

10. ENGINEERED BARRIER SYSTEM TRANSPORT

Section 10 describes the new information developed to produce a more realistic model for transport of radionuclides through the engineered barrier system (EBS). More specifically, this new information is designed to quantify uncertainties and reduce conservatisms in the EBS radionuclide transport abstraction for the *Total System Performance Assessment for the Site Recommendation* (TSPA-SR) (CRWMS M&O 2000 [DIRS 153246]). The new information provides supplemental models or analysis in six areas: (1) diffusive transport within the waste package, (2) transport from the waste package to the invert, (3) diffusive transport through the invert, (4) sorption of dissolved radionuclides, (5) transport via colloids, and (6) transport via microbes. Table 10-1 summarizes the rationale for the supplemental models and analyses in these six areas and identifies the specific section that documents the new information.

Diffusion in the waste package, diffusion from the waste package to the invert, sorption of dissolved radionuclides, and microbial sorption and transport are based on new conceptual models for transport through the EBS. While these new conceptual models provide a more realistic simulation of the transport process, they also include parameters that represent the uncertainties in long-term EBS performance. Diffusion through the invert and colloidal transport of radionuclides primarily involve better definition of the unquantified uncertainties in the previous TSPA-SR models (CRWMS M&O 2000 [DIRS 153246]).

Transport processes in the EBS have no impact on alternative thermal operating modes for the repository. However, the thermal operating mode does influence transport through the EBS, both directly and indirectly. A direct influence exists because the diffusion coefficient is a function of the temperature. The indirect influences exist because the diffusion coefficient is a function of liquid saturation and the adsorption of water vapor on surfaces is a function of the relative humidity. The time-dependent values for liquid saturation and relative humidity are both functions of the thermal operating mode.

Finally, multiple lines of evidence are provided for sorption, colloidal transport, and microbial transport. The supporting evidence for sorption is based on laboratory column tests, which are similar to the downward migration of radionuclides through materials representing the waste form and invert. The supporting evidence for colloidal transport is based on numerous investigations of colloid stability and transport properties; common principles have been employed in the development of this model. The supporting evidence for microbial transport of radionuclides is based on a substantial experimental basis documenting radionuclide uptake by microbes and their subsequent movement as colloidal particles in unsaturated environments.

10.1 INTRODUCTION AND CONCEPTUAL MODEL

The waste form is the source of all radionuclides in the EBS. Radionuclides can be transported downward from breached waste packages, through the invert, and into the unsaturated zone. Transport can occur through advection, in which radionuclides are carried along by a fluid when there is fluid flow through the waste package and invert. Transport can also occur by diffusion, whereby radionuclides migrate from a zone of high concentration to a region of lesser concentration. Both advective and diffusive transport can occur simultaneously when there is a fluid flux through the waste package and invert. Diffusion can occur in the absence of an

Table 10-1. Summary of Supplemental Models and Analyses

Key Attributes of System	Process Model (Section of S&ER)	Topic of Supplemental Scientific Model or Analysis	Reason For Supplemental Scientific Model or Analysis			Section of Volume 1	Performance Assessment Treatment of Supplemental Scientific Model or Analysis ^a	
			Unquantified Uncertainty Analysis	Update in Scientific Information	Lower-Temperature Operating Mode Analysis		TSPA Sensitivity Analysis	Included in Supplemental TSPA Model
Limited Release of Radionuclides from the Engineered Barriers	EBS (Invert) Degradation and Transport (4.2.6, 4.2.7)	Diffusion inside waste package	X	X		10.3.1	X	X
		Transport pathway from inside waste package to invert	X	X		10.3.2		
		Sorption inside waste package	X	X		10.3.4	X	X
		Sorption in invert	X	X		10.3.4	X	X
		Diffusion through invert	X			10.3.3	X	X
		Colloid stability in the invert	X			10.3.5		
		Microbial transport of colloids	X	X		10.3.6		

NOTE: S&ER = Yucca Mountain Science and Engineering Report (DOE 2001 [DIRS 153849]).

^a Performance assessment treatment of supplemental scientific model or analysis discussed in SSPA Volume 2 (McNeish 2001 [DIRS 155023]).

advective liquid flux if there is a continuous liquid pathway, possibly in the form of thin films, on the waste form, the waste package, the invert, and solid surfaces. Note that gaseous transport of volatile radionuclides has been screened out of the nominal scenario for the total system performance assessment (TSPA) because of low consequence (CRWMS M&O 2000 [DIRS 150806], FEP 3.2.10.00.00).

Advective and diffusive transport in the engineered barrier system may occur through unsaturated porous media or liquid films. The invert, with a granular backfill material, is conceptualized to behave as an unsaturated porous medium. It will have both advective and diffusive transport in those regions of the repository where in-drift seepage or imbibition from the host rock create an advective flux through the invert. Liquid films can exist on EBS components, even in repository regions without seepage, because water vapor will adsorb onto surfaces with corrosion products. Transport through very thin liquid films will be primarily by diffusion through corrosion products because the advective velocity is negligible. Thicker liquid films may have large advective fluxes within which advection is the dominant transport mechanism.

A one-dimensional transport model has been used to represent advection and diffusion in the EBS. This approach is appropriate because (1) the major transport path is downward, from the waste package to the invert to the unsaturated zone, and (2) lateral pressure and saturation gradients directly beneath the waste package are anticipated to be minor, so a one-dimensional model should maximize releases to the unsaturated zone. Further, because the advective travel time through the invert is anticipated to be very fast in comparison to the travel times through the unsaturated and saturated zones, dispersivity is neglected in the transport model for the EBS.

Radionuclides are transported in two physical forms: as dissolved chemical species and as colloidal particles. Dissolved and colloidal radionuclides will diffuse through thin films of water and stress corrosion cracks in the waste package lids. They may also migrate by advection through larger patches formed by general corrosion. Migration through the invert may be by diffusion, advection, or both.

Colloid-facilitated transport of radionuclides is important for certain radionuclides that have limited solubility (as dissolved species) but strong affinity for colloidal-size particles that are mobile in water. Two general classifications of colloids can be defined. First, abiotic colloids are small particulates, with a typical size range of 10^{-3} to 10^{-6} mm (Freeze and Cherry 1979 [DIRS 101173], p. 127), that can physically or chemically bind with ions in an aqueous environment. They often occur naturally in the geologic environment because clay minerals and some geochemical weathering products of rocks are of colloidal size and can persist in aqueous solutions for long periods of time. Three types of abiotic colloids are expected in the EBS: (1) waste form colloids, (2) colloids produced from corrosion of repository materials, and (3) natural colloids in the partially saturated media and groundwater at the repository horizon. Second, microbes also behave similarly to colloids and can be considered biotic colloids. Radionuclides in waste form colloids may be irreversibly embedded or reversibly attached by chemical sorption. Radionuclides in corrosion-product and groundwater colloids are likely to be reversibly attached, although sorption of metal ions to iron-(hydr)oxide colloids can be quite strong.

10.1.1 Alternative Conceptual Models

Several alternative conceptual models for transport were considered but, because they are improbable or not supported by available data, were not incorporated in the TSPA-SR (CRWMS M&O 2000 [DIRS 153246]) conceptual model for EBS transport. These models are described in the following paragraphs.

It is possible that ponding could occur in the emplacement drifts due to clogging in the invert or in the host rock that drains the invert. Drainage pathways could become clogged with fine materials from geochemical alteration of EBS materials, dust from long-term ventilation of the drifts, fines from rockfalls, or precipitates of uranium compounds derived from the waste form. Possible consequences include an increased rate of radionuclide transport to and through the unsaturated zone. For example, radionuclides might be transported laterally along the drift to a major fault or fracture zone where rapid drainage through the host rock could occur. In this situation, transport through the unsaturated zone could occur faster than if the drainage was more uniform. However, the fracture permeability and drainage capacity of the host rock is large enough that ponding is sufficiently unlikely (CRWMS M&O 2000 [DIRS 133329], Section 6.6) and has not been included in the EBS flow abstraction for the TSPA-SR (CRWMS M&O 2000 [DIRS 153246], Section 3.6.2.1).

It is possible that radionuclides can be sorbed by steel corrosion products, and that episodes of increased fluid flux could cause temporarily increased rates of radionuclide release. However, the increased flux would cause dilution downstream, which would tend to mitigate the effect on dose rate in the biosphere.

It is possible that precipitates and salts could accumulate in the invert during the thermal period. Any change in invert porosity could alter the invert transport properties. However, the salts would be readily dissolved when water returned during cooldown, leaving the less soluble precipitates (mainly of silica and calcite) at later times, when waste package failure is most likely to occur. These precipitates would occupy only a portion of the available porosity (CRWMS M&O 2000 [DIRS 133329], Section 6.1). Consequently, the effect on transport properties of the invert ballast material from precipitation in the interparticle porosity would be limited. If water entering the drift is imbibed into the intraparticle porosity and evaporates there, the relative changes from precipitation may be greater; however, the effects on invert hydrologic properties and transport properties have not been evaluated.

10.2 REVIEW OF TOTAL SYSTEM PERFORMANCE ASSESSMENT-SITE RECOMMENDATION TREATMENT

Over tens of thousands of years, the drip shields and waste packages will gradually degrade, leading to the mobilization and transport of radionuclides through the EBS. The primary transport medium through the engineered barriers is (liquid) water. Flowing water or a continuous film of water is necessary for radionuclide transport out of the waste package to the invert and through the invert into the unsaturated zone.

Once a waste package is breached, water may enter the package as water vapor or as drips. This water will come into contact with the metal cladding of commercial spent nuclear fuel rods or

with the stainless steel canister surrounding vitrified high-level waste. If the metal cladding that encases the spent nuclear fuel pellets is also breached, radionuclides may dissolve in the water and be transported out of the waste package. Similarly, if the stainless steel canister surrounding the vitrified waste form is breached, the glass and its associated radionuclides may dissolve and be mobilized for transport out of the waste package. Figure 10.2-1 illustrates this transport process for patches formed by general corrosion of the drip shield and waste package. As shown in this figure, the patches provide a path for dripping water to enter the top of the waste package, contact the waste form, mobilize radionuclides, and carry these radionuclides out the bottom of the waste package through the invert and into the unsaturated zone. Patches are large areas on the surface of the waste package that form due to general corrosion. The timing and size of patches are predicted by waste package degradation models, independent of the EBS flow and transport abstractions.

The dissolved concentration of each mobilized radionuclide cannot exceed the radionuclide solubility limit unless colloids are present. Colloids are important for transport because they can increase the mobilized concentration of radionuclides. Colloids can also increase the transport velocity of radionuclides, although this will be a minor effect over the short distances in the EBS.

Radionuclides that are mobilized as dissolved species or as colloidal particles may be transported by advection or diffusion. Both advection and diffusion are important for transport through patches produced by general corrosion of the waste package. Advective transport is anticipated to be the main transport mechanism through patches if there is a significant dripping flux through the waste package, while diffusive transport through patches will be important in the dry areas of the repository. In the TSPA-SR (CRWMS M&O 2000 [DIRS 153246], p. 3-134), a one-dimensional advection-diffusion transport model combines both of these mechanisms. Diffusive transport is anticipated to be the dominant mechanism through stress corrosion cracks because their small size and associated capillary forces resist an advective flux.

Once outside the package, radionuclides will be transported through the invert by diffusion if fluid velocities are sufficiently small, or by diffusion and advection if fluid velocities are large.

Microbial transport and sorption were not included in the EBS transport abstraction for the TSPA-SR model (CRWMS M&O 2000 [DIRS 153246], Section 3.6.2.2).

10.2.1 Transport Abstraction

The waste form is the source of all radionuclides in the EBS. After a breach of the waste package, radionuclides can be transported downward through the invert and into the unsaturated zone (UZ), as shown in Figure 10.2-1. Advective and diffusive transport can occur through patches formed by general corrosion of the waste package, as discussed above. Transport can also occur by diffusion through stress corrosion cracks. The transport abstraction conservatively assumes that diffusion begins immediately after stress corrosion cracks form, regardless of whether conditions are consistent with the existence of a continuous liquid pathway.

Colloid-facilitated transport of radionuclides is included as an additional source term. Radionuclides are transported from the waste package either as dissolved species or bound to colloids. The total concentration for certain radionuclides, particularly plutonium and

americium, can be increased well above the solubility limit by colloidal transport. There are three types of colloids in the engineered barrier system: (1) waste form colloids, (2) iron-(hydr)oxide colloids, and (3) groundwater colloids. The waste form colloids may have irreversibly attached (embedded) or reversibly attached (sorbed) radionuclides. The iron-(hydr)oxide and groundwater colloids have only reversibly attached radionuclides.

The diffusion coefficient for dissolved species in the invert is based on the self-diffusivity of water as an upper bound. Each radionuclide complex could be assigned a unique value for its free water diffusion coefficient. The complexity of the time-dependent chemistry in the waste package makes this a challenging task, so a simpler approach has been incorporated into the TSPA-SR (CRWMS M&O 2000 [DIRS 153246], p. 3-138). The value of the free water diffusion coefficient for all radionuclides is set equal to the self-diffusivity of water at 25°C. This is a reasonable and conservative approximation because the self-diffusivity of water has been shown to be a bounding value for all radionuclides of interest (CRWMS M&O 2000 [DIRS 153940], Section 6.4.1) in the TSPA-SR.

The value of the free water diffusion coefficient must be corrected for the presence of a porous medium in the invert. The functional dependence of these corrections is given in the *EBS Radionuclide Transport Abstraction* (CRWMS M&O 2000 [DIRS 153940], Section 6.4.1):

$$D = D_0 s^{1.849} \phi^{1.3} f(T)$$

where

- D = the time-dependent diffusion coefficient
- D_0 = the self-diffusivity of water at 25°C
- s = the time-dependent liquid saturation in the invert
- ϕ = the (constant) porosity of the invert
- $f(T)$ = the correction for invert temperature, T .

Finally, the diffusion coefficient for radionuclides bound to colloids is given by the diffusion coefficient for the dissolved species divided by 100:

$$D_{colloid} = D / 100 = (0.01) D_0 s^{1.849} \phi^{1.3} f(T)$$

The rationale for the factor of 100 reduction is based on an approximation of the ratio of the ionic radii of a dissolved species to that of a colloid (CRWMS M&O 2000 [DIRS 125156], Section 6.17).

Diffusive transport calculations through the invert also require boundary conditions on the top and bottom of the invert. The boundary condition on the top of the invert is simply the radionuclide concentration within the waste package. The boundary condition on the bottom of the invert, at the boundary with the UZ, is a zero concentration (swept away) boundary condition. The zero concentration boundary condition is implemented by defining a flow cell with a small volume of water but a very high advective outflow, effectively sweeping all radionuclides away from the lower boundary. This is a reasonable approximation when advective fluxes in the host rock are large enough to sweep radionuclides away from the invert,

diluting the local concentrations below it. This can be a conservative assumption if the advective fluxes in the host rock are small, so that seepage into the drift is negligible and the dominant transport mechanism is diffusion. In this case, the radionuclide concentrations in the host rock directly beneath the invert may be large enough to substantially reduce diffusive transport through the invert. This conservatism has not been quantified in the present studies because quantifying the uncertainties in sorption and in-package diffusion were expected to be more important for EBS performance.

Corrosion products from the waste package and spent nuclear fuel have the potential to strongly sorb actinides. Sorption on corrosion products will be beneficial to performance because this process can retain radionuclides in the EBS and delay their release to the UZ. The potential advantages of retardation were conservatively ignored in the transport abstraction.

10.2.2 Conservatisms and Uncertainties in the Transport Abstraction

The transport abstraction described above is based on a reasonable approach that bounds the transport and release of radionuclides to the UZ. The use of reasonable bounds is appropriate because of potentially large uncertainties in the response of a very complex engineered system over long periods of time. Following are the noteworthy conservatisms and uncertainties in the TSPA-SR (CRWMS M&O 2000 [DIRS 153246]) abstractions:

Diffusion from the Waste Package Is Maximized—The abstraction has a number of assumptions that maximize diffusive releases:

1. All mobilized radionuclides are immediately available to diffuse through any breaches in the waste package. For example, the potential delay associated with in-package diffusion between fuel rods and a stress corrosion crack is conservatively neglected in the transport abstraction.
2. Stress corrosion cracks and the invert are covered with a thin film of liquid that supports diffusive transport at all times. The thermal effect from evaporation drying out selected elements of the system, such as the emplacement pallet or surface of the waste package, is conservatively ignored.
3. The waste package is assumed to be in contact with the invert, providing a short, continuous pathway for diffusion from the waste package to the invert. The potential delay associated with diffusion through the longer pathway along the outer surfaces of the waste package and emplacement pallet is (conservatively) ignored.

The result of these assumptions is that radionuclides will be released by diffusion through a patch or a stress corrosion crack, even when the drip shield is intact and there is no advective flux into the waste package. The thermal effect referred to in Item 2 may have tremendous benefit for defense-in-depth and degraded barrier sensitivity studies, such as a waste package juvenile failure scenario.

The Diffusion Coefficient Is Based on a Bounding Abstraction—The free water diffusion coefficient for all radionuclides is based on the self-diffusivity of water at 25°C. This approach provides a bounding value for the free water diffusivity of all radionuclide species relevant to the

TSPA. The self-diffusivity of water is conservative (larger) than the radionuclide-specific values by a factor of 1 to 3.8, depending on the ionic charge (see Section 10.3.3.3.2). This assumption therefore enhances diffusive transport by a factor of 1 to 3.8. In addition, the correction for porosity of the invert is conservative by about 40 percent.

Sorption Is Ignored in the Waste Package and Invert—Reversible sorption is known to be an important process for contaminant transport when iron corrosion products are present in a system, as will occur in the waste package and invert (see Section 10.3.4). Irreversible sorption is known to be an important process for transport of plutonium, thorium, and neptunium (see Section 10.3.4.3.3.4). The transport abstraction (conservatively) ignores retardation in the EBS.

The next section provides model abstractions to quantify the uncertainty and conservatism associated with diffusion inside the waste package, transport along the outer surface of the waste package and the emplacement pallet, the bounding abstraction for the diffusion coefficient in the invert, sorption of dissolved species, colloidal-mediated transport, and the effects of microbial populations on the transport process.

10.3 UNCERTAINTY ANALYSES

The conservatisms and uncertainties in the TSPA-SR transport abstraction (CRWMS M&O 2000 [DIRS 153246], Section 3.6.3.1) are quantified in this section. The relationships between the conservatisms in Section 10.2.1 and the uncertainty analyses in this section are described below.

Diffusion from the Waste Package—The conservative or bounding assumptions for the TSPA-SR diffusive transport abstraction (CRWMS M&O 2000 [DIRS 153246], p. 3-141) abstraction have been analyzed in three steps: diffusion in the waste package (see Section 10.3.1), diffusion from the waste package to the invert (see Section 10.3.2), and diffusion through the invert (see Section 10.3.3).

Diffusion Coefficient—The conservatisms in the calculation of the free water diffusion coefficient and the diffusion coefficient in unsaturated granular media are quantified in Section 10.3.3.

Sorption—The potential for sorption of radionuclides in the EBS is evaluated in Section 10.3.4, and ranges of partition coefficients for seven radionuclides are provided in that section.

Colloidal/Microbial Transport—Although not identified as a conservatism in the TSPA-SR abstraction (CRWMS M&O 2000 [DIRS 153246], Section 3.6.3.1), the potential uncertainties in radionuclide transport via colloids and microbes are discussed in Sections 10.3.5 and 10.3.6.

10.3.1 Diffusion in the Waste Package

10.3.1.1 Goal of the Model

The goal of this model is to quantify the impact of in-package diffusion on radionuclide transport through the waste package. Transport within the waste package can occur through advective or diffusive mechanisms. Advective transport occurs when a radionuclide, either as a dissolved species in an aqueous solution or attached to a colloidal particle, moves with a flowing fluid.

Diffusive transport occurs when a radionuclide, either as a dissolved species in aqueous solution or attached to a colloidal particle, moves from a region of high concentration to a region of lower concentration in a stagnant film or body of water. Both advective and diffusive transport will occur for those waste packages exposed to a dripping environment in the repository. Only diffusive transport is anticipated to occur in those waste packages in the dry (non-seeping) regions of the repository. Since approximately 87 percent of the waste packages are in a dry region of the repository (CRWMS M&O 2000 [DIRS 153246], pp. 4-5), in-package diffusion is an important process for release of radionuclides from the waste package. This section provides a model to quantify the impact of in-package diffusion on repository performance.

10.3.1.2 Identification of Unquantified Uncertainties in Total System Performance Assessment-Site Recommendation

Dripping from seeps is not expected to occur in about 87 percent of the potential repository at Yucca Mountain (CRWMS M&O 2000 [DIRS 153246], pp. 4-5). In this situation, advective transport of radionuclides within waste packages will be negligible for the bulk of the repository. However, diffusive transport is still possible through the thin film of adsorbed water that will cover all surfaces exposed to the humid air in the repository drifts. The objective of this analysis is to develop an abstraction for calculating the diffusive releases from waste packages where no drips or other advective releases occur.

The current TSPA-SR transport model for the waste package (CRWMS M&O 2000 [DIRS 153246], p. 3-141) conservatively assumes that all radionuclides released by the waste form are immediately available to diffuse through any breaches in the package. In other words, the potential delay between release of radionuclides from the pellets in a commercial spent nuclear fuel (SNF) fuel rod and their arrival at the surface of the waste package is ignored. Similarly, the potential delay between the release of radionuclides at the surface of a vitrified form and their arrival at the surface of the waste package is ignored. This approach is equivalent to assuming instantaneous in-package diffusion, which is a conservative approach.

Alternative thermal operating modes will affect the in-package diffusion model in two ways. First, the diffusion coefficient for in-package corrosion products is a direct function of temperature (CRWMS M&O 2000 [DIRS 153940], p. 62). Second, the thermal operating mode will indirectly affect the thickness of in-package water films and the saturation of in-package corrosion products because these quantities are functions of the thermally-dependent relative humidity in the repository, as discussed in Sections 10.3.1.3.2 and 10.3.1.3.5.

10.3.1.3 Quantification of Previously Unquantified Uncertainty

The focus in this section is on diffusive releases from commercial SNF waste packages in non-dripping regions of the repository. A diffusive release model for U.S. Department of Energy (DOE) high-level radioactive waste packages is not being implemented for the TSPA-SR sensitivity studies because the glass dissolution process may result in advective releases from the waste package if the relative humidity is high enough (see Section 10.3.1.3.1.1).

10.3.1.3.1 Conceptual Model for the Commercial SNF In-Package Environment

Fuel rods are expected to be extremely robust because the Zircaloy cladding around the fuel pellets is highly corrosion-resistant; at 100°C, the cladding will remain intact for at least 100,000 years (CRWMS M&O 2000 [DIRS 136058], p. 48) barring damage from rockfalls. However, some fuel rods may be damaged while in use or during handling and shipping to the repository. A number of mechanisms cause fuel rod failure inside a reactor core, including damage from debris striking the rods, manufacturing defects, radiation-enhanced corrosion resulting in splitting of the rods, pitting corrosion, and chafing where the rods contact the assembly spacer grids. Because estimated failure rates of fuel rods due to corrosion are essentially zero after emplacement in the potential repository, the TSPA-SR model (CRWMS M&O 2000 [DIRS 153246], p. 3-112) assumed that the cladding will fail in a certain fraction of the fuel rods over specified periods of time. These failed rods will release radionuclides through diffusion once a continuous film of liquid water is present on the internal components of the waste package.

Baskets and guides support fuel rod assemblies inside a waste package for commercial SNF. These support components are fabricated from carbon steel and will begin to corrode once a waste package is breached. Corrosion begins when the relative humidity becomes great enough to produce aqueous conditions on the surface. A threshold value of 70 percent has been estimated (CRWMS M&O 2000 [DIRS 151951], Assumption 5.3.9, p. 45), although the presence of deliquescent salts can result in aqueous conditions at lower values of relative humidity. As the support components become thinner due to corrosion, they will weaken and eventually allow fuel rod assemblies to fall to the bottom of the waste package.

Corrosion of the internal support components will increase the surface area for adsorption of water and increase the area for diffusive transport, resulting in greater diffusive releases from the waste package. The fuel rods could also be bent if sections of the support components fail sooner than other parts. This could result in enhanced rod failure rates, with a greater mass of radionuclides available to diffuse out of a waste package.

The waste package inner liner, made of Stainless Steel Type 316NG, has a very long lifetime as computed from known general corrosion rates. However, the potential performance credit of the stainless steel layer was not included in the nominal TSPA-SR analysis (CRWMS M&O 2000 [DIRS 146427], p. 32). As with the baskets and other waste form components (except for the fuel rods), the degradation of the inner liner will provide additional surface area for adsorption of water and additional cross-sectional area for diffusion of radionuclides through the water film.

10.3.1.3.1.1 Conceptual Model for U.S. Department of Energy High-Level Radioactive Waste In-Package Environment

When glass is exposed to humid air, water molecules will adsorb onto specific sites on the glass surface (primarily silanol and alkali metal). The amount of water that adsorbs on the glass will depend on the relative humidity of the air, the temperature of the glass surface, and the hygroscopicity of the glass surface. The adsorption isotherm for water on a reference waste glass made with Savannah River Laboratory 165 frit has been measured at about 23°C (Ebert et al. 1991 [DIRS 111028], p. 134, Figure 1b). The measured isotherm for Savannah River

Laboratory 165U glass was fit using the following equation (CRWMS M&O 2001 [DIRS 153846], p. 35):

$$\theta = \left[\frac{-3.2}{\ln(RH)} \right]^{1/1.5} \quad (\text{Eq. 10-1})$$

where θ is the number of layers of water adsorbed and RH is the relative humidity. The first layer forms at a relative humidity of only a few percent. This corresponds to adsorption at the primary sites. Subsequent layers form as water vapor bonds with adsorbed water to form beads of water on the glass surface. At relative humidities above about 80 percent (CRWMS M&O 2001 [DIRS 153846], pp. 35), a sufficient amount of water has condensed to coalesce into a thin film covering the entire surface.

The DOE high-level radioactive waste, in the form of glass logs, will eventually degrade completely from the reactions at the outer surface. Once glass degradation has begun, a film of water will exist on the outer surface of the glass logs. This coating will provide a pathway for radionuclides to diffuse through breaches in the waste package.

The film of water may also be thick enough to result in advective flow within the waste package. The rate of degradation of the glass is provided by the glass degradation model (CRWMS M&O 2001 [DIRS 153846], pp. 39 to 40). The concentrated solutions containing dissolved glass are hygroscopic, and will continue to absorb water and further degrade the glass. In this situation, the thickness of the water film can be related to the degradation rate, but the water film thickness may not increase; rather, once a certain thickness is reached, it will drain off the glass and either pool in the bottom of the waste package or flow out of breaches in the waste package into the invert. The rate of flow will be equal to the rate of condensation, which in turn will be proportional to the rate of degradation, with fresh condensation offsetting the dissolution and concentration of glass degradation products.

Thus, two transport mechanisms may be occurring simultaneously—diffusion and advection—even when there is no dripping or other flow of liquid water into a waste package (i.e., when water vapor diffuses into a waste package and adsorbs or condenses on the waste package internals). The TSPA-SR model ignores the beneficial effects from a partly saturated and degraded waste form on in-package transport (CRWMS M&O 2000 [DIRS 153246], p. 3-141) for all types of waste packages. Considering the lack of information on adsorption of water vapor into films containing dissolved glass, this approach seems to be reasonable for the codisposal waste packages that contain vitrified glass waste forms. An in-package diffusion model for DOE high-level radioactive waste has therefore not been implemented in the sensitivity studies.

10.3.1.3.2 Adsorption of Water Vapor

All surfaces exposed to water vapor will adsorb water. The amount of adsorbed water vapor depends principally on the nature of the material and the relative humidity. In many cases, the first layer of water adsorbed is chemically bound to the surface and is difficult to remove except at high temperatures, considerably higher than will exist in the repository. Subsequent layers are

less tightly bound, being attracted simply by van der Waals forces to lower water layers. The first few layers of water often form an ice-like structure with little mobility. As the relative humidity approaches 100 percent, the outer layers of water begin to behave more like bulk liquid; at 100 percent relative humidity, bulk condensation of water occurs, forming a liquid phase.

Except for inert metals such as gold and platinum, most metals form an oxide surface layer when exposed to oxygen or water. In the case of Alloy 22, stainless steel, Zircaloy, and aluminum—metals found in the waste package or waste form—the surface oxide layer is passivating. Oxygen diffuses very slowly through the oxide layer, protecting the metal underneath. Thus, all metals in a waste package contain a surface oxide layer on which water adsorption takes place.

Adsorption isotherms define the amount of water adsorbed as a function of relative humidity or relative pressure, provided sufficient time is allowed for equilibrium to take place. Extensive measurements have been made for a few substances, such as iron oxide and titanium oxide, but adsorption isotherms are only available for a few materials. Isotherms for metal oxides found in waste packages have been measured for NiO, Fe₂O₃, and ZrO₂. Isotherms for other major components of stainless steel, such as Cr₂O₃ and Mo₂O₃, are not readily available in the open literature. However, the oxides of iron, nickel, and zirconium make up the bulk of oxides in a package and are representative of in-package materials. Figure 10.3.1-1 presents the adsorption isotherms for Fe₂O₃, NiO, and ZrO₂, each of which is discussed in the following sections.

10.3.1.3.2.1 Iron Oxide Isotherm

The adsorption isotherm of α -Fe₂O₃, a form of hematite, has been extensively measured and reported in the literature (McCafferty and Zettlemyer 1970 [DIRS 154382]; Jurinak 1964 [DIRS 154381]). These measurements are directly relevant to the repository because (1) hematite should be the predominant form of iron oxide in a degrading waste package (YMP 1998 [DIRS 104441]), and (2) hematite should comprise the bulk of the corrosion products in the waste package. The second point follows because steel accounts for most of the mass in a waste package and iron is the major component of both carbon steel and stainless steel.

Although it is not the most recent measurement of water vapor adsorption on hematite, Jurinak (1964 [DIRS 154381], p. 486) provides a functional relationship for the coverage (i.e., number of monolayers of water adsorbed) as a function of relative humidity based on the Frenkel-Halsey-Hill (FHH) equation for multilayer adsorption:

$$\log_{10} P/P_0 = -\frac{1.1}{(V/V_m)^{2.45}}$$

where

- P = partial pressure of water [Pa]
- P_0 = vapor pressure of water [Pa]
- V = volume of water vapor adsorbed at reference conditions [m³]
- V_m = volume of adsorbed water vapor that provides a one-monolayer coverage on the surface [m³].

The ratio of water vapor partial pressure to vapor pressure is the relative humidity (RH). The ratio of V to V_m is the number of monolayers of water (i.e., the number of layers of individual water molecules) adsorbed on the surface, assuming complete and uniform coverage. Letting $\theta_a = V/V_m$ and $RH = P/P_0$, Jurinak's correlation may be written in general terms with parameters k and s :

$$\ln(RH) = -\frac{k}{\theta_a^s \log_{10} e}$$

or

$$\theta_a = \left(\frac{k}{\log_{10} e} \right)^{\frac{1}{s}} [-\ln(RH)]^{-1/s}$$

With $k = 1.1$ and $s = 2.45$:

$$\ln(RH) = -2.5328\theta_a^{-2.45}$$

or

$$\theta_a = 1.461296[-\ln(RH)]^{-0.40816} \quad (\text{Eq. 10-2})$$

This isotherm is plotted in Figure 10.3.1-2 with the data of McCafferty and Zettlemoyer (1970 [DIRS 154382]) for comparison.

The average thickness of a monolayer of water can be computed from the cross-sectional area of a water molecule. Although Jurinak (1964 [DIRS 154381], p. 480) assumes an area of 10.8 \AA^2 per molecule, an area of 10.6 \AA^2 seems to be more commonly used (McCafferty and Zettlemoyer 1970 [DIRS 154382], p. 454); Holmes et al. 1974 [DIRS 154379], p. 368), while Gregg and Sing (1982 [DIRS 153010], p. 264) indicate that 10.5 \AA^2 per molecule represents a "close-packed" monolayer. Using 10.6 \AA^2 per molecule and a water density at 25°C of 997.0449 kg/m^3 (Weast 1985 [DIRS 111561], p. F-4), the thickness of a water monolayer, t_f , is:

$$t_f = \frac{18.01528 \times 10^{-3} \frac{\text{kg}}{\text{mol}}}{\left(10.6 \times 10^{-20} \frac{\text{m}^2}{\text{molec}} \right) \left(997.0449 \frac{\text{kg}}{\text{m}^3} \right) \left(6.0221367 \times 10^{23} \frac{\text{molec}}{\text{mol}} \right)} \quad (\text{Eq. 10-3})$$

$$= 2.83 \times 10^{-10} \text{ m.}$$

At 50°C , the density of water is 988.0363 kg/m^3 (Weast 1985 [DIRS 111561], p. F-5) and the adsorbed water monolayer thickness is $2.85 \times 10^{-10} \text{ m}$, which shows that the monolayer thickness is not highly sensitive to temperature.

10.3.1.3.2.2 NiO Isotherm

Pure nickel reacts spontaneously with oxygen in air to form a NiO film that is 16Å to 32Å thick after 3 to 48 hours (Lee 1994 [DIRS 154380], p. 56). The NiO(s) film is highly insulating and coherent. The NiO(s) film is highly insulating and coherent. It retains its identity as a chemical species when in contact with water vapor or bulk water.

Lee (1994 [DIRS 154380], pp. 276 to 277) found that an oxide layer forms on the nickel surface in N₂/H₂O, but no further oxidation occurs. Oxide grows on nickel with relative humidity in the air and water at a constant temperature. The amount of water adsorbed on nickel is not affected by the thickness of nickel oxide (Lee 1994 [DIRS 154380], p. 251). Multilayer and capillary condensation occur as the relative humidity increases. At 25°C, the amount of water adsorbed on nickel at RH = 80 percent is about 2.10×10^{-7} g/cm² (Lee 1994 [DIRS 154380], Figure 4.48). Using a monolayer coverage of 3.1033×10^{-8} g/cm² (Lee 1994 [DIRS 154380], p. 173) and a surface roughness factor of 4 (Lee 1994 [DIRS 154380], p. 231), the mass gain data in g/cm² from Lee (1994 [DIRS 154380], Figure 4.48) are converted to monolayer coverage by dividing by $(3.1033 \times 10^{-8})(4) = 1.24132 \times 10^{-7}$. These results (Lee 1994 [DIRS 154380], Figure 4.48) are for N₂ carrier gas, rather than for air; however, the amount of water adsorbed from air appears to be slightly less than from N₂ (Lee 1994 [DIRS 154380], Figures 4.49 and 4.50), so using these data should be conservative in terms of overestimating the amount of water available for diffusion of radionuclides. The data of Lee (1994 [DIRS 154380]) at 25°C, converted from g/cm² mass gain to monolayers of water by dividing by 1.24132×10^{-7} , are shown in Figure 10.3.1-3.

The NiO film is very thin, and the adsorption isotherm for NiO results in a film thickness that is less than the film thickness for iron oxide at all values of relative humidity, as shown in Table 10.3.1-1. The iron oxide isotherm has therefore been used to estimate film thickness for the corroded waste package internal components because it is conservative relative to the adsorption isotherm for NiO.

10.3.1.3.2.3 ZrO₂ Isotherm

The adsorption isotherm for water vapor on ZrO₂ at 25°C (Holmes et al. 1974 [DIRS 154379], p. 367, Figure 3) is shown in Figure 10.3.1-4. Measurements by Holmes et al. (1974 [DIRS 154379]) during adsorption-desorption cycling revealed that the sample irreversibly adsorbed 4.8 mg water/g sample, which compares favorably with the estimated chemisorption capacity of 5.7 mg/g. In the initial outgassing of the sample, the weight loss between 25°C and 500°C was equivalent to about 2.3 monolayers of chemisorbed water. The monolayer capacities are equivalent to specific surface areas of about 14 to 15 m²/g, based on 10.6 Å² per adsorbed water molecule. Nitrogen and argon adsorption data on the water-covered zirconium oxide surface gave specific surface areas of 18.6 m²/g for nitrogen and 17.8 m²/g for argon. This difference emphasizes the specificity involved in water adsorption on oxide surfaces and the accompanying uncertainty in specific surface areas estimated from such data. Using 14.5 m²/g for specific surface area, the amount adsorbed per monolayer of water is:

$$\frac{\left(14.5 \frac{\text{m}^2}{\text{g ZrO}_2}\right) \left(18.0153 \times 10^3 \frac{\text{mg H}_2\text{O}}{\text{mol}}\right)}{\left(10.6 \times 10^{-20} \frac{\text{m}^2}{\text{molecule}}\right) \left(6.0221367 \times 10^{23} \frac{\text{molecule}}{\text{mol}}\right)} = 4.092 \frac{\text{mg H}_2\text{O}}{\text{g ZrO}_2} / \text{monolayer}$$

The data for the adsorption of water onto ZrO_2 are presented graphically in Holmes et al. (1974 [DIRS 154379], Figure 3). For easier use, these data have been fit to the commonly-used FHH multilayer adsorption isotherm equation (Lee 1994 [DIRS 154380], p. 96). The FHH isotherm is attractive for its simple mathematical form and its applicability to multilayer adsorption, which is observed for water vapor on ZrO_2 :

$$\ln RH = -\frac{k}{\theta_a^s}$$

or equivalently,

$$\theta_a = \left(\frac{-k}{\ln RH}\right)^{1/s}$$

which relates the number of monolayers of water, θ_a , to the relative humidity, RH . The parameter k and exponent s are obtained by a linear least squares fit of data read from Holmes et al. (1974 [DIRS 154379], Figure 3). The FHH equation can be linearized in terms of k and s by taking the log of both sides of the equation:

$$-\ln[-\ln(RH)] = s \ln(\theta_a) - \ln(k).$$

This equation is for a straight line:

$$Y = sX - \ln k$$

where

$$Y = -\ln[-\ln(RH)]$$

$$X = \ln(\theta_a)$$

Table 10.3.1-2 presents the least squares analysis of the transformed data performed using Microsoft® Excel 97. The Add Trendline capability was used for the linear regression, resulting in the relationship:

$$Y = 1.8318X - 1.8976$$

where s is the slope (1.8318) and $-\ln k = -1.8976$ is the intercept, so $k = 6.67$. The coefficient of determination for the linear regression is $R^2=0.984$.

Thus, the data from Holmes et al. (1974 [DIRS 154379], Figure 3) as fit to an FHH multilayer adsorption isotherm correlation become:

$$\theta_a = \left(\frac{-6.67}{\ln RH} \right)^{1/1.8318}$$

The predicted relative humidity is based upon a least squares fit linear regression analysis. The slope $s = 1.8318$, and the intercept $\ln(k) = -1.8976$.

10.3.1.3.2.4 Behavior of Thin Water Films

Water at solid surfaces varies in nature from a highly structured form on hydrophilic substrates to a loose, entropic form on more hydrophobic substrates possessing hydrophilic sites (Lee 1994 [DIRS 154380], p. 74). The adsorption of water on solids depends on the capacity of the surface to orient the water dipoles, usually with the proton outward. Near polar surfaces of solids such as metal and oxides, the source of orientation of water molecules at the interface could be either hydrogen bonding or dipole-dipole interactions, depending on the chemical nature of the solid. Depending on the dissimilarity between the ordered (dipole-dipole), induced structure near the interface and the bulk structure, various thicknesses of the ordered layers are possible (Lee 1994 [DIRS 154380], p. 75).

The structure of liquid water is considered to consist of unbonded molecules and of molecules hydrogen-bonded in clusters that have a mean size of about 90 molecules at 0°C (Lee 1994 [DIRS 154380], p. 79). At hydrophilic surfaces, such as oxides, the structure of water resembles that of ice (McCafferty and Zettlemoyer 1971 [DIRS 154378], p. 239). This behavior is attributed to the existence of a monolayer in which the adsorbed water is held rigidly to the solid surface at fixed sites. The first layer is localized by double hydrogen bonding of a single water molecule to two surface hydroxyls. This highly constrained first layer relaxes in the next layers, where the water molecules start to possess a rotational degree of freedom, being singly hydrogen-bonded. The second layer becomes more ordered when hydrogen bonds to a third layer, and so on, until the ordering effect of the surface is overcome and bulk liquid layers form farther from the surface. On a hydrophobic surface, such as silica, different behavior is observed. When half of the surface hydroxyls on silica are occupied by water, the water starts to agglomerate into clusters instead of adsorbing uniformly over the surface.

Layers of water adsorbed on an oxide surface can promote lateral ion movement, which sets up localized electrochemical cells due to inhomogeneities in the underlying metal (Lee 1994 [DIRS 154380], p. 141). Such cells promote pitting corrosion. Surface water dipoles may act to shield oxygen ions from an internal field that promotes ion movement. On the other hand, the gel-like structure of a metal-(hydr)oxide may not support the charge separation that normally accounts for the field-driven process. Instead, ion movement may take place under the influence of a concentration gradient. The first layers of adsorbed water often do not contain ions from the solid (Lee 1994 [DIRS 154380], p. 73). This suggests that multiple water layers are needed in order for solid species (such as radionuclides) to dissolve and diffuse.

10.3.1.3.3 Specific Surface Areas of Component Materials

Most studies of the nature of adsorbed water at solid surfaces have been done with solid powders whose specific surface area is at least $5 \text{ m}^2/\text{g}$. Such high interfacial areas are required for sufficient sensitivity in the measurements of adsorbed mass using routine gravimetric techniques. However, the use of surface areas of 10 to $20 \text{ m}^2/\text{g}$ typical of the samples used in adsorption studies for Fe_2O_3 , NiO , and ZrO_2 should be conservative in the sense that predicted quantities of adsorbed water will be larger than might be realistically expected, resulting in an overestimation of the amount of radionuclides released by purely diffusive mechanisms.

Table 10.3.1-3 lists the specific areas of waste form component oxides. Jurinak (1964 [DIRS 154381], p. 480) measured surface area of Fe_2O_3 by nitrogen adsorption ranging from 9.60 to $9.70 \text{ m}^2/\text{g}$, whereas water adsorption surface areas ranged from 6.52 to $9.10 \text{ m}^2/\text{g}$. It was concluded that about one-third of the Fe_2O_3 is covered with chemisorbed water which, unless removed by activation (i.e., heating to at least 425°C), blocks water adsorption sites on the surface. Jurinak (1964 [DIRS 154381]) assumed a cross-sectional area of 10.8 \AA^2 for water. McCafferty and Zettlemyer (1970 [DIRS 154382], p. 453) report a single value of $10 \text{ m}^2/\text{g}$ for "nominal argon surface area" and assume a cross-sectional area of the water molecule of 10.6 \AA^2 . For comparison, Gregg and Sing (1982 [DIRS 153010], p. 188) report surface area measurements of a material identified only as "iron oxide" by mercury porosimetry and by nitrogen adsorption; these respective values are shown in Table 10.3.1-3.

For ZrO_2 , Holmes et al. (1974 [DIRS 154379], pp. 367 to 368) measured specific surface areas after outgassing at 500°C of $23.7 \text{ m}^2/\text{g}$ by nitrogen adsorption and of $23.9 \text{ m}^2/\text{g}$ by argon adsorption. Monolayer capacities for water were equivalent to specific surface areas of about 14 to $15 \text{ m}^2/\text{g}$ based on 10.6 \AA^2 per adsorbed water molecule; the average value of $14.5 \text{ m}^2/\text{g}$ is shown in Table 10.3.1-3. Nitrogen and argon adsorption data on the water-covered ZrO_2 surface gave specific surface areas of $18.6 \text{ m}^2/\text{g}$ for nitrogen and $17.8 \text{ m}^2/\text{g}$ for argon. "This difference emphasizes the specificity involved in water adsorption on oxide surfaces and the accompanying uncertainty in specific surface areas estimated from such data" (Holmes et al. 1974 [DIRS 154379], p. 368).

10.3.1.3.3.1 Interior Surface Area for Commercial Spent Nuclear Fuel Waste Package

The internal surface area of an as-emplaced waste package (i.e., in an undegraded state) containing commercial SNF can be approximated if the dimensions and numbers of fuel rods, baskets, side guides, and other support components are known. Since the surface area will increase by orders of magnitudes as the waste package components degrade, the initial surface area is useful only as a limiting value, but one that can be estimated fairly accurately (unlike the surface area of corrosion products). Typical measurements for a 21-PWR waste package are given in Table 10.3.1-4. The surface areas of fuel assembly spacer grids and end connections are ignored. The total internal surface area of a 21-PWR waste package as emplaced is approximately $1,023 \text{ m}^2$. The surface area of basket components is computed as shown in Table 10.3.1-4 (footnote a) by dividing the total mass of each component by the density of the material (which gives the volume of material), then dividing by the thickness of the component. This results in the area of component material as though it were a plate, ignoring the area of

edges. To account for both sides of the component being exposed to air and able to adsorb water, the area is multiplied by two.

The calculation shown in Table 10.3.1-4 assumes that all the fuel rods are intact. The surface area of intact fuel rods accounts for about 62 percent of the total surface area. It is estimated that an average of 2.2 fuel rods per assembly in a 21-PWR waste package have failed by the time they are emplaced (CRWMS M&O 2000 [DIRS 151659], p. 53), during reactor operation, in dry storage, or due to damage in transportation. Fuel rods that are estimated to have failed cladding may also be susceptible to cladding unzipping and fuel dissolution when the waste package fails. The interior surface of failed rods, as well as the fuel pellets themselves, may adsorb water. The inside cladding surface of these rods will increase the total surface area only slightly. SNF pellets are generally highly fractured and can contribute more significantly to the surface area available for adsorption when a waste package is first breached.

The calculation of pore volume and porosity for a commercial SNF waste package is summarized in Table 10.3.1-5. The porosity of an average 21-PWR waste package is $4.9724/7.6047 = 0.6539$. In the TSPA-SR sensitivity analyses, the impact on waste package porosity and surface area from volume changes resulting from oxide formation is ignored.

In *Total System Performance Assessment - 1995: An Evaluation of the Potential Yucca Mountain Repository* (CRWMS M&O 1995 [DIRS 100198], Section 5.6.1), the presence of cladding was conservatively ignored. The surface area of the SNF was taken to be $39.6 \text{ cm}^2/\text{g}$ (CRWMS M&O 1998 [DIRS 102839], p. 18). The total surface area of the fuel, which was all fully exposed, was computed as $96,200 \text{ cm}^2/\text{kg}$ water, with the assumption that the entire void space of the waste package was filled with J-13 well water (CRWMS M&O 1998 [DIRS 102839], p. 27). Using the pore volume of a 21-PWR waste package of 4.9724 m^3 (as calculated in Table 10.3.1-5) and a density of J-13 well water assumed to be $1,000 \text{ kg}/\text{m}^3$ (CRWMS M&O 1998 [DIRS 102839], p. 6, Assumption 3.2), the surface area of the SNF is:

$$SA_{fuel} = \left(96200 \frac{\text{cm}^2}{\text{kg water}} \right) \left(1000 \frac{\text{kg}}{\text{m}^3} \right) (4.9724 \text{ m}^3) \left(10^{-4} \frac{\text{m}^2}{\text{cm}^2} \right) = 47834.5 \text{ m}^2$$

The initial surface area of fuel baskets and other internal waste package structures remains the same as in Table 10.3.1-4. However, the calculation of SNF surface area (CRWMS M&O 1998 [DIRS 102839], pp. 18 and 27) did not include the Zircaloy cladding, so the waste package internal surface area for this calculation is $1023.201 - 636.933 + 47834.5 = 48220.8 \text{ m}^2$, or a factor of 47 larger than the surface area when all fuel rods are intact.

Another way to estimate the initial internal surface area of a waste package would be to assume that an average of 2.2 rods per assembly have failed at the time of emplacement (CRWMS M&O 2000 [DIRS 151659], p. 53), but that all other fuel rods are intact. In a 21-PWR waste package, the SNF in $2.2 \times 21 = 46.2$ fuel rods would be assumed to be fully exposed, although the cladding is still present, with the inside and outside surfaces of the 46.2 fuel rods exposed. The surface area of SNF in 46.2 rods per waste package is computed (CRWMS M&O 1998 [DIRS 102839], pp. 18 and 27) using a specific surface area of SNF of $39.6 \text{ cm}^2/\text{g}$ and a mass of

fuel in each rod of 1.98219 kg/rod (CRWMS M&O 1998 [DIRS 100733], Attachment I, Table 1):

$$SA_{fuel} = \left(1.98219 \frac{\text{kg fuel}}{\text{rod}}\right) (46.2 \text{ rod}) \left(39.6 \frac{\text{cm}^2}{\text{g}}\right) \left(10^{-4} \frac{\text{m}^2}{\text{cm}^2}\right) \left(10^3 \frac{\text{g}}{\text{kg}}\right) = 362.646 \text{ m}^2$$

It is clear that the highly fractured SNF contributes greatly to the exposed surface area inside a waste package. Including the exposed fuel surface area of the 46.2 rods per waste package with the total obtained in Table 10.3.1-5 results in 1,385.847 m². The inside surface area of the 46.2 fuel rods, where the cladding thickness is 0.0225 in. = 0.05715 cm (DOE 1992 [DIRS 102588], p. 2A-30), is:

$$SA_{cladding} = \pi(0.94996 - 0.05715 \text{ cm})(384.96 \text{ cm}) \left(10^{-4} \frac{\text{m}^2}{\text{cm}^2}\right) (46.2) = 4.988 \text{ m}^2$$

In this case, the total internal surface area of a 21-PWR waste package is initially 1023.214 + 362.646 + 4.988 = 1390.848 m². The materials making up this surface are: (1) about 26 percent SNF, composed mostly of UO₂ (about 95 mole percent [CRWMS M&O 1998 [DIRS 102839], Table 5.2.1-1, p. 23]); (2) about 46 percent ZrO₂; and (3) about 28 percent products of corrosion of various steels, mostly Fe₂O₃ and NiO.

Over time, the fraction of steel corrosion products surface area would be expected to increase greatly relative to the surface areas of SNF and ZrO₂, since the cladding is predicted to degrade and fail at an extremely slow rate. The amount of additional SNF exposed as fuel rods fail will increase at a correspondingly slow rate; however, because of the high surface area of SNF in each fuel rod, the surface area will increase in discrete amounts of about 8 m² (7.85 m² of SNF and 0.11 m² of inside cladding surface) as each fuel rod fails. This assumes that the entire contents of a fuel rod are accessible by water vapor diffusion when the fuel rod is breached.

In principle, the surface area inside a waste package can be computed as a function of time, if the degradation rates of the basket components and the stainless steel inner liner are known, and the failure rate of fuel rods. The calculation is complicated by the different compositions of each component of the waste package. Spatial variability in degradation rates due to variations in accessibility to water vapor further complicate the picture. For example, the fuel rod assemblies in 44-BWR waste packages are enclosed in flow tubes that provide added protection from corrosion over 21-PWR fuel rod assemblies. However, an average corrosion rate for a 21-PWR waste package should be an acceptably conservative approximation from which surface areas and quantities of adsorbed water can be computed.

The complete degradation of a waste package gives an estimated upper bound on the surface area available for adsorption. For this bounding estimate, the assumption is made that all corrodible material inside a 21-PWR waste package is iron that completely oxidizes to Fe₂O₃. The mass of each major component for three types of waste package is listed in Table 10.3.1-6. The amounts and composition of each waste package component are converted to total moles of material in Table 10.3.1-7.

Assume that the inner liner stainless steel fully corrodes, but that the Alloy 22 outer liner remains intact (except for breaches, the sizes of which are assumed to be negligible). Assume that the Zircaloy fuel claddings and assembly grid spacers do not degrade because the Zircaloy will remain uncorroded for tens of thousands of years after the steel has fully corroded. The surface area of SNF, even if fully exposed, is relatively small ($47,834 \text{ m}^2$, as calculated above), and, as will be seen, can be ignored in this estimate.

The masses of materials differ little between the two types of waste packages for commercial SNF (21-PWR and 44-BWR), and all other types of packages comprise a much smaller fraction of the total waste in the repository. Therefore, the calculation will be done for the 21-PWR waste package as representative of all packages in the repository.

The computational procedure is as follows. Based on the elemental composition of each material (CRWMS M&O 2000 [DIRS 151561]) shown in Table 10.3.1-7, convert the mass of each material listed in Table 10.3.1-6 to moles by element. Add up the total moles, assume all moles are iron, and determine the stoichiometrically equivalent amount of Fe_2O_3 in the waste package. Using the measured surface area of Fe_2O_3 , calculate the total surface area for adsorption from the basket materials and liners. This value provides an estimated upper bound for the surface area for adsorption in a completely degraded waste package. The atomic weights for conversion to moles (Weast 1985 [DIRS 111561]) are as follows:

- Iron 0.055847 kg/mol
- Molybdenum 0.09594 kg/mol
- Chromium 0.051996 kg/mol
- Nickel 0.05871 kg/mol
- Aluminum 0.0269815 kg/mol
- Oxygen 0.0159994 kg/mol.

The total amount of material in a 21-PWR waste package (treated as though it were iron) is 355,218 moles (see lower right-hand entry in Table 10.3.1-7). This iron will oxidize to $177,609 \text{ mol Fe}_2\text{O}_3 \times 0.1596922 \text{ kg/mol} = 28,363 \text{ kg Fe}_2\text{O}_3$. Using a specific surface area of $9.1 \text{ m}^2/\text{g}$ for the oxide (Jurinak 1964 [DIRS 154381]; see also Table 10.3.1-3), the estimated upper bound for total surface area for adsorption in a 21-PWR waste package is $(28,363 \text{ g})(9.1 \times 10^3 \text{ m}^2/\text{kg}) = 2.58 \times 10^8 \text{ m}^2/\text{package}$.

Table 10.3.1-8 summarizes the various estimates of surface area within a 21-PWR waste package.

10.3.1.3.4 Mass Balance Considerations

It is generally assumed that there is no limitation on the amount of water vapor available to adsorb onto surfaces within a waste package. However, this may be an overly conservative assumption, particularly at early times when the only breaches in a waste package are small stress corrosion cracks. Even at later times, when general corrosion patches are present, the patches are modeled as filled with corrosion products (Lee et al. 1996 [DIRS 100913], p. 5-62) that severely limit the diffusion of water vapor into the waste package. The following calculation shows that the rate of water vapor diffusion through stress corrosion cracks is

probably high enough to provide all the water that adsorbs onto internal waste package surfaces. However, there is not overwhelming excess, so the assumption of plentiful water vapor for adsorption may be conservative.

Another consideration is the rate at which water or oxygen is consumed by corrosion relative to the rate of diffusion of water vapor and oxygen into the waste package. A calculation will show that the diffusion rate is just adequate for assumed corrosion rates. Assume a diffusion distance of $\Delta x = 2$ cm (thickness of waste package outer liner). Assume that the temperature of the waste package and drift air is 50°C, the relative humidity in the drift is 90 percent, and the relative humidity is zero inside the waste package. Then the humidity is 0.082 kg water/kg dry air (Perry 1963 [DIRS 119529], Figure 15-3). Using molecular weights for water of 0.01801528 kg/mol and for air of 0.028964 kg/mol (Weast 1985 [DIRS 111561], p. F-150), the molal humidity is 4.55169 mol H₂O/34.5256 mol dry air, or 0.1165 mol H₂O/mol wet air. With an ideal gas molar density of 22,414 cm³/mol (at 0°C and 1 atmosphere) (Weast 1985 [DIRS 111561], p. F-194), the concentration of water vapor in air at 50°C and 90 percent relative humidity is:

$$C_{wv} = \frac{\left(0.1165 \frac{\text{mol H}_2\text{O}}{\text{mol air}}\right) \left(18.01528 \frac{\text{g H}_2\text{O}}{\text{mol H}_2\text{O}}\right)}{\left(22414 \frac{\text{cm}^3}{\text{mol}}\right) \left(\frac{323.15 \text{ K}}{273.15 \text{ K}}\right)} = 7.915 \times 10^{-5} \frac{\text{g H}_2\text{O}}{\text{cm}^3 \text{ air}}$$

For the binary diffusion coefficient, the following equation is used (Bird et al. 1960 [DIRS 103524], Equation 16.3-1):

$$D_{AB} = a \left(\frac{T}{\sqrt{T_{cA} T_{cB}}} \right)^b (p_{cA} p_{cB})^{1/3} (T_{cA} T_{cB})^{5/12} \left(\frac{1}{M_A} + \frac{1}{M_B} \right)^{1/2} p^{-1}$$

where

D_{AB} is the diffusion coefficient [cm²/s] for water (A) in air (B)

T is absolute temperature [K]

p is pressure [atm]

M is molecular weight [g/mol]

a and b for H₂O with a nonpolar gas are 3.640×10^{-4} and 2.334, respectively
subscript c refers to critical properties.

For water, $T_{cA} = 374.1^\circ\text{C} = 647.25\text{ K}$, $p_{cA} = 218.3\text{ atm}$ (Weast 1985 [DIRS 111561], p. F-64), and $M_A = 18.01528\text{ g/mol}$; for air, $T_{cB} = 132\text{ K}$, $p_{cB} = 36.4\text{ atm}$ (Bird et al. 1960 [DIRS 103524], p. 744), and $M_B = 28.964\text{ g/mol}$ (Weast 1985 [DIRS 111561], p. F-150). Substituting these values into the above equation:

$$D_{AB} = (3.640 \times 10^{-4}) \left(\frac{323.15}{\sqrt{(374.1)(132.)}} \right)^{2.334} [(218.3)(36.4)]^{1/3} [(374.1)(132.)]^{5/12} \cdot \left(\frac{1}{18.01528} + \frac{1}{28.964} \right)^{1/2} (1.0)^{-1} = 0.4715959\text{ cm}^2/\text{s}$$

Then the rate of diffusion of water vapor is:

$$q = D_{AB} A \frac{\Delta C}{\Delta x} = D_{AB} A \frac{C_{wv}}{\Delta x} = \left(0.472 \frac{\text{cm}^2}{\text{s}} \right) A \left(\frac{7.915 \times 10^{-5} \frac{\text{g}}{\text{cm}^3}}{2\text{ cm}} \right) = 1.87 \times 10^{-5} A\text{ (g/s)}$$

where A is the cross-sectional area [cm^2] of stress corrosion cracks through which water vapor can diffuse. The typical cross-sectional area of a stress corrosion crack is $4.08 \times 10^{-6}\text{ m}^2$ per stress corrosion crack (CRWMS M&O 2000 [DIRS 153940], p. 51), and an average of 25 stress corrosion cracks per waste package is expected (CRWMS M&O 2000 [DIRS 146427], p. 81); then $A = 1.02 \times 10^{-4}\text{ m}^2 = 1.02\text{ cm}^2$, and the rate of diffusion of water vapor is $q = 1.907 \times 10^{-5}\text{ g/s} = 33.40\text{ mol H}_2\text{O/yr}$.

When stress corrosion cracks first appear, water vapor that diffuses through will probably be consumed by corrosion of the most reactive materials within a waste package, namely the A 516 carbon steel that makes up the baskets. These steel components will have a median lifetime of 168 years (CRWMS M&O 2000 [DIRS 151561], Table 32). From Table 10.3.1-6, the total mass of A 516 steel in a 21-PWR waste package is 5,723.68 kg, or 102,489 mol Fe (see Table 10.3.1-7). The consumption rate of iron is then $102489\text{ mol}/168\text{ yr} = 610\text{ mol Fe/yr}$. Assuming a stoichiometry of 3 mol $\text{H}_2\text{O}/2\text{ mol Fe}$ (to form Fe_2O_3), corrosion of A 516 carbon steel consumes 915 mol $\text{H}_2\text{O/yr}$, which is a factor of 27 greater than the rate of diffusion of water vapor through stress corrosion cracks.

If the corrosion rate is limited by the rate of diffusion of water vapor, then the lifetime of the carbon steel components will be considerably greater than 168 years. The diffusion rate of 33.40 mol $\text{H}_2\text{O/yr}$ will allow 22.27 mol Fe/yr to corrode, thereby requiring $102,489\text{ mol Fe}/(22.27\text{ mol Fe/yr}) = 4,602\text{ years}$ for all A 516 steel components to degrade fully once stress corrosion cracks appear.

This assumes that the stress corrosion cracks remain fully open and are not plugged with corrosion products, and that water is not consumed by any other corrosion process or evaporation. If water is preferentially consumed by corrosion reactions, none will be available to adsorb onto surfaces to form a thin film through which radionuclides can diffuse. Thus, the carbon steel will act as a water getter as long as water vapor diffusion into a waste package is limited by stress corrosion cracks and precludes releases of radionuclides.

Since dry air oxidation can also proceed once stress corrosion cracks appear, the rate of oxygen diffusion through cracks should also be considered. Using the appropriate parameters for oxygen (A) diffusing in air— $T_{ca} = 154.58$ K, $p_{ca} = 5.043$ MPa = 49.77 atm (Weast 1985 [DIRS 111561], p. F-62), and $M_A = 31.9988$ g/mol—it follows that:

$$D_{AB} = (3.640 \times 10^{-4}) \left(\frac{323.15}{\sqrt{(154.58)(132.)}} \right)^{2.334} [(49.7)(36.4)]^{1/3} [(154.58)(132.)]^{5/12} \cdot \left(\frac{1}{31.9988} + \frac{1}{28.964} \right)^{1/2} (1.0)^{-1} = 0.477721 \text{ cm}^2/\text{s}.$$

Assume the oxygen concentration in air in a drift outside a waste package is the same as in the atmosphere: 20.946 volume-percent (Weast 1985 [DIRS 111561], p. F-156) or 0.20946 mol O₂/mol air. With 22414 cm³/mol, the O₂ concentration is $C_{O_2} = 9.34505 \times 10^{-6}$ mol O₂/cm³ air at 0°C, or 7.89912×10^{-6} mol O₂/cm³ at 50°C. Inside a waste package, assume the oxygen concentration is essentially zero. For 25 stress corrosion cracks with a total cross-sectional area of 1.02 cm², the rate of diffusion of oxygen is:

$$q = D_{AB} A \frac{\Delta C_{O_2}}{\Delta x} = \left(0.477721 \frac{\text{cm}^2}{\text{s}} \right) (1.02 \text{ cm}^2) \left(\frac{9.34505 \times 10^{-6} \frac{\text{mol}}{\text{cm}^3}}{2 \text{ cm}} \right) (3.1556926 \times 10^7 \text{ s/yr}) = (2.2768 \times 10^{-6} \text{ mol/s}) (3.1556926 \times 10^7 \text{ s/yr}) = 71.849 \text{ mol O}_2/\text{yr}$$

With corrosion stoichiometry of 3 moles of O₂/4 mol Fe to produce Fe₂O₃, the rate of corrosion allowed by diffusion of oxygen through stress corrosion cracks is (71.849)(4/3) = 95.8 mol Fe/yr. Again, the corrosion rate is limited by diffusion through stress corrosion cracks and the lifetime of A 516 carbon steel components in the waste package will be 102489/95.8 = 1,070 yr.

If both water vapor and oxygen can diffuse simultaneously through the stress corrosion cracks without hindering each other, then the total diffusion-limited corrosion rate would be the sum of the diffusion rates of water vapor and oxygen, 95.8 + 33.4 = 129.2 mol Fe/yr. At this rate, the

A 516 carbon steel in a 21-PWR waste package would consume H₂O and O₂ as fast as they diffuse into a waste package for 102,489/129.2 = 793 years after stress corrosion cracks appear. On the other hand, if corrosion of the Stainless Steel Type 316NG inner liner is also accounted for, then consumption of water by corrosion could preclude adsorption of water and diffusion of radionuclides for a much longer period of time.

In view of the assumptions and uncertainties in corrosion rates and stress corrosion crack behavior in this simple model of gas diffusion and corrosion of steel waste package components, it can only be stated that the rates of diffusion of oxygen and water vapor into a waste package are comparable to their rate of consumption by corrosion of A 516 steel. Calculations show that corrosion of A 516 steel may consume all water vapor that diffuses into a waste package for several thousands of years following a breach by stress corrosion cracks. In this situation, the assumption that sufficient water vapor is available for thin water films to adsorb onto all surfaces inside a waste package is fairly conservative. Even in a humid drift environment, the assumption that radionuclides can diffuse out of a waste package via the hypothetical water films is conservative, since the water film may not exist as long as stress corrosion cracks are the only breaches in a waste package. Of course, once general corrosion patches penetrate both the inner and outer layers of the waste package, diffusion of H₂O or O₂ through the openings will no longer limit corrosion rates or adsorption of water. But the first patches often appear much later than the first stress corrosion cracks in the current corrosion models, so the capability of corrosion to limit formation of a diffusive pathway is important.

These calculations suggest that a more accurate mass balance for water and oxygen inside a waste package could greatly reduce predicted releases of radionuclides to the invert, and thus to the accessible environment. Releases could be delayed for several thousand years compared with current estimates as the corrosion of fuel baskets and inner liner components scavenges water and oxygen that diffuse through small stress corrosion cracks. Formation of a diffusive pathway may then be delayed until corrosion of iron-based materials is largely completed. This possibility has not been included in the TSPA-SR sensitivity analyses.

10.3.1.3.5 Cross-Sectional Areas and Effective Diffusivity

10.3.1.3.5.1 Cross-Sectional Area for the Waste Package

The rate of diffusion of radionuclides, q [kg/s], from a waste package to the exterior is given by:

$$q = D_s A \frac{\partial C}{\partial x}$$

where

- D_s = the effective diffusion coefficient [m²/s]
- A = the cross-sectional area of the diffusive pathway [m²]
- C = the concentration of the radionuclide [kg/m³]
- x = the length of the path [m].

The amount of water vapor that adsorbs on a surface has been determined. This provides the thickness of the water film. To calculate the cross-sectional area of the pathway, the width of the water film is also needed. Because of the difficulty in characterizing the waste, not only initially but especially as it degrades, this width (and consequently, the cross-sectional area) is very difficult to calculate. The length of the diffusive path is also highly variable because the radionuclide sources may develop at random locations within a waste package and the path length will depend on the geometry of the film connecting the source to a breach. Finally, the effective diffusion coefficient itself depends on the complex interactions of source term composition, water chemistry, porosity, water saturation, and tortuosity, none of which can be characterized in a deterministic fashion. Thus, each term in the above equation— D_s , A , and Δx —needs to be sampled, and a reasonable range and distribution for each has to be determined. All three terms are interrelated through the geometry assumed for the waste package interior, and all are effectively a function of relative humidity and time.

In the simplest model, a single fuel rod has failed in one location, a point source, and an adsorbed water film covers the fuel rod and provides direct connection to a breach. In this case, the cross-sectional area for diffusion is that of the film uniformly covering the cylindrical fuel rod. The thickness of the film is obtained from the adsorption isotherm of water vapor adsorbed on ZrO_2 at the known relative humidity. Thus,

$$A = \frac{\pi}{4} \left[(D_0 + t_f)^2 - D_0^2 \right]$$

$$= \frac{\pi t_f}{4} (2D_0 + t_f),$$

where D_0 is the diameter of the fuel rod [m] and t_f is the adsorbed water film thickness [m]. A reasonable value for the diffusion coefficient would be the bulk water coefficient, as given in the *EBS Radionuclide Transport Abstraction* (CRWMS M&O 2000 [DIRS 153940], pp. 58 to 60). In this simple case, the minimum path length, Δx , would be the shortest distance along a solid surface from a fuel rod to the exterior of a waste package. This minimum length is 7 cm, which is the combined thickness of the two waste package liners. In this instance, the fuel rod would have to have intimate contact with the waste package inner liner at an insignificant distance from the source for the value of A to remain consistent. The maximum value for Δx would be the length of a fuel rod plus the maximum distance from a fuel rod to the exterior (approximately the diameter of a waste package), for a total of 3.85 m + 1.56 m = 5.41 m (using a waste package outer diameter of 1.56 m [CRWMS M&O 2000 [DIRS 144128]], Attachment I, Sketch SK-0175). A uniform distribution is reasonable for Δx in this case.

At a relative humidity of 95 percent (used as an example throughout this section), the adsorbed water film on ZrO_2 is 56 monolayers thick, as shown in Figure 10.3.1-4, based on data from Holmes et al. (1974 [DIRS 154379], Figure 3). From Equation 10-3, the thickness of a water monolayer is $t_f = 2.83 \times 10^{-10}$ m, so the cross-sectional area on a 0.94996-cm diameter fuel rod is:

$$\begin{aligned} A &= \pi(2.83 \times 10^{-10} \text{ m}) \left[2(0.94996 \times 10^{-2} \text{ m}) + 2.83 \times 10^{-10} \text{ m} \right] / 4 \\ &= 4.22 \times 10^{-12} \text{ m}^2 \\ &= 4.22 \times 10^{-6} \text{ mm}^2 \end{aligned}$$

This is a very small area through which radionuclides will diffuse, and releases from a single failed rod should be insignificantly small. However, if the average 2.2 rods per assembly, or 46.2 rods per waste package, have failed initially, then the total cross-sectional area of adsorbed water films on fuel rods for a waste package is $1.95 \times 10^{-4} \text{ mm}^2$, which is still very small but not insignificant.

Another approach to determining the cross-sectional area is to ignore the dispersion of water over all surfaces within a waste package. Assume that all the water adsorbed on surfaces is collected into a tube, connecting the source to the exterior surface. As shown in Table 10.3.1-4, the total initial surface area in a waste package is $1,023.2 \text{ m}^2$, neglecting any exposed SNF in failed fuel rods. Most of the surfaces are oxidized steel, so it is appropriate to use the Fe_2O_3 adsorption isotherm. From Figure 10.3.1-2 or Equation 10-2, at an example 95 percent relative humidity, the amount of water adsorbed is 4.91 monolayers. Using a monolayer thickness of 2.83×10^{-10} m, the water film is 1.39×10^{-9} m thick. The total volume of adsorbed water is then $(1023.2 \text{ m}^2)(1.39 \times 10^{-9} \text{ m}) = 1.42 \times 10^{-6} \text{ m}^3$. If the length of the diffusion pathway is the total inside length of a waste package (4.775 m), then the cross-sectional area for diffusion is $(1.42 \times 10^{-6} \text{ m}^3)/(4.775 \text{ m}) = 2.97 \times 10^{-7} \text{ m}^2 = 0.30 \text{ mm}^2$, equivalent to a square about 0.5 mm on a side. This is a relatively large area for diffusion, considering that diffusion will take place for thousands of years. Since porosity, saturation, and tortuosity have been neglected, this is an extremely conservative estimate for cross-sectional area.

To carry this estimate further, consider the initial surface area when (1) an average of 46.2 fuel rods per waste package have failed initially, and (2) cladding is neglected. The surface area for adsorption is $1,390.835 \text{ m}^2$ and $48,220.8 \text{ m}^2$, respectively, for these two cases. For a diffusive path the length of the inside of a waste package, the cross-sectional areas are $4.05 \times 10^{-7} \text{ m}^2 = 0.405 \text{ mm}^2 = (0.636 \text{ mm})^2$ and $1.40 \times 10^{-5} \text{ m}^2 = 14.0 \text{ mm}^2 = (3.75 \text{ mm})^2$, respectively. Again, these are relatively large diffusive areas, considering the time over which diffusion will occur. These are also extremely conservative estimates.

At the other extreme in time and waste package condition, consider the cross-sectional area available when the interior of a waste package is fully degraded, at least to the extent that all iron-containing basket and inner liner components have completely corroded. The Alloy 22 outer layer should still be largely intact at this point; a number of general corrosion patches will have penetrated the waste package, but it will still provide some overall structural support. By this time, a large number of fuel rods will have failed by pitting or unzipping, but the Zircaloy

spacer grids will provide enough support to hold assemblies together and support assemblies collapsed on top of them. Interspersed throughout the assemblies are porous corrosion products. In this scenario, the source is dispersed throughout the waste package interior. Diffusion will occur through the porous medium in which all surfaces are coated with the thin film of adsorbed water.

The cross-sectional area can be conservatively estimated for this degraded state. The fully degraded surface area is derived in Section 10.3.1.3.3.1 and summarized in Table 10.3.1-8 to be $2.58 \times 10^8 \text{ m}^2$. At an example 95 percent relative humidity, the film thickness is $1.39 \times 10^{-9} \text{ m}$, so the diffusion area over a path the length of a waste package is $0.075 \text{ m}^2 = (0.27 \text{ m})^2$. Although this estimate is exceedingly conservative, the magnitude is clearly large enough to conclude that there will be essentially no resistance to diffusion inside a fully degraded waste package.

A more realistic estimate must take into account the saturation and porosity of the corrosion products. For homogeneous porous media such as soils, the diffusion coefficient is modified by a tortuosity factor to account for the increased path length and decreased cross-sectional area of the diffusing solute in an unsaturated porous medium. In the absence of an advective flux and negligible vapor phase transport, one-dimensional transient diffusion is given by:

$$\frac{\partial C}{\partial t} = D_s \frac{\partial^2 C}{\partial x^2}$$

where the diffusion coefficient D_s [m^2/s] is defined as (CRWMS M&O 2000 [DIRS 150793], p. 29):

$$D_s = \frac{D_e}{\theta} = \frac{D_e}{\phi S_e}$$

Here, D_e [m^2/s] is the effective dispersion-diffusion coefficient, θ is the volumetric moisture content, ϕ is the porosity, and S_e is the effective water saturation. With no advective flux, D_e is equal to the solute diffusion coefficient, D_{sl} , which in turn is a function of the binary diffusion coefficient in water, D_{wl} , and of the liquid tortuosity factor, $\xi(\theta)$:

$$D_e = D_{sl} = \xi(\theta) D_{wl}$$

Various correlations have been proposed for $\xi(\theta)$; the *EBS Radionuclide Transport Model* (CRWMS M&O 2000 [DIRS 150793], pp. 30 to 31) compares a Modified Millington Quirk correlation with Archie's Law (CRWMS M&O 2000 [DIRS 153940], p. 60) for application to diffusion in the invert, which is composed of a granular material. These correlations are:

$$\begin{aligned} \xi(\theta) &= \theta^{10/3} \phi^{-2} && \text{Modified Millington Quirk} \\ \xi(\theta) &= \theta^2 \phi^{-0.7} && \text{Archie's Law} \end{aligned}$$

Thus, the diffusion coefficient using each of these correlations would be:

$$\left. \begin{aligned}
 D_s &= \frac{D_e}{\theta} = \frac{\xi(\theta)D_{wl}}{\theta} \\
 &= \theta^{7/3} \phi^{-2} D_{wl} \\
 &= \theta^{10/3} \phi^{-3} S_e^{-1} D_{wl} \\
 &= \phi^{1/3} S_e^{7/3} D_{wl}
 \end{aligned} \right\} \text{Modified Millington Quirk}$$

$$\left. \begin{aligned}
 D_s &= \frac{D_e}{\theta} = \frac{\xi(\theta)D_{wl}}{\theta} \\
 &= \theta^2 \phi^{-0.7} D_{wl} \\
 &= \theta^3 \phi^{-1.7} S_e^{-1} D_{wl} \\
 &= \phi^{1.3} S_e^2 D_{wl}
 \end{aligned} \right\} \text{Archie's Law}$$

The exponents in Archie's law are typical values, and will vary for different materials (Bear 1988 [DIRS 101379], p. 116). The typical values (1.3 and 2) are used throughout this section to estimate in-package diffusion coefficients.

Conca and Wright (1992 [DIRS 100436]) performed measurements for the diffusion coefficient of unsaturated soil, gravel, bentonite, rock, and crushed tuff from Yucca Mountain over a broad range of water contents (DTN: MO9810SPA00026.000 [DIRS 137076]). These data have been used to analyze the dependence of diffusion coefficient on volumetric moisture content, θ , for a variety of granular materials, as explained in Section 10.3.3.3.1. The resulting equation for diffusivity as a function of porosity and saturation (Equation 10-14), with the notation changed to that of this section, is:

$$D_s = \phi^{1.849} S_e^{1.849} D_{wl} \quad (\text{Eq. 10-4})$$

Equation 10-4 is consistent with Archie's law, except that the exponents are based on a statistical fit to experimental data for a variety of granular materials.

Either the Modified Millington Quirk or Archie's Law might be appropriate in the later stages of waste package degradation, since the package would be nearly filled with porous corrosion products. Equation 10-4 has been selected for the TSPA sensitivity calculations because it is based on measured data for granular materials and is consistent with the calculation of the diffusion coefficient for the invert, as discussed in Section 10.3.3.3.1. No experimental data exist for the degraded waste package materials, so it cannot be determined which of these (or some other correlation) is correct.

The self-diffusion coefficient for water is used as a bounding value for the binary diffusion coefficient in water, D_{wl} , as discussed in Section 10.3.3 (CRWMS M&O 2000 [DIRS 153940], p. 58).

The effective water saturation, S_e , is obtained from adsorption isotherms as a function of relative humidity. Assume that the corrosion products are Fe_2O_3 . The water saturation is given by:

$$S_e = \frac{V_w \left(\frac{s_{WP}}{s_{N_2}} \right)}{V_{WP}}$$

where

V_w is the volume of water adsorbed [$\text{m}^3 \text{H}_2\text{O}/\text{g Fe}_2\text{O}_3$]

V_{WP} is the pore volume of a waste package [m^3 pore volume]

s_{WP} is the surface area of a waste package [m^2]

s_{N_2} is the surface area of the porous degraded waste form [$\text{m}^2/\text{g Fe}_2\text{O}_3$], typically obtained by BET nitrogen adsorption measurements.

Since V_w is normalized to the surface area of Fe_2O_3 , it must be multiplied by (s_{WP}/s_{N_2}) to obtain the volume of water in an entire waste package. V_w/s_{N_2} is the volume of water adsorbed per unit surface area, which is multiplied by the total surface area of the waste package to get the volume of water adsorbed in the entire waste package; it is divided by the pore volume of the waste package to obtain the saturation. V_w/s_{N_2} is obtained from an FHH multilayer adsorption isotherm model (Jurinak 1964 [DIRS 154381], p. 486), shown in Section 10.3.1.3.2.1, that gives the fractional surface coverage, or number of monolayers θ_a covering a surface:

$$\theta_a = \frac{V_w}{V_m} = \frac{m_w}{m_m} = \left(\frac{-1.1}{\log_{10} RH} \right)^{\frac{1}{2.45}}$$

where

V_m is the volume of adsorbed water vapor that provides a one monolayer coverage on the surface [m^3]

m_w is the mass adsorbed per unit mass of adsorbent [$\text{kg H}_2\text{O}/\text{kg Fe}_2\text{O}_3$]

m_m is the mass of one monolayer of adsorbate per unit mass of adsorbent [$\text{kg H}_2\text{O}/\text{kg Fe}_2\text{O}_3$].

The mass of a monolayer is obtained from the cross-sectional area of a water molecule, $A_w = 10.6 \text{ \AA}^2 = 10.6 \times 10^{-20} \text{ m}^2/\text{molecule}$ (see discussion preceding Equation 10-3 in Section 10.3.1.3.2.1). An upper bound for the specific surface area of Fe_2O_3 , s_{N_2} , is $9.1 \text{ m}^2/\text{g}$ (Jurinak 1964 [DIRS 154381], Table I; see also Table 10.3.1-3), as deduced from BET N_2 adsorption measurements. The molecular weight of water is $M_w = 18.01528 \times 10^{-3} \text{ kg H}_2\text{O}/\text{mol}$.

Avogadro's number is $N_A = 6.0221367 \times 10^{23}$ molecule/mol; then the specific mass of a monolayer coverage on Fe_2O_3 is:

$$\begin{aligned}
 m_m &= \frac{s_{N_2} M_w}{A_w N_A} \\
 &= \frac{\left(9.1 \frac{\text{m}^2}{\text{g Fe}_2\text{O}_3} \right) \left(18.01528 \times 10^{-3} \frac{\text{kg H}_2\text{O}}{\text{mol}} \right)}{\left(10.6 \times 10^{-20} \frac{\text{m}^2}{\text{molecule}} \right) \left(6.0221367 \times 10^{23} \frac{\text{molecule}}{\text{mol}} \right)} \\
 &= 2.56818 \times 10^{-6} \frac{\text{kg H}_2\text{O}}{\text{g Fe}_2\text{O}_3} \\
 &\approx 2.57 \frac{\text{mg H}_2\text{O}}{\text{g Fe}_2\text{O}_3}
 \end{aligned}$$

Assume that bulk liquid properties apply to the adsorbed water, in particular that the density of adsorbed water is equal to that of liquid water. Then

$$m_w = \rho_w V_w$$

and

$$m_m = \rho_w V_m$$

Combining these expressions with the definition of θ_a ,

$$\begin{aligned}
 m_w &= m_m \theta_a \\
 &= \frac{s_{N_2} M_w}{A_w N_A} \theta_a \\
 &= \rho_w V_w
 \end{aligned}$$

Then the quantity (V_w / s_{N_2}) needed for the saturation is:

$$\begin{aligned}
 \frac{V_w}{s_{N_2}} &= \frac{M_w}{\rho_w A_w N_A} \theta_a \\
 &= \frac{M_w}{\rho_w A_w N_A} \left(\frac{-1.1}{\log_{10} RH} \right)^{\frac{1}{2.45}}
 \end{aligned}$$

Inserting this expression into S_e gives the effective water saturation of the entire waste package:

$$S_e = \frac{V_w s_{WP}}{s_{N_2} V_{WP}} \quad (\text{Eq. 10-5})$$

$$= \frac{s_{WP}}{V_{WP}} \frac{M_w}{\rho_w A_w N_A} \left(\frac{-1.1}{\log_{10} RH} \right)^{\frac{1}{2.45}}$$

The parameters used in this expression include the surface area and void volume of the waste package. As summarized in Table 10.3.1-8, estimates of the surface area can vary over five orders of magnitude. The initial void volume, as shown in Table 10.3.1-5, is 4.9724 m³. This volume will decrease somewhat as corrosion products form, since the oxides occupy greater volume than the metals from which they are formed. However, the change depends on time and extent of corrosion, so for simplicity the initial void volume will be used. To give some idea of the effect of water saturation on surface area, some values of saturation are listed in Table 10.3.1-9 for various relative humidity values. The value used for the density of water is 988.0363 kg/m³ at 50°C. The surface areas used are those summarized in Table 10.3.1-8 for different degradation states of the waste package. It is clear that the saturation can change enormously between the initial condition when the surface area is on the order of 1,000 m² to the time when the steel components are fully degraded.

Inserting S_e into the expression for the diffusion coefficient, and using water density at 50°C and the initial waste package porosity of 0.6539 (Section 10.3.1.3.3.1),

$$D_s = \phi^{1.3} S_e^2 D_{wl}$$

$$= \phi^{1.3} \left(\frac{s_{WP}}{V_{WP}} \frac{M_w}{\rho_w A_w N_A} \right)^2 \theta_a^2 D_{wl}$$

$$= (0.6539)^{1.3} \left[\frac{s_{WP} \left(18.01528 \times 10^{-3} \frac{\text{kg H}_2\text{O}}{\text{mol}} \right)}{\left(4.9724 \text{ m}^3 \right) \left(988.0363 \frac{\text{kg H}_2\text{O}}{\text{m}^3} \right) \left(10.6 \times 10^{-20} \frac{\text{m}^2}{\text{molec.}} \right) \left(6.0221367 \times 10^{23} \frac{\text{molec.}}{\text{mol}} \right)} \right]^2 \theta_a^2 D_{wl}$$

$$D_s = 1.89957263654 \times 10^{-21} s_{WP}^2 \left(\frac{-1.1}{\log_{10} RH} \right)^{\frac{2}{2.45}} D_{wl}$$

$$= 2.05326900807 \times 10^{-21} s_{WP}^2 (-\log_{10} RH)^{-0.816326530612} D_{wl}$$

For consistency with other uses of adsorption models, use natural logarithms instead of base 10 logs, using the relation

$$-\log_{10} RH = -\log_{10} (e^{\ln RH}) = -\ln RH \log_{10} e$$

Then the final expression for the diffusion coefficient is:

$$D_s = 4.05631924941 \times 10^{-21} s_{WP}^2 (-\ln RH)^{-0.816326530612} D_{wf} \quad (\text{Eq. 10-6})$$

Table 10.3.1-10 lists some values for D/D_{wf} for surface areas from Table 10.3.1-8 over a range of relative humidity values, showing the range of factors that impact the diffusion coefficient.

The difficulty in specifying the diffusion coefficient lies in determining at what point a correlation such as Archie's Law is valid and what type of correlation would be more appropriate at an intermediate degraded state. The approach used here is to compute diffusive fluxes using both a correlation for diffusion through porous media and a calculation for diffusion along failed fuel rods, then compare the results to determine which calculation is more appropriate or conservative.

If radionuclide sources (i.e., failed fuel rods) are distributed more or less uniformly throughout a waste package, then the source can be thought of as residing at the inside surface of the waste package, particularly if the inside of the package is largely degraded. In this case, the diffusive path is very short: the distance through the breach in the corrosion-resistant outer layer. The cross-sectional area for diffusion is the area of the water film covering the material that fills the corrosion patch. If the corrosion patch is mostly empty space, then diffusion must occur through a much smaller area around the perimeter of the breach. This situation will occur if the corroded Alloy 22 falls away, leaving a gaping hole where the breach occurs. In any event, the size of the breach, rather than the diffusive path area inside the waste package, will be the limiting factor for diffusion out of a waste package.

10.3.1.3.5.2 Diffusion Through General Corrosion Patches

Lee et al. (1996 [DIRS 100913]) developed a model for steady-state and "quasi-transient" diffusive releases from waste packages into the invert. In this model, perforations in the package are assumed to be cylindrical in shape. The diffusion path consists of the approach to the opening of the perforation from the waste form side; the path through the cylindrical portion of the perforation, which is filled with corrosion products; and the path through the exit disk separating the perforation from the invert. The waste is assumed to be distributed uniformly inside the waste container. The package is approximated by an equivalent spherical configuration, and the underlying invert is represented by a spherical shell surrounding the package.

The model of Lee et al. (1996 [DIRS 100913]) is suitable for the late stages of package degradation, when the waste form has become a mass of porous corrosion products. Although Lee et al. (1996 [DIRS 100913]) assumed the packages failed by pitting corrosion, which is no longer expected to occur (CRWMS M&O 2000 [DIRS 147648], p. 27), this model should be equally applicable to failure by patches from general corrosion.

The assumption of Lee et al. (1996 [DIRS 100913]) that the waste (i.e., the radionuclide source) is uniformly distributed inside the waste package restricts the applicability of the model to late times. The object of the present in-package diffusion model is to provide more realism at earlier and intermediate times, when the waste cannot yet be considered a uniform porous medium. On

the other hand, as discussed above, the fundamental assumption that diffusive releases are controlled by diffusion through breaches that are filled with porous corrosion products may be valid over much of the waste package lifetime, including early times, when stress corrosion cracks are the first breaches to appear. Lee et al. (1996 [DIRS 100913], p. 5-67) assume that the porosity of the perforations is $\phi_{cp} = 0.4$ and the percent volumetric water content is $\Phi = 10$ percent (i.e., $\Phi = 10$), so the water saturation in the perforations is a constant $S = \Phi / (100\phi_{cp}) = 0.25$. They compute a diffusion coefficient, D [cm^2/s] (Lee et al. 1996 [DIRS 100913], p. 5-67), for the porous corrosion products filling the perforations based on data from Conca and Wright (1990 [DIRS 101582]; 1992 [DIRS 100436]):

$$\log_{10} D = -8.255(\pm 0.0499) + 1.898(\pm 0.0464) \log_{10} \Phi \quad (\text{Eq. 10-7})$$

where the numbers in parentheses are one standard deviation. For $\Phi = 10$ percent, $D = 4.4 \times 10^{-7} \text{ cm}^2/\text{s}$ for comparison, they assume that the diffusion coefficient inside the waste package is $10^{-5} \text{ cm}^2/\text{s}$ (Lee et al. 1996 [DIRS 100913], p. 5-67). As a further comparison, the self-diffusion coefficient for water is $2.299 \times 10^{-5} \text{ cm}^2/\text{s}$ (CRWMS M&O 2000 [DIRS 153940], p. 58), and for many actinides the diffusion coefficient in water is roughly $5 \times 10^{-6} \text{ cm}^2/\text{s}$ (CRWMS M&O 2000 [DIRS 153940], Table 7). The value for D given by Equation 10-7 accounts for porosity and saturation, and so is comparable to the value for D_s given by Equation 10-6. If the self-diffusion coefficient for water is used for D_{wt} , then Equation 10-7 gives $D/D_{wt} = 1.91 \times 10^{-2}$. This is greater than the largest value in Table 10.3.1-10, indicating that the Lee et al. (1996 [DIRS 100913]) model for D represents very high relative humidity and very high surface area if adsorption is the sole mechanism for water appearing in the corrosion products. If no advection takes place, the assumption of a saturation of 0.25 is excessive. Using the lower saturations obtained from adsorption isotherms brings the diffusion coefficient from Equation 10-7 into closer agreement with the values in Table 10.3.1-10. For example, if $S = 10^{-5}$, then Equation 10-7 would give $D/D_{wt} = 9 \times 10^{-11}$. A more detailed calculation can be done to estimate the surface area of corrosion patches, the amount of water adsorbed at various relative humidity values, the resulting water saturation of the patches, and obtain a diffusion coefficient using Equation 10-6 or Equation 10-7.

10.3.1.3.5.3 Cross-Sectional Areas of General Corrosion Patches

The nominal area of a general corrosion patch is fixed in the current waste package degradation model (i.e., WAPDEG V4.0) at $2.346 \times 10^4 \text{ mm}^2$, based on the equivalent area of 1,000 nodes on the surface of the package (CRWMS M&O 2000 [DIRS 153940], p. 37). If the patch exists through the Alloy 22 layer, which is 2 cm thick, the volume of the patch is $4.692 \times 10^{-4} \text{ m}^3$. If the porosity, ϕ_{cp} , is 0.4, as used by Lee et al. (1996 [DIRS 100913]), the solids volume is $2.8152 \times 10^{-4} \text{ m}^3$. Using a density for Fe_2O_3 of $\rho_{\text{Fe}_2\text{O}_3} = 5,240 \text{ kg/m}^3$ (Weast 1985 [DIRS 111561], p. B-104), the mass of corrosion products filling the corrosion patch is 1.475 kg. The surface area of Fe_2O_3 in the patch, with a specific surface area of $\bar{s}_{\text{Fe}_2\text{O}_3} = 9.1 \times 10^3 \text{ m}^2/\text{kg}$, is $1.342 \times 10^4 \text{ m}^2$. The water saturation within the corrosion patch, $S_{e,cp}$, can be obtained as a function of RH using Equation 10-5, where V_{wp} and s_{wp} are replaced by V_{cp} , the total volume of

the corrosion patch (not the pore volume), and s_{cp} , the surface area of the patch (instead of the entire package). Since the surface area of corrosion products is:

$$\begin{aligned} s_{cp} &= m_{cp} \bar{s}_{Fe_2O_3} \\ &= \rho_{Fe_2O_3} V_{cp} (1 - \phi_{cp}) \bar{s}_{Fe_2O_3} \end{aligned}$$

where m_{cp} is the mass of corrosion products [kg], the ratio of surface area to volume of the corrosion patch can be expressed as:

$$\frac{s_{cp}}{V_{cp}} = \rho_{Fe_2O_3} \bar{s}_{Fe_2O_3} (1 - \phi_{cp}),$$

and the effective saturation of the patch is given by:

$$\begin{aligned} S_{e,cp} &= \frac{s_{cp}}{V_{cp}} \frac{M_w}{\rho_w A_w N_A} \left(\frac{-1.1}{\log_{10} RH} \right)^{2.45} \\ &= \frac{\rho_{Fe_2O_3} \bar{s}_{Fe_2O_3} (1 - \phi_{cp}) M_w}{\rho_w A_w N_A} \theta_a \\ &= 1.19419 \times 10^{-2} (-\ln RH)^{-1/2.45} \end{aligned} \quad (\text{Eq. 10-8})$$

The equivalent of Equation 10-6, which gives the effective diffusion coefficient based on Archie's Law, can similarly be obtained for the patch:

$$\begin{aligned} D_s &= \phi_{cp}^{1.3} S_{e,cp}^2 D_{wl} \\ &= (0.4)^{1.3} \left[1.19419 \times 10^{-2} (-\ln RH)^{-1/2.45} \right]^2 D_{wl} \\ &= 4.33337 \times 10^{-5} (-\ln RH)^{-0.816326530612} D_{wl} \end{aligned} \quad (\text{Eq. 10-9})$$

Alternatively, the diffusion coefficient can be obtained using Equation 10-7, in which

$$\Phi = 100 S_{e,cp} \phi_{cp} = 0.477676 (-\ln RH)^{-0.40816}$$

then

$$\begin{aligned} \log_{10} D &= -8.255 + 1.898 \log_{10} \Phi \\ &= -8.255 + 1.898 [-0.320866 - 0.40816 \log_{10} (-\ln RH)] \\ &= -8.864 - 0.775 \log_{10} (-\ln RH) \end{aligned} \quad (\text{Eq. 10-10})$$

For example, at RH = 95 percent, and using $D_{wl} = 2.299 \times 10^{-9} \text{ m}^2/\text{s}$, self-diffusion coefficient for water (CRWMS M&O 2000 [DIRS 153940], p. 10), the effective diffusion coefficient for the patch using Archie's Law (Equation 10-9) is $D_s = 1.13 \times 10^{-12} \text{ m}^2/\text{s}$, and using Equation 10-10,

$D = 1.37 \times 10^{-8} \text{ m}^2/\text{s}$. For comparison with earlier estimates, such as Table 10.3.1-10 or Section 10.3.1.3.5.2, $D_s / D_w = 4.90 \times 10^{-4}$ and 5.95 for these respective cases.

10.3.1.3.5.4 Cross-Sectional Areas of Stress Corrosion Cracks

When stress corrosion cracks first appear and are the only breaches in the package, the steel components will be largely intact and the surface area and cross-sectional areas of internal components will control diffusive releases. The total area of stress corrosion crack openings (assuming a mean of 25 stress corrosion cracks per waste package) is 1.02 cm^2 , as shown above. Since even the very conservative estimate of initial cross-sectional area for diffusion within a package is $2.97 \times 10^{-7} \text{ m}^2 = 2.97 \times 10^{-3} \text{ cm}^2$, it is the adsorbed water film inside the package that controls diffusive releases. This viewpoint is appropriate when corrosion products fill the stress corrosion cracks, as they eventually will, and radionuclides diffuse through these products.

If the stress corrosion crack is not filled with corrosion products, diffusion can still occur through an adsorbed water film on the sides of the stress corrosion cracks. In this case, the cross-sectional area through the stress corrosion cracks is computed from the perimeter of the stress corrosion crack and the film thickness. The *EBS Radionuclide Transport Abstraction* (CRWMS M&O 2000 [DIRS 153940], p. 51) gives a maximum crack length of 4 cm. Although a stress corrosion crack is theoretically ellipsoidal in shape, it is so narrow that the perimeter is approximately twice the length, or 8 cm. With 25 stress corrosion cracks/package, the total width of the diffusive path is 200 cm. The water film thickness, assuming adsorption on Fe_2O_3 at RH = 95 percent, as an example, is $1.39 \times 10^{-9} \text{ m}$ (4.91 monolayers of thickness $t_f = 2.83 \times 10^{-10} \text{ m}$), so the cross-sectional area for diffusion on the sides of stress corrosion cracks is $2.78 \times 10^{-5} \text{ cm}^2$, or a factor of 100 less than the high estimate for cross-sectional area inside the waste package. While it is not unreasonable for the actual diffusive area inside the waste package to be at least two orders of magnitude less than the conservative estimate, the area for diffusion along the walls of the stress corrosion cracks is at least as small as the diffusive area in the interior of the waste package, and may in fact be the controlling dimension. If the stress corrosion cracks are filled with corrosion products, then the area inside the waste package is more likely to be controlling, as discussed in the preceding paragraph.

Expressions for the effective saturation and diffusion coefficient based on Archie's Law in a stress corrosion crack are identical to those obtained above for general corrosion patches, as long as the same porous material properties are assumed. In Equation 10-8 (effective saturation), the ratio of the surface area to the volume of patches, s_{cp} / V_{cp} , is independent of the dimensions of the penetration, since $s_{cp} / V_{cp} = \bar{s}_{\text{Fe}_2\text{O}_3} \rho_{\text{Fe}_2\text{O}_3} (1 - \phi_{cp})$, where $\bar{s}_{\text{Fe}_2\text{O}_3}$ is the specific surface area of Fe_2O_3 [m^2/kg], whose density is $\rho_{\text{Fe}_2\text{O}_3}$ [kg/m^3], and porosity is ϕ_{cp} . Hence, the effective saturation and diffusion coefficient will be identical if the same porous material properties are valid.

10.3.1.3.6 Diffusive Path Length

For stress corrosion cracks, the diffusion path length may be as long as the waste package or longer, depending on the tortuosity. It may also be only a few centimeters, the shortest distance

from a fuel rod through a stress corrosion crack to the exterior of a waste package. The distance for corrosion patches will generally be shorter, since by then the waste package should be filled with porous corrosion products through which a more direct path will exist from failed fuel rods to the exterior. This is the key assumption of the Lee et al. (1996 [DIRS 100913]) model: that the interior of a waste package is a uniformly mixed source and the invert is contiguous to the exterior of the waste package.

When a package is first breached and the interior components have not yet degraded (except for the few initially failed fuel rods), a range of path lengths can be estimated with some certainty. As the steel components inside a package corrode, the diffusion path will likely become more tortuous on a microscopic scale, but more direct on a larger scale. The uncertainty in related parameters—porosity, saturation, cross-sectional area—will be so great that range and uncertainty in path length become relatively unimportant.

10.3.1.3.7 Comparison of Diffusive Release Estimates

In Table 10.3.1-11, the cross-sectional diffusion areas are summarized for the conditions described above. In addition, the quantity $D_s A / \Delta x = q / \Delta C$ is computed to provide a consistent comparison among the different states and conditions for a waste package. Based on these results, the highest releases are predicted to occur when all the adsorbed water is consolidated into a single bulk water pathway in a package with fully degraded internal components. However, this result is based on the most extreme degradation state and on the most conservative approach to calculating diffusive releases from a waste package. More realistic estimates for this quantity range from 10^{-15} to 10^{-11} m³/s.

10.3.1.3.8 Implementation of In-Package Diffusion Model

This section summarizes the general approach, major assumptions, main steps in the computational algorithm, and the stochastic parameters for the in-package diffusion model for TSPA-SR sensitivity studies. The mathematical equations for the in-package diffusion model are described in Section 10.4.1.

10.3.1.3.8.1 General Approach

The general approach for the 21-PWR and 44-BWR waste packages is to consider three limiting pathways for diffusion: (1) along failed fuel rods; (2) through porous corrosion products inside the waste package; and (3) through porous corrosion products filling breaches (either stress corrosion cracks or general corrosion patches) in the outer layer of the waste package. Starting from the time when a package is first breached, the extent of degradation is determined. This gives the amount of corrosion products present inside a package and the size of penetrations, and allows water saturations and effective diffusion coefficients to be computed. The diffusive flux for releases by way of failed fuel rods and through corrosion products within the package is calculated, and the larger of these two is selected. Next, the diffusion rate through breaches in the package is computed. Since these two diffusion rates are in series, the smaller rate controls the overall diffusive release, so the smaller of the in-package diffusion rate and the breach diffusion rate is selected as the diffusive release.

10.3.1.3.8.2 Assumptions and Algorithms

The major assumptions for the in-package diffusion model are:

- This analysis applies when the seepage or dripping flux into the drifts is zero. This model also applies when the seepage flux is less than the rate of evaporation from the drip shield and waste package.
- The TSPA-SR model for transport in the waste package (CRWMS M&O 2000 [DIRS 153246], Section 3.6.1.2) will be used for those waste packages exposed to seepage because advective flow and transport through the waste package is anticipated to dominate diffusion in the seeping regions of the repository.
- This analysis applies to commercial SNF waste packages. Releases from DOE high-level radioactive waste packages should be calculated using the TSPA-SR models (CRWMS M&O 2000 [DIRS 153246], Section 3.6.1.2).
- There are no diffusive releases from any waste package until a breach occurs.
- Archie's Law is used to calculate the diffusion coefficient for unsaturated porous media. The exponents for porosity and saturation are based on experimental data for granular materials (see Section 10.3.1.3.5.1).

The major steps in the computational algorithm for in-package diffusion of commercial SNF waste packages are:

1. Determine the extent of degradation of the iron-based internal components of the waste package and the resulting surface area available for adsorption of water vapor. The extent of degradation is estimated from the lifetime of the internal components. More specifically, the effective surface area for adsorption is interpolated between the initial surface area and the fully degraded surface area as a function of the component lifetimes and the current simulation time.
2. Using the adsorption isotherm for Fe_2O_3 , and assuming that the waste package void volume remains constant at 4.97 m^3 (Table 10.3.1-5), compute the amount of water vapor adsorbed (number of monolayers and film thickness) and the water saturation in the package.
3. Compute the effective diffusion coefficient for steel corrosion products, using Archie's Law and the water saturation obtained in Step 2. Calculate the total cross-sectional area of the corrosion products, depending on the main direction (axial or radial) for diffusion. Use axial diffusion if only stress corrosion cracks are present in the waste package; use radial diffusion once a patch forms.
4. Compute the amount of water adsorbed using the adsorption isotherm for ZrO_2 , calculate the cross-sectional area for diffusion (not of the oxide layer) on the failed fuel rods, assuming axial diffusion, and assume that the effective diffusion coefficient is equal to the diffusion coefficient of radionuclides in water.

5. Calculate the diffusion rates through the steel corrosion products and along failed fuel rods. Use the larger of these two quantities as the in-package diffusion rate through the waste package. These two pathways are in parallel, so the larger rate will dominate diffusive transport.
6. Using the adsorption isotherm for Fe_2O_3 , compute the amount of water vapor adsorbed (number of monolayers and film thickness) and the water saturation in breaches in the waste package. Compute the effective diffusion coefficient, using Archie's Law and the water saturation obtained in Step 6. Obtain the total area of all breaches (stress corrosion cracks and patches) in the waste package. Calculate the diffusion rate through patches. This approach assumes that all breaches are filled with Fe_2O_3 corrosion products.
7. Compare the diffusion rates for in-package diffusion (Step 6) and diffusion through breaches (Step 7), and select the smaller quantity as the rate of diffusion out of the waste package. These two pathways are sequential, so the smaller rate will limit diffusive transport.

The only sampled parameters that are not already used in another model are the diffusion path length, the corrosion rate of steel components, and the surface area factor for the waste package. The sampled parameters and their distributions are summarized in Table 10.3.1-12.

10.3.2 Diffusion from the Waste Package to the Invert

10.3.2.1 Goal of Model

The goal of this model is to quantify the impact of radionuclide transport on the outer surface of the waste package and on the emplacement pallet. Transport between the waste package and invert can occur through advective or diffusive mechanisms. Advective transport occurs when a radionuclide moves with a flowing fluid, such as droplets or films, on the surface of the waste package and emplacement pallet. Diffusive transport occurs when a radionuclide moves from a region of high concentration to a region of lower concentration on the surface of the waste package. Advective and diffusive transport will occur for those waste packages exposed to a dripping environment in the repository. Diffusive transport may be the primary transport mechanism in the dry regions of the repository. Because 87 percent of the waste packages are not expected to be subject to dripping seepage at ambient conditions (CRWMS M&O 2000 [DIRS 153246], p. 4-5), diffusion is an important process for release of radionuclides from the waste package to the invert. This section provides a model to evaluate the potential impact of these transport processes on repository performance.

10.3.2.2 Identification of Unquantified Uncertainties in Total System Performance Assessment-Site Recommendation

In 87 percent of the potential repository in Yucca Mountain, dripping from seeps is not expected to occur. In these no-drip regions, diffusive transport is always possible, with diffusion of radionuclides occurring through a thin film of adsorbed water that will cover all surfaces exposed to the humid air in the repository drifts. Advective transport is also possible if the thin films become thick enough to advect under gravity. The objective of this analysis is to develop an

abstraction for calculating radionuclide transport between the waste package and invert in the regions of the repository without seepage.

The TSPA-SR transport model for the waste package (CRWMS M&O 2000 [DIRS 153246], p. 3-141) conservatively assumes that the waste package is always in contact with the invert. In other words, the diffusive path length is essentially zero between the waste package and the invert because the emplacement pallet is assumed to have failed. This is a conservative assumption because the emplacement pallet support members are fabricated from Alloy 22 (CRWMS M&O 2000 [DIRS 150953], Section 2.3.3), a corrosion-resistant material, and because the design specification for the pallet and invert requires that they maintain the horizontal position of the waste package for 10,000 years (CRWMS M&O 2000 [DIRS 150953], Section 1.2.1.21).

Alternative thermal operating modes could affect the model for transport between the waste package and the invert in two ways. First, as discussed in Section 10.3.3.2, solute diffusion coefficients vary as a direct function of temperature. Second, as discussed in Section 5.3.1.4, the time-history of relative humidity in the drifts differs according to the thermal operating mode. Relative humidity affects the thickness of water films (Section 10.3.2.3) and the saturation of corrosion products (Section 10.3.1.3.2).

10.3.2.3 Quantification of Previously Unquantified Uncertainty

10.3.2.3.1 Water Films and Their Relevance to Transport

Water films can act as a medium for diffusive or advective transport of radionuclides, particularly on the outer surfaces of the waste package and pallet. Both mechanisms will occur simultaneously, but if diffusion predominates, radionuclide transport will be slow and the so-called "diffusive barrier" will contribute to waste isolation. The following discussion develops an estimate for the value of relative humidity at which advection on vertical or sloping surfaces could overwhelm diffusion and eliminate the diffusive barrier on the waste package/pallet surfaces.

Evidence for solute transport in water films is provided by the laboratory tracer testing of Tokunaga et al. (2000 [DIRS 152914]), which was conducted at a relative humidity greater than 99.9 percent. In addition, dye tracer migration in films has been observed in the niche studies conducted in the Exploratory Studies Facility (Wang et al. 1998 [DIRS 154423], Section 2).

Films will accumulate on solid surfaces because of adsorption and long-range ordering and because of capillarity on rough surfaces with dust or other granular material. Film thickness will increase with relative humidity in the drift environment because the films will be in moisture potential equilibrium with the gas phase (except where dripping seepage forms thicker films). Thinner films may form if they are not in full equilibrium with water vapor, as may occur with moving films.

Film thickness greater than 0.1 μm is known to occur on rock or prepared glass surfaces only at values of relative humidity approaching 100 percent. Such conditions will not occur during preclosure ventilation or early in the postclosure period because the relative humidity will be too

low. But relative humidity may approach 100 percent after cooldown begins, particularly in cooler regions of the emplacement areas, where there may be localized condensing-humidity conditions.

The following discussion pertains to the potential for advective movement of a water film without regard to water composition. Gradients in total water potential, including the effects of chemical gradients, could also drive the movement of films, as described by Landau and Lifschitz (1959 [DIRS 155006], pp. 241 to 244).

10.3.2.3.2 Film Thickness Relationships

Film thickness depends on the composite effect from different types of forces acting near the solid-liquid interface and the liquid-vapor interface. These forces can alter the liquid density, the liquid composition, and the orientation (ordering) of the liquid molecules. The combined effects from the solid-liquid and liquid-vapor interfaces determine the free energy of the film, so the energy depends on film thickness.

Long-range forces include double-layer effects and van der Waals forces, which can affect film behavior for thicknesses up to approximately 1 micron (de Gennes 1985 [DIRS 154424]). The relative contribution from each type of force depends on the nature of the solid and liquid materials. For thicker films, in the approximate range of 0.1 to 1 micron, capillarity becomes increasingly important, depending on the scale of surface roughness (Philip 1977 [DIRS 152255]). The important point is that the transition from surface-dominated to capillary-dominated behavior occurs in the same range of film thickness as the transition from relatively immobile to mobile film flow characteristics. This transition range corresponds to a relative humidity of approximately 98 to 99 percent, which is likely to occur in the repository during cooldown.

Measured data and predictive relationships for film thickness selected from the scientific literature are plotted in Figure 10.3.2-1. The various results from the literature that are shown in this figure are plotted against the variable $\log(1-RH)$ to show the important relative humidity range above 99 percent. Measurements for aqueous films contacting air are taken from Tokunaga and Wan (1997 [DIRS 139195], Figure 7) and Tokunaga et al. (2000 [DIRS 152914], Figure 6), for Bishop tuff and roughened glass, respectively. These data are plotted directly from the sources, with conversion of values on the abscissas from matric head to $\log(1-RH)$.

The predictive relationship from Philip (1977 [DIRS 152255], p. 5074) (power-law expression for film potential, F , versus film thickness, v) is also plotted in Figure 10.3.2-1. This relation is reported to be consistent with limited available published data for films on wetting surfaces (Philip 1977 [DIRS 152255], pp. 5072 to 5074). The Hamaker equation (Middleman 1995 [DIRS 144046], Equation 9.2-2) is also plotted for comparison; this equation is typically applied for wetting, nonpolar liquids (such as lubricant films) on metal surfaces and is not strictly applicable to water-wetting surfaces. Water films are more complex because of the possibility of interfering double-layer effects from the solid-liquid and liquid-vapor interfaces and hydrogen bonding at the solid surface (Middleman 1995 [DIRS 144046], p. 242).

Figure 10.3.2-1 indicates that film thickness decreases rapidly with lower relative humidity and that surface roughness tends to increase the apparent average film thickness, but the contribution of roughness to the supporting data for the predictive relationships is unknown. Thus, the measured data (and the predictive relationships) may tend to indicate greater film thickness for the same relative humidity.

10.3.2.3.3 Film Transmissivity and Flow Velocity

Tokunaga et al. (2000 [DIRS 152914]) developed estimates for film transmissivity that represent the average volumetric flow rate under a unit potential gradient (i.e., gravity). Transmissivity, T , is defined as a function of film thickness, h , as:

$$T(h) = D(h) \frac{dh}{dF} \quad (\text{Eq. 10-11})$$

where D is the diffusivity and dh/dF is the derivative of film thickness with moisture potential. This equation corresponds to Equation 1 from Tokunaga et al. (2000 [DIRS 152914]), with a change of notation to conform to Philip (1977 [DIRS 152255]). Diffusivity D was measured directly on prepared samples using transient methods from unsaturated zone hydrology (Tokunaga et al. 2000 [DIRS 152914], pp. 1739 to 1741). The film thickness potential relationship was measured directly using a gravimetric method.

The transmissivity can be used to estimate the average film velocity (averaged through the film thickness), \bar{v} , on a vertical surface under the impetus of gravity (Tokunaga et al. 2000 [DIRS 152914], p. 1744):

$$\bar{v} = \frac{T(h)}{h} \quad (\text{Eq. 10-12})$$

The resulting plot of average film velocity for roughened glass over the range of film thickness investigated by Tokunaga et al. (2000 [DIRS 152914], Figure 10) is presented in Figure 10.3.2-2. Another approach to estimating average velocity is based on application of the Navier-Stokes equations to one-dimensional flow of a Newtonian fluid (Tokunaga and Wan 1997 [DIRS 139195], Equation 1). This approach is also plotted on Figure 10.3.2-2 for comparison, and shows that the average velocity can be much greater if viscous dissipation (from long-range ordering) and surface roughness effects are neglected.

10.3.2.3.4 Application of Film Flow Concepts to Performance Assessment

The available information for film behavior can be used to estimate how environmental conditions in the emplacement drifts can affect the transport of radionuclides released from the waste packages. More specifically, thin film behavior can be used to determine whether transport on the external surfaces of the waste package and pallet becomes advection-dominated at high humidity such that releases to the invert would not be diffusion-limited.

In the following discussion, the term “potential” refers to the additive sum of hydrostatic pressure, capillary, osmotic, and adsorptive potential components. The potential in thin films of

dilute water on smooth surfaces is dominated by the adsorptive potential, but the importance of the capillary potential increases as film thickness or surface roughness increases. The relative humidity of a gas phase contacting a water film is assumed to be at equilibrium to the potential, because each of the potential components affects the chemical activity of water. The literature data are based on tests that vary only matric potential, but the conversion to relative humidity for discussion purposes is still valid.

Recent laboratory work on roughened glass surfaces has extended the reported range of potential for direct measurement of average film thickness down to approximately -50 kPa (Tokunaga et al. 2000 [DIRS 152914], p. 1743 and Figure 6), corresponding to an equilibrium relative humidity of approximately 99.99 percent (condensing humidity) at 25°C , according to the Kelvin equation (Atkins 1990 [DIRS 111464], p. 148, Equation 13b). At this equilibrium relative humidity, the measured film thickness was $0.75\ \mu\text{m}$ (Tokunaga et al. 2000 [DIRS 152914], p. 1743), corresponding to an average vertical film flow velocity of approximately $1\ \text{cm/yr}$ (Tokunaga et al. 2000 [DIRS 152914], Figure 10). Further reduction in velocity can be expected at a lower relative humidity because of the strong relative humidity dependence observed in these tests, and because viscous dissipation intensifies for thinner films. As film thickness approaches $0.1\ \mu\text{m}$, long-range forces promote molecular ordering of the liquid and greater viscous resistance to flow (de Gennes 1985 [DIRS 154424], p. 857). The effect of increased viscous dissipation decreases the film transmissivity and average film flow velocity (i.e., in response to gravity). As the film thickness approaches $0.01\ \mu\text{m}$, viscous dissipation can be "very strong" (de Gennes 1985 [DIRS 154424], p. 853).

Glass is water-wetted, as are tuffaceous minerals (Tokunaga and Wan 1997 [DIRS 139195]) and metal-oxides (de Gennes 1985 [DIRS 154424], p. 830). Wetting properties of common soda glass are similar to rock dust and the corrosion products that will exist on the surfaces of waste packages and emplacement pallets. The porous surface texture of roughened glass reported by Tokunaga et al. (2000 [DIRS 152914], p. 1740) represents a scale of roughness that is likely to be present on the machined surfaces of the waste package and pallet, along with roughness at other scales. Roughness at larger scales could contribute to increased average film transmissivity when conditions are sufficiently humid (see discussion of heterogeneity effects below). Roughness at smaller scales could accumulate liquid water at lower values of moisture potential (more negative), but this would be associated with smaller values of film transmissivity because of the thinner films that exist at those potentials. Consequently, the results for roughened glass are considered to be suitable for approximating the minimum relative humidity for which film mobility could become important in the EBS.

The results of Tokunaga et al. (2000 [DIRS 152914]) were limited to a moisture potential of approximately -50 kPa, but other estimates of film thickness at drier conditions are available, as discussed above. The Philip (1977 [DIRS 152255]) model predicts thicker films than Tokunaga et al. (2000 [DIRS 152914]). These estimates support an inference that the equilibrium film thickness on the waste package and pallet at more negative moisture potential (lower relative humidity) will be very small.

From the Navier-Stokes solution for film flow (Tokunaga and Wan 1997 [DIRS 139195], Equation 1), the average film velocity on a vertical surface is less than $1\ \text{cm/yr}$ for a film thickness less than $0.01\ \mu\text{m}$ (Figure 10.3.2-2). In fact, the average thickness is probably much

less than the value predicted by the Philip model, which does not explicitly account for the effects of surface roughness and long-range molecular interactions that increase when water films become very thin. Similarly, the average film velocity is probably much less than that calculated using the Navier-Stokes solution; for example, the Tokunaga et al. (2000 [DIRS 152914]) results show that this approach greatly overestimates film mobility for roughened glass (Figure 10.3.2-2).

10.3.2.3.5 Uncertainties and Limitations

Solutes affect the activity of water in solution and may change the free energy of a thin film. Ionic solutes tend to shorten the length scale for electrostatic interactions, which would affect the free energy for thin films (e.g., less than 1 μm , where adsorption becomes much more important, as discussed previously). Surface tension (against vapor) for aqueous solutions of common salts increases with concentration, but is relatively insensitive (Weast and Astle 1981 [DIRS 100833], p. F-34). By analogy, film behavior may also be relatively insensitive to the effect of solutes. The associated uncertainty in the average velocity of film flow is probably less than that associated with surface roughness heterogeneity.

This discussion is limited to film flow on wettable surfaces, which is generally applicable to metal-oxide surfaces in the EBS. However, there is a possibility that metallic surfaces in the EBS could have nonwetting characteristics, which would tend to decrease film thickness and mobility, but could also induce the formation of droplets. If droplets were in moisture equilibrium with the gas phase, their sizes could range from a few microns to a few millimeters in the relative humidity range of 99 to 99.99 percent or greater. The transport characteristics of such droplets are not addressed here.

Effects of surface heterogeneity produce channeling of flow, as observed by Tokunaga et al. (2000 [DIRS 152914], p. 1743 and Figure 5) in comparing transient film movement on roughened plate glass versus glass cast of a natural fracture surface. The macroscopic average film flow velocity may be increased because movement of thicker films in channels is less hindered by viscous dissipation. Fluid film thickness in channels may be increased by capillarity, depending on the scale of surface roughness. Capillarity was probably important in the results presented by Tokunaga et al. (2000 [DIRS 152914], p. 1740) because the surface exhibited roughness at scales similar to the average film thickness, and because the relative humidity was sufficiently high that the potential equilibrium capillary radius-of-curvature for the film surface was of the same order as the scale of surface roughness.

The Philip approach for estimating film free energy (corresponding to matrix potential) is empirical, based on selection of a functional form to represent available measured data (Philip 1977 [DIRS 152255], Equation 33). The approach would suggest that film free energy increases with absolute temperature (Philip 1977 [DIRS 152255], Equation 34), such that a thicker, more mobile film would form in equilibrium with a given value of relative humidity. However, the surface tension of pure water against air (Weast and Astle 1981 [DIRS 100833], p. F-36), and thus the energy associated with this interface, decreases with increasing temperature. This appears to be inconsistent based on an analogy between liquid-vapor and solid-liquid interactions, and is not supported by empirical data. Thus, the approach is

appropriate for estimating film behavior at ambient temperatures, but not at temperatures that differ markedly from 25°C.

10.3.2.3.6 Application to Total System Performance Assessment

The results in Figures 10.3.2-1 and 10.3.2-2 provide a basis for a rough estimate of the maximum relative humidity required for diffusion to dominate transport between the waste package and the invert in the non-seeping areas of the repository. Assuming that the advective travel time on the surfaces of the waste package and pallet must be more than 10,000 years for diffusion to dominate transport, then the advective velocity must be less than 10^{-4} m/yr ($1 \text{ m}/10,000 \text{ yr} = 10^{-4} \text{ m/yr}$) for a characteristic length scale of 1 m between the waste package and invert. Figure 10.3.2-2 shows that the film thickness must be less than $0.001 \mu\text{m}$ for the advective velocity to be less than 10^{-4} m/yr, based on the Navier-Stokes equation. The corresponding limit on relative humidity is given in Figure 10.3.2-1 as 90 percent for the Phillip model. (The Hamaker equation is ignored here because water is a polar molecule.) In other words, the relative humidity must be less than 90 percent for the film thickness to be small enough that advective transport will take 10,000 years or more on the surface of the waste package and emplacement pallet.

An alternative (less conservative) approach is to use the Tokunaga data in Figure 10.3.2-2 instead of the Navier-Stokes equation. In this case, the film thickness must be less than $1 \mu\text{m}$ and the upper limit on relative humidity becomes 99.99 percent (Figure 10.3.2-1). Clearly, the range of response for relative humidity is quite large, varying from 90 percent to more than 99.99 percent.

At the low extreme, the relative humidity in the repository is expected to rise above 90 percent during the long cooldown period. This means that advective transport must be considered on the waste package and pallet if the Phillip model is valid. At the high extreme, the relative humidity may never reach 99.99 percent in the general repository and advective transport can be ignored, except perhaps near cooler waste packages or cooler regions of the repository. In this situation, the significance of advective transport will depend on the detailed three-dimensional thermal-hydrologic response of the repository for the emplaced waste packages.

The baseline model for transport between the waste package and the invert will be used until additional information is available on thin film flow and until TSPA-SR sensitivity results are analyzed to determine the impacts from the other models introduced in this section. A detailed advective-diffusive transport model between the waste form and the invert may be implemented when (1) three-dimensional predictions of relative humidity and waste package temperature are available to the required level of detail, (2) the effects of surface roughness and heterogeneity for the repository system can be quantified, and (3) the maximum value of relative humidity that will prevent advective transport within the repository system can be determined.

10.3.3 Diffusion Through the Invert

10.3.3.1 Goal of Model

The goal of this model is to quantify the impact of the uncertainty in the diffusion coefficient on radionuclide transport through the invert. The diffusion coefficient abstraction for the TSPA-SR (CRWMS M&O 2000 [DIRS 153246], pp. 3-138 to 3-139) already includes the effects of invert porosity, invert saturation, invert temperature, and the uncertainty in experimental measurements of the diffusivity of granular materials. The analysis for this model will eliminate a conservatism in the dependence of diffusivity on porosity, quantify the conservatism in using the self-diffusivity of water as a bounding value for all radionuclides of interest for the TSPA-SR, and evaluate the uncertainty in using a volume-averaged saturation for the invert rather than a more detailed saturation gradient for diffusive transport.

10.3.3.2 Identification of Unquantified Uncertainties in Total System Performance Assessment-Site Recommendation

The current model represents the diffusion coefficient in the waste package and invert as a function of porosity, saturation, and temperature (CRWMS M&O 2000 [DIRS 153940], Section 6.4.1). The TSPA-SR abstraction for diffusion coefficient is as follows:

- The self-diffusivity of water is a bounding value for the free water diffusivity of all radionuclides at 25°C.
- The free water diffusion coefficient is corrected for the porosity and (liquid) saturation of the invert as a porous medium. The correction for porosity and saturation is conservatively represented, based on Archie's law and experimental data for granular media.
- The diffusion coefficient for a partly saturated medium is corrected for the temperature of the invert.
- The effects of concentrated solutions are neglected in the TSPA-SR. The rationale for this choice (CRWMS M&O 2000 [DIRS 153940], Section 6.4.1.4) is that the maximum correction to diffusivity for a highly concentrated solution of potassium iodide is an increase of 27 percent. This increase is on the same order as the bounding approximation inherent in using the self-diffusion coefficient of water for all radionuclides, so it is neglected in the TSPA-SR.

Two of the conservatisms/uncertainties associated with this model have been quantified in previous work (CRWMS M&O 2000 [DIRS 153940]). These features are the uncertainty of the diffusivity of an unsaturated, porous medium and the use of a bounding value for free water diffusivity for all radionuclides. These conservatisms are discussed in Sections 10.3.3.3.1 and 10.3.3.3.2, respectively.

A third uncertainty relates to the use of a uniform saturation for the invert, based on the volume-averaged saturation from the NUFT multiscale model (CRWMS M&O 2000

[DIRS 139610]). An alternate approach, using a more detailed computational grid to evaluate the saturation gradient within the invert and its potential effect on diffusive transport, has been evaluated to quantify this uncertainty. These computational results are discussed in Section 10.3.3.3.3.

Alternative thermal operating modes will affect the diffusion coefficient directly, because of its functional dependence on invert temperature, and indirectly, because of its functional dependence on invert saturation.

10.3.3.3 Quantification of Previously Unquantified Uncertainty

10.3.3.3.1 Uncertainty for Unsaturated Porous Media

Conca and Wright (1992 [DIRS 100436]) measured the diffusion coefficient of unsaturated soil, gravel, bentonite, rock, and crushed tuff from Yucca Mountain over a broad range of water contents (DTN: MO9810SPA00026.000 [DIRS 137076]). These measured data have been used to analyze the dependence of the diffusion coefficient on volumetric moisture content for a variety of granular materials (CRWMS M&O 2000 [DIRS 150418], p. 3-138). Figure 10.3.3-1 presents a summary of the diffusivity data for various granular media and for volumetric moisture content between 0.5 percent and 40 percent.

A statistical analysis (CRWMS M&O 2000 [DIRS 150418], pp. 21 to 25) produced an excellent fit to the diffusivity data using a power law dependence on moisture content in the range of 1.5 percent to 66.3 percent. The statistical fit to the diffusion coefficient, D , is based on a linearizing transformation to the variables X and Y , defined as:

$$Y = \log(D / D_0)$$

$$X = \log(\theta) - 2$$

where

D = the diffusion coefficient

D_0 = free water diffusivity

θ = volumetric moisture content (CRWMS M&O 2000 [DIRS 150418], Equation 31).

The slope of the X - Y relationship is evaluated to be 1.849 (CRWMS M&O 2000 [DIRS 150418], Equation 37), leading to the following linear equation for Y as a function of X :

$$Y = (1.849)X$$

$$\log\left(\frac{D}{D_0}\right) = (1.849)(\log(\theta) - 2) \quad (\text{Eq. 10-13})$$

In this equation, θ , the volumetric moisture content, is defined as $\theta = 100\phi s$, where ϕ is porosity and s is the liquid saturation of the porous medium. Both ϕ and s are nondimensional, with values between 0 and 1. Substituting the definition of θ into the linear fit and exponentiating both sides as powers of 10 results in:

$$D = D_0 \phi^{1.849} s^{1.849} \quad (\text{Eq. 10-14})$$

A slightly different representation of the diffusion coefficient was used in the TSPA-SR (CRWMS M&O 2000 [DIRS 153246], p. 3-138):

$$D = D_0 \phi^{1.3} s^{1.849} \quad (\text{Eq. 10-15})$$

This equation has the same exponent for saturation as the statistical fit, but the exponent for porosity is set equal to the cementation factor for unconsolidated sand (CRWMS M&O 2000 [DIRS 150418], Section 4.1.2, p. 7). The rationale for using Equation 10-15 in the TSPA-SR (CRWMS M&O 2000 [DIRS 153246]), rather than the direct statistical fit (Equation 10-14), is that the statistical analysis is based on a single parameter—the volumetric moisture content—and does not treat porosity as an independent variable. In reality, the porosity of the various granular materials varies. Given this situation, it seemed appropriate to use the slightly more conservative representation in Equation 10-15. For example, the diffusion coefficient is 46 percent greater for a porosity of 50 percent with the TSPA-SR representation, assuming the same value for liquid saturation.

Given the robustness of the data set, which includes crushed tuff (Figure 10.3.3-1), and the accuracy of the statistical fit over a broad range of moisture contents, it is appropriate to use the (full) statistical fit for the TSPA-SR sensitivity studies, thereby eliminating the 40 percent conservatism from using an exponent for porosity based on unconsolidated sand.

The statistical fit for the diffusion coefficient has uncertainty because of the scatter of data points in Figure 10.3.3-1. This uncertainty approximates a normal distribution for the residuals in log-log space (CRWMS M&O 2000 [DIRS 150418], Figure 4). This normal distribution has a mean value of 0.0 and a standard deviation of 0.223 (CRWMS M&O 2000 [DIRS 150418], Equation 38). The uncertainty can be incorporated into the statistical fit as an additional factor on the (full) statistical fit.

$$D = D_0 \phi^{1.849} s^{1.849} 10^{ND(a=0, \sigma=0.223)} \quad (\text{Eq. 10-16})$$

where ND represents a normal distribution with a mean, a , of 0 and a standard deviation, σ , of 0.223. ND is in the exponent because the residuals are calculated in the log-log space of the statistical fit.

Figure 10.3.3-2 presents the statistical fit (solid line) and the upper and lower bounds (dashed lines) at two standard deviations above and below the fit. The dashed lines encompass almost all the data points, as would be expected because ± 2 standard deviations includes 97.7 percent of the area under a normal distribution. The above equation therefore accurately represents the uncertainty in the diffusivity data for the TSPA calculations.

The normal distribution was sampled for each realization of the TSPA-SR calculations (CRWMS M&O 2000 [DIRS 153246]), thereby incorporating the uncertainty of the experimental data into the diffusivity. A similar procedure should also be used for the final TSPA-SR calculations.

10.3.3.3.2 Uncertainty in the Self-Diffusivity of Water as an Upper Bound

The self-diffusion coefficient for water, 2.299×10^{-5} cm²/s at 25°C, provides a conservative bound for the diffusion of ionic and neutral inorganic and organometal species that may be released from a waste package (CRWMS M&O 2000 [DIRS 153940], Section 6.4.1.1). This assertion is based on the following:

- A survey of compiled diffusion coefficients at 25°C shows that simple cation and anion species (excluding the proton and hydroxyl species, which are not appropriate analogues for diffusing radionuclide species) have diffusion coefficients smaller than that of water.
- The self-diffusion coefficient for water at 90°C is larger than compiled diffusion coefficients for simple inorganic species at 100°C.
- Diffusion coefficients for simple lanthanide and actinide cations are much smaller than the self-diffusion coefficient of water, and are expected to be even smaller for their hydroxyl and carbonate complexes.

An alternative approach is to use four diffusion coefficients to provide a more realistic model. One coefficient could be used for each charge (monovalent, divalent, and trivalent species) and one for the hydroxyl and carbonate complexes of the actinides and lanthanides. At 25°C, the monovalent, divalent, and trivalent species have ranges of diffusion coefficients, as shown in Figure 10.3.3-3 (CRWMS M&O 2000 [DIRS 153940], Figure 5). The free water diffusivity is shown as the dashed line on this figure. The conservatism for the monovalent, divalent, and trivalent species is indicated by the size of the vertical “gap” between the data points and the dashed line; it varies between factors of 1.07 and 2.6 for monovalent species, between factors of 2.1 to 3.8 for divalent species, and by a factor of 3.8 for the trivalent species.

Given the potential variability of the in-drift chemical environment, it is not feasible to characterize the various radionuclide complexes that may exist in the invert. The current approach, using the self-diffusivity of water as an upper bound for the free water diffusivity of all radionuclides relevant to the TSPA, will be maintained in the TSPA-SR (CRWMS M&O 2000 [DIRS 153246], p. 3-138). This approach is conservative by a factor between 1 and 3.8 for the monovalent, divalent, and trivalent species in the invert.

10.3.3.3.3 Uncertainty in the Average Saturation for the Invert

The TSPA-SR analyses (CRWMS M&O 2000 [DIRS 153246], p. 3-134) use the saturation in the invert, as defined by the abstraction of thermal-hydraulic calculations, to determine the diffusivity in the invert. If a substantial saturation gradient exists in the invert, then the calculation of diffusivity from the volume-averaged saturation may be overly conservative. For example, it is possible that the liquid saturation at the top of the invert could be substantially lower than its average value if capillarity cannot draw liquid upward throughout the invert. In

this situation, the diffusion coefficient will be substantially smaller at the top of the invert, providing a barrier to diffusive transport. This decrease can be calculated for an example 50 percent reduction in liquid saturation as follows:

$$\frac{D_{top}}{D_{vol-avg}} \propto \left(\frac{s_{top}}{s_{vol-avg}} \right)^{1.849} \propto \left(\frac{0.5}{1} \right)^{1.849} = 0.28 \quad (\text{Eq. 10-17})$$

where the subscripts *top* and *vol-avg* indicate the parameter values at the top surface or volume-averaged throughout the invert. A similar calculation for an order of magnitude decrease in saturation shows that the diffusion coefficient decreases by a factor of 70 (i.e., $(0.1)^{1.849} = 0.014 = 1/70$). Clearly, the value of the diffusion coefficient is sensitive to the liquid saturation along the transport pathway in the invert.

A new analysis was performed with the NUFT, RADPRO, and XTOOL computer codes to evaluate the saturation gradient in the invert. Qualified software for this analysis is:

- NUFT 3.0s for modeling fully coupled, unsaturated-saturated flow of multiple phases and multiple components under non-isothermal conditions
- RADPRO 3.22 for defining radiation connectivity within the drift
- XTOOL 10.1, which is a postprocessor for NUFT output.

The new analysis is based on the same inputs, assumptions, and qualified software used in *In-Drift Thermal-Hydrological-Chemical Model* (CRWMS M&O 2000 [DIRS 131150]) for an equivalent continuum model, with the following exceptions:

- Backfill is not present in the space between the drip shield and the drift wall because the design basis for the TSPA-SR is a repository without backfill (CRWMS M&O 2001 [DIRS 153681], p. 2-18).
- An effective thermal conductivity of 0.40 W/m/K is used for air between the drip shield and the drift wall. This value in the outer annulus is a result of model calibration and validation.
- An approximately-round shape for the waste package and a letter-box shape (a rounded top and vertical sides) for the drip shield are included in the model.
- The air gap below the drip shield extends through the space between the waste package and the invert (i.e., the waste package is not in contact with the invert).
- Simulation time is 0 to 10,000 years. This duration allows the liquid saturation in the invert to approach an approximately steady-state value.
- A lower-temperature operating mode is based on the thermal loading for the latest design (BSC 2001 [DIRS 154461]).

- The grid for the simulation (Figure 10.3.3-4) is finer than that used for typical calculations with the multiscale thermal-hydrologic model (CRWMS M&O 2000 [DIRS 139610], Figure 6-3). This finer grid provides more resolution in the invert.

Figures 10.3.3-5 and 10.3.3-6 depict the liquid saturation in the EBS and in the invert at 10,000 years, respectively. The NUFT calculation predicts constant saturation in the invert underneath the drip shield, demonstrating that the saturation beneath the waste package, in the transport pathway for radionuclides through the invert, is essentially constant (uniform). In this case, the use of a volume-averaged saturation for the invert provides acceptable accuracy for calculating the effect of saturation on the diffusion coefficient.

10.3.4 Sorption of Dissolved Radionuclides

10.3.4.1 Goal of Model

The goal of this model is to quantify the impact of sorption processes on radionuclide transport through the EBS. Transport through the EBS is a function of the adsorption and desorption of radionuclides on the materials in the waste package and invert. Adsorption describes the uptake of a radionuclide by a solid surface when in contact with a radionuclide-laden aqueous solution. This uptake typically occurs when a bond is formed by surface sites that have a chemical affinity for the radionuclide. Progressive inflow of fluids with low radionuclide concentrations would thermodynamically favor desorption of the original population of sorbed radionuclides back into solution. The fully reversible sorption and desorption of radionuclides is often described by a linear isotherm, using a partition coefficient (K_d).

Irreversible sorption refers to the tendency in natural systems for desorption to be incomplete. In other words, the amount of sorbed contaminant available for desorption in natural systems is typically less than the total sorbed mass due to chemical and physical processes occurring at or beneath the mineral surface. Sorption processes will be referred to as adsorption if the process occurs on the surface or absorption if the process occurs beneath the surface.

This section defines a conceptual model for transport through the degraded EBS, including appropriate ranges of K_d values for americium, iodine, neptunium, plutonium, technetium, thorium, and uranium, and the defensibility of irreversible sorption for these radionuclides.

10.3.4.2 Identification of Unquantified Uncertainties in Total System Performance Assessment-Site Recommendation

The current TSPA-SR transport model for the EBS assumes no sorption or retardation of dissolved species of radionuclides (CRWMS M&O 2000 [DIRS 153246], p. 3-134). This assumption is very conservative for several reasons:

- A large mass of iron-(hydr)oxides, including species such as hematite, will be generated through corrosion of mild steel and stainless steels within the waste package and invert. The iron-(hydr)oxides are known to be excellent sorbers of many radionuclide species (Table 10.3.4-1).

- Some sorbed radionuclides, such as plutonium, appear not to desorb in many geologic environments (Section 10.3.4.3.3.4). In effect, the sorption process appears partly irreversible and a substantial percentage of sorbed radionuclides would appear to be permanently attached to the corrosion products in the EBS. But it is difficult to quantify irreversibility because the time scale for laboratory experiments or field observations is much shorter than repository time scales. In this situation, the short-term data may provide misleading information about long-term irreversibility. The net effect of irreversible sorption on EBS transport will depend on two competing effects: (1) irreversible sorption on the in-drift materials will decrease releases from the EBS, and (2) irreversible sorption to stable colloidal particles will increase transport through the EBS.
- Copper is present along the top of the invert as an electrical conductor. Two corrosion products produced by the alteration of elemental copper can strongly sorb iodine and technetium species (Table 10.3.4-1), an important feature for decreasing releases of two elements that generally have minimal sorption in oxidizing environments.

Partition coefficients are typically measured for groundwaters and substrates at ambient or near ambient temperatures. There is little or no experimental data for partition coefficients at the elevated temperatures that may occur in the EBS with either the repository design and operating mode described in the *Yucca Mountain Science and Engineering Report* (DOE 2001 [DIRS 153849]) or an alternative thermal operating mode. In this situation, the available data for partition coefficients have been used to define the ranges of K_d values for TSPA analyses, but it is not possible to distinguish alternative thermal operating modes in this model.

10.3.4.3 Quantification of Previously Unquantified Uncertainty

10.3.4.3.1 Conceptual Model for the In-Drift Environment

The mild steel and stainless steel in the waste package and invert (Table 10.3.4-2) are expected to degrade to iron-(hydr)oxides more rapidly than the corrosion-resistant materials in the EBS (e.g., Alloy 22 and titanium). The time sequence for corrosion of iron-based components in the EBS is:

- Mild steel in the invert (support beams, cap plate, and gantry rails) will begin to degrade after closure of the potential repository because the invert is directly exposed to the relative humidity and temperature environment within the drifts. Corrosion begins when the relative humidity becomes great enough to produce aqueous conditions on the surface. A threshold value of 70 percent has been estimated (CRWMS M&O 2000 [DIRS 151951], Assumption 5.3.9, p. 45), although the presence of deliquescent salts can result in aqueous conditions at lower values of relative humidity.

The steel and copper are in the top portion of the invert. More specifically, the longitudinal and transverse support beams are in the top half of the invert, based on *Committed Materials in Repository Drifts* (BSC 2001 [DIRS 154441], Figure 3). The transverse support beams are spaced at about 5-ft intervals, so the corrosion products from the beam will not always be directly beneath the emplacement pallet or stress

corrosion cracks. Below these beams, the invert is filled to depth with a granular ballast that does not contain any steel.

- Stainless steel rods in the emplacement pallet will corrode more slowly than mild steel (see footnote to Table 10.3.4-2). Again, the rods are directly exposed to the in-drift temperature and relative humidity after closure. The rods in the emplacement pallet are located directly beneath the waste package, in the anticipated flow path from the waste package.
- Mild steel (i.e., A 516 and borated steels) inside the waste package can begin to degrade after stress corrosion cracks form in the waste package. The earliest cracks form approximately 10,000 years after closure of the potential repository in the current TSPA-SR model (CRWMS M&O 2000 [DIRS 153246], p. F3-61, Figure 3.4-19 middle plot). Water vapor can enter the waste package once a crack forms, and this vapor will be adsorbed on the steel surfaces, providing an environment for corrosion within the waste package.
- Stainless steel inside the waste package can also corrode, albeit more slowly than mild steel, after a stress corrosion crack forms in the lid weld.

All mild steel components in the invert and emplacement pallet will degrade to iron-(hydr)oxides by the time the first stress corrosion cracks form at 10,000 years. In other words, iron-(hydr)oxides will be present in the invert before any radionuclides are transported from the waste package. After stress corrosion cracks form, the mild steel internals in the waste package will also degrade relatively rapidly, adding more iron-(hydr)oxides to the in-package environment. Most iron-based in-package materials will degrade to corrosion products by 25,000 years (Table 10.3.4-2), relatively early in the waste package lifetime.

The degradation products from corrosion of iron, aluminum, and copper-based materials in the waste package will include hydrous metal oxides and clays from degradation of high-level radioactive waste glass. These corrosion products are assumed to form a residue that is similar to a highly iron-rich soil or sediment in terms of its bulk chemical properties for determining appropriate ranges of K_d . The degradation products from the corrosion of iron, aluminum, and copper-based materials in the invert will include iron-(hydr)oxides and minerals from the granular backfill. The iron-(hydr)oxides are assumed to dominate the sorptive properties of the invert corrosion products for determining appropriate ranges of K_d , although the aluminum oxides and manganese oxides are also highly sorptive. These corrosion products occur in the top portion of the invert because all steel and copper is located in the top half of the invert (BSC 2001 [DIRS 154441], Figure 3).

The in-package degradation products are envisioned to be composed of unconsolidated particulates and larger agglomerations of clays, iron-(hydr)oxides, and other mineral assemblages that first slump to the bottom of the waste package and eventually collect on the top of the invert (floor of the drift) after the waste package and emplacement pallet fail. The invert degradation products are initially located near the top of the invert, but may move into the mass of granular backfill during seismic events. Any seepage through the waste package is expected to flow through this sludge of corrosion products because the invert corrosion products form

before any radionuclides can be released from the waste package and are in the flow path (i.e., at the bottom of the waste package and the top of the invert).

The sludge of corrosion products is reasonably described as a single porosity medium, given the granularity of the corrosion products and the randomness of the slumping process. Rapid flow paths with no sorption, as in the discrete fractures of a dual porosity medium, are not anticipated to occur in this unconsolidated sludge. The conceptual model for this uncertainty analysis assumes that the radionuclides have access to the mass of corrosion products. An alternative conceptual model, with corrosion products that form a contiguous mass that has a low permeability and tight pore structure, would limit access to the full sorptive capacity of the corrosion products. Similarly, if the transverse or longitudinal beams in the invert are outside the transport pathway, their efficiency as a sorber will be limited. These limitations are implicitly acknowledged in the selection of broad distributions with small minimum values for the partition coefficients (Table 10.4.4-1).

The initial sorption of radionuclides on the corrosion products is assumed to be described by a linear isotherm (i.e., a K_d). Descriptions of sorption based on a K_d are approximate because this approach is empirical, with little if any information about underlying mechanisms, and is therefore not easily extendable to different chemical environments and physical substrates (sorptive media). The use of a linear isotherm is also approximate because it does not predict saturation of the sorption sites with sorbed species that may include natural components of the groundwater. The mass of iron-(hydr)oxides from waste package corrosion is large (Table 10.3.4-3), so each waste package provides many sites for sorption. For these reasons, the K_d approach is at best an order of magnitude measure of contaminant uptake in geologic environments (Davis and Kent 1990 [DIRS 143280]).

The use of K_d to represent the subsequent release of radionuclides into fresh recharge (i.e., the desorption process) is often inconsistent with observations in geologic media. Typically, contaminants become more closely attached to a mineral surface after sorption, either adsorbed at high energy sites on the surface or absorbed through overcoating and buried due to other mineral surface reactions. The net result is that only a fraction of the original sorbed population remains available at the surface and able to react with adjacent solutions or be accessed by microorganisms. A K_d approach, on the other hand, assumes that all sorbed radionuclides are able to desorb from the substrate.

As an example, recent reviews of field and laboratory measurements indicate that the fraction of sorbed plutonium that is available for desorption rarely exceeds 1 percent (Brady et al. 1999 [DIRS 154421]; Davis and Kent 1990 [DIRS 143280]). Recognition of the strong role of irreversible sorption is implicit in models for watershed transport (Graf 1994 [DIRS 154419]) that focus solely on particulate transport. In these cases, desorption is ignored because it is rarely seen to occur with plutonium. However, as noted previously, the time scales for these observations are much shorter than the regulatory time period for repository performance (10,000 years), so the fraction of plutonium that is irreversibly sorbed in TSPA calculations has a substantial uncertainty.

10.3.4.3.2 Representation in the Total System Performance Assessment Model

The EBS should be represented as two sets of cells for the TSPA calculations. The in-package environment should be represented as a single cell. This mixing cell would include the mass of in-package corrosion products and the partition coefficients for these corrosion products. The invert should be represented by multiple cells. The cell or cells that represent the top one-third to one-half of the invert should include the mass of corrosion products in the invert and use the partition coefficients for these corrosion products. Any additional cells in the invert can represent granular backfill without corrosion products. This is a reasonable approach because most steel in the invert is in the top portion of the invert. The K_d s for the invert cells without corrosion products can be based on the partition coefficients for tuff in the unsaturated zone (CRWMS M&O 2001 [DIRS 154024]).

Irreversible sorption prevails to some extent in the natural environment for most radionuclides of interest to TSPA, as discussed above. In effect, the assumption of fully reversible sorption for radionuclides like plutonium and thorium may be conservative, although the degree of conservatism over repository time scales is difficult to evaluate. TSPA-SR calculations will be performed with a linear isotherm, which is conservative. Future TSPA calculations could be performed with irreversible sorption if a suitable implementation can be determined.

10.3.4.3.3 Sorption Parameters

This section presents and analyzes appropriate sorption parameters for the EBS. First, the mass of corrosion products (sorbers) is calculated for the potential repository design. Second, the available values for K_d are used to estimate the distributions of partition coefficients for the oxidizing in-drift environment in the waste package and invert. Third, an alternative method based on the concept of tolerance interval is used to estimate the ranges of values for K_d . The tolerance interval approach is appropriate when there is a limited sample set, as is often the case with K_d measurements. Finally, the available data on irreversible sorption of metals that are relevant to EBS transport are presented.

10.3.4.3.3.1 Mass of Corrosion Products

The mass of sorbing material in the waste package has been estimated using data from *In-Drift Microbial Communities* (CRWMS M&O 2000 [DIRS 151561], Attachment III). The mass of sorbing material in the waste package is based on the iron contents of Stainless Steel Type 304L, Stainless Steel Type 316L, Stainless Steel Type 316NG, A 516 carbon steel, Neutronit A 978, and the masses of these alloys in the four waste package types. The mass of corrosion products, assumed to be Fe_2O_3 , is then calculated based on the ratio of molecular weight for iron (as Fe_2) to that for Fe_2O_3 (Table 10.3.4-3).

The mass of sorbing material in the invert has been estimated using the data from *In-Drift Microbial Communities* (CRWMS M&O 2000 [DIRS 151561], Attachment II). The iron content of the steel invert and the gantry rails is included in this calculation. The iron in the steel set ground support, the rock bolts, and the welded wire fabric steel has been ignored, even though the corrosion products from these components may fall on the invert. The contribution from the rail fittings is ignored because it is a small fraction (about 8 percent) of the contribution from the

gantry rails. The mass of corrosion products is again estimated by assuming that iron converts to Fe_2O_3 during the corrosion process. In lithophysal and nonlithophysal areas, the mass of iron (703 kg/m) converts to 1,004 kg/m of Fe_2O_3 .

Finally, the amount of elemental copper in the drift is given by the nominal weight of the solid copper conductor bar rail, 1.73 kg/m, plus the copper in the communication cable, which is 50 percent by weight of the total cable weight of 0.79 kg/m (BSC 2001 [DIRS 154441], Assumptions 3.1.7, 3.1.9, and 3.2.1.3). The total weight of elemental copper per meter of drift is then $(1.73 + (0.5)(0.79))$ or a total of 2.13 kg/m. These values are based on the nominal mass of elemental copper, rather than the upper bound values, for conservatism. The mass of elemental copper is not explicitly represented in the TSPA model, but its presence when oxidized is important because of its role as a sorber for iodine and technetium.

The mass of copper is significant relative to that for iodine and technetium. Using a waste package length of 5.165 m for the commercial spent nuclear fuel waste package (BSC 2001 [DIRS 154441], Table III-1), there is 11.0 kg per commercial spent nuclear fuel waste package of elemental copper in the invert. This value (11.0 kg) can be compared to approximately 7.68 kg of technetium-99 and 1.80 kg of iodine-129 per commercial spent nuclear fuel waste package. Thus, there is more elemental copper than iodine or technetium using a mass or molar basis. Similarly, the 5-DHLW/DOE SNF Short waste package has a length of 3.59 m (BSC 2001 [DIRS 154441], Table III-3), implying that there is 7.63 kg of elemental copper per 5-DHLW/DOE SNF Short waste package in the invert. This mass is greater than the approximately 0.115 to 0.729 kg of technetium-99 or the 0.0251 to 0.0480 kg of iodine-129 in the codisposal waste packages (DTN: SN0009T0810599.014 [DIRS 152980]).

10.3.4.3.3.2 Partition Coefficient Values for Corrosion Products

As discussed previously, the use of a linear isotherm is an empirical, order-of-magnitude description of mineral surface processes because it is not based on underlying physical or chemical mechanisms. In essence, a K_d value is valid only for the specific substrate and chemical conditions under which it is measured. More defensible models of contaminant uptake by mineral surfaces require a more comprehensive mechanistic understanding of the chemical reactions involved (Davis et al. 1998 [DIRS 154436]). In lieu of a more involved mechanistic treatment based on surface complexation that includes a provision for irreversible sorption, K_d s can provide a first-order picture of the sorption process, using generic ranges based on soils and iron-(hydr)oxides. The rationale for this approach is described below.

The pH of waste package fluids (CRWMS M&O 2000 [DIRS 153246], Tables 3.3-7 through 3.3-9) is expected to fall within the range observed in soils and groundwaters (pH values between 4 and 10). Although the composition of in-package fluids will vary with time due to degradation of the waste package components (primarily steels, Zircaloy cladding, spent nuclear fuel, and waste glass), major element characteristics (such as alkalinity and system redox state) will likely be controlled by equilibrium with atmospheric carbon dioxide and free oxygen. The primary reactive components in the degraded waste package environment are likely to be iron hydroxides, the same mineral phases that tend to dominate trace element sorption in soils. Oxides of copper are also expected to be present. The only major element species that will be

present in waste package fluids, but that tend to be scarcer in natural soils and groundwaters, are those containing uranium.

The trace element composition of waste package fluids will differ due to the presence of metal components and various radiogenic isotopes. On the other hand, the waste package and invert environments are expected to contain greater volumes of iron hydroxides than all but the most iron-rich soils. Consequently, sorption calculations using ranges of K_d s measured on iron-containing soils or iron hydroxides probably provide a reasonable measure of sorption inside the waste package and invert.

Partition coefficients often vary by at least an order of magnitude. Each range of K_d represents the compilation of many experimental measurements with wide variations in soil composition, contaminant level, soil solution composition, and method of measurement.

Partition coefficients values for a linear, reversible isotherm can be interpreted physically (Stumm 1992 [DIRS 141778], Section 4.12). For example, a contaminant with a K_d of 1,000 ml/g will move at one ten-thousandth the rate of the carrier fluid for a rock porosity of 20 percent and a rock density of 2,000 kg/m³. A contaminant with a K_d of 1 ml/g will move at one-eleventh the velocity of the carrier fluid, and a contaminant with a K_d of 0 moves at the velocity of the fluid, both for the same values of rock porosity and rock density. These effective transport velocities provide an estimate of the delay for first breakthrough of the contaminant; after the sorption sites are completely saturated, changes in mass flow rate will be delayed only by the fluid travel time through the system.

The K_d ranges for iodine and technetium require additional discussion. Balsley et al. (1998 [DIRS 154439], pp. 125 to 141) experimentally identified and classified potential sorbent backfills for the anions I and TcO₄⁻. Under the oxidizing conditions that are conservatively assumed to prevail in the EBS, iodine and technetium will exist as the anions I and TcO₄⁻. Balsley et al. (1998 [DIRS 154439], p. 126) report that neither I or TcO₄⁻ form insoluble salts or sorb appreciably to common soil minerals. Consequently, the sorption coefficients for these radionuclides are generally assumed to be very low (Brady et al. 1999 [DIRS 154421], Appendix E). For near-neutral pH, which is typical of unsaturated or alkaline soils, hydrotalcites and copper oxides are efficient sorbers (Balsley et al. 1998 [DIRS 154439], p. 140). It is then reasonable to assume nonzero K_d s for technetium and iodine because copper oxides are expected to be present in the invert.

Median values and ranges for K_d for americium, iodine, neptunium, plutonium, technetium, thorium, and uranium on typical soils or corrosion products, or under oxidizing conditions, from a variety of sources are summarized in Table 10.3.4-1. The detailed reference citations, including table and page numbers as appropriate, are identified in Table 10.3.4-1 but are not repeated in the text to enhance readability. Because the sources provide broad ranges of K_d s for a variety of materials and because the in-drift chemical environment will vary with time, a reasonable but conservative approach has been used to define the ranges of partition coefficients.

The range of values for the americium partition coefficient is based on a uniform distribution with a minimum of 85 ml/g and a maximum of 5,000 ml/g. This distribution is based on the minimum value from Onishi et al. (1981 [DIRS 154420]) and the maximum value in

Unsaturated Zone and Saturated Zone Transport Properties (U0100) (CRWMS M&O 2001 [DIRS 154024]). It is a subset of the range in Onishi et al. (1981 [DIRS 154420]), and it is more conservative than the ranges in the Electrical Power Research Institute (EPRI) (2000 [DIRS 154149]), *Unsaturated Zone and Saturated Zone Transport Properties (U0100)* (CRWMS M&O 2001 [DIRS 154024]), and Sheppard and Thibault (1990 [DIRS 109991]) for loam. Values at the extreme low end of the range for sand (Sheppard and Thibault 1990 [DIRS 109991]) were ignored because the other data for iron oxides and oxidizing environments are generally greater than the minimum value for sand.

The range of values for the iodine partition coefficient is based on a uniform distribution with a minimum of 0 and a maximum of 10 ml/g. This distribution is based on the minimum or best estimate value from EPRI (2000 [DIRS 154149]) and the median value from Onishi et al. (1981 [DIRS 154420]). It is a subset of the range in Onishi et al. (1981 [DIRS 154420]) and more conservative than the ranges for sand and loam from Sheppard and Thibault (1990 [DIRS 109991]). This maximum value (10 ml/g) is also much less than the range of values for sorption on copper oxide and copper sulfide determined by Balsley et al. (1998 [DIRS 154439]). The upper limit of 1 ml/g in EPRI (2000 [DIRS 154149]) was ignored because of data from the other sources.

The range of values for the neptunium partition coefficient is based on a uniform distribution with a minimum of 0.1 and a maximum of 79 ml/g. This distribution is consistent with the minimum value from EPRI (2000 [DIRS 154149]) and the maximum value for loam from Sheppard and Thibault (1990 [DIRS 109991]). It is more conservative than all the ranges in Table 10.3.4-1.

The range of values for the plutonium partition coefficient is based on a uniform distribution with a minimum of 100 ml/g and a maximum of 5,000 ml/g. This distribution is based on the minimum value of 100 ml/g from Onishi et al. (1981 [DIRS 154420]) and the maximum value of 5,000 ml/g from *Unsaturated Zone and Saturated Zone Transport Properties (U0100)* (CRWMS M&O 2001 [DIRS 154024]). Larger maximum values are defined in the other three references (Table 10.3.4-1), but these are ignored for conservatism. The values at the extreme low end of the range for sand (Sheppard and Thibault 1990 [DIRS 109991]) were ignored because other data for iron oxides and oxidizing environments are generally greater than the minimum value for sand.

The range of values for the technetium partition coefficient is based on a uniform distribution with a minimum of 0 ml/g and a maximum of 5 ml/g. This distribution is based on the possibility of zero sorption under extreme oxidizing conditions and the median value from Onishi et al. (1981 [DIRS 154420]). This range is consistent with the measurements by Bird and Schwartz (1997 [DIRS 154488]), and it is a conservative subset of the ranges in Onishi et al. (1981 [DIRS 154420]), EPRI (2000 [DIRS 154149]), and Sheppard and Thibault (1990 [DIRS 109991]) for sand. The maximum value (5 ml/g) is less than the range of values (30 to 60 ml/g) for sorption on copper oxide and copper sulfide determined by Balsley et al. (1998 [DIRS 154439]). The upper limit of 0.4 ml/g, in Sheppard and Thibault (1990 [DIRS 109991]) for loam, was ignored because of data from the other sources.

The range of values for the thorium partition coefficient is based on a uniform distribution with a minimum of 1,000 ml/g and a maximum of 5,000 ml/g. This distribution is based on the smallest value in three sources (1,000 ml/g; Table 10.3.4-1) and the maximum value of 5,000 ml/g from *Unsaturated Zone and Saturated Zone Transport Properties (U0100)* (CRWMS M&O 2001 [DIRS 154024]). This range is a conservative subset of the ranges in Onishi et al. (1981 [DIRS 154420]), EPRI (2000 [DIRS 154149]), and *Unsaturated Zone and Saturated Zone Transport Properties (U0100)* (CRWMS M&O 2001 [DIRS 154024]). EPRI (2000 [DIRS 154149]) and Onishi et al. (1981 [DIRS 154420]) provide greater maximum values that are ignored for conservatism. The values at the extreme low end of the range for sand (Sheppard and Thibault 1990 [DIRS 109991]) were ignored because the other data for iron oxides and oxidizing environments are generally greater than the minimum value for sand.

The range of values for the uranium partition coefficient is based on a uniform distribution with a minimum of 0.2 ml/g and a maximum of 1,000 ml/g. This distribution is based on the minimum value from Sheppard and Thibault (1990 [DIRS 109991]) for loam and the maximum value of 1,000 ml/g from *Unsaturated Zone and Saturated Zone Transport Properties (U0100)* (CRWMS M&O 2001 [DIRS 154024]) and Onishi et al. (1981 [DIRS 154420]). This range is a conservative subset of all the ranges in Table 10.3.4-1, except for the minimum value for sand (Sheppard and Thibault 1990 [DIRS 109991]). The values at the extreme low end of the range for sand (Sheppard and Thibault 1990 [DIRS 109991]) were ignored because the other data for iron oxides and oxidizing environments are generally greater than the minimum value for sand. EPRI (2000 [DIRS 154149]) provides a higher maximum value (10,000 ml/g), which was ignored for conservatism.

10.3.4.3.3 Partition Coefficients Based on Small Sample Sizes

An alternative approach to estimating the appropriate ranges of values for partition coefficients is based on the concept of tolerance intervals. Tolerance intervals provide a statistical estimate of parameter ranges at a given confidence level from a small data set. In other words, the tolerance interval provides an estimate of the uncertainty inherent in a finite set of data. As a reminder, there are many conceptual uncertainties associated with linear isotherms and K_{ds} , as discussed in Section 10.3.4.3.1. The tolerance interval approach does not represent these uncertainties for sorption behavior; rather, the goal here is to quantify the uncertainty represented by the ranges of K_d data reported in the literature. The use of this technique is illustrated here with the partition coefficients compiled by Sheppard and Thibault (1990 [DIRS 109991]).

Sheppard and Thibault (1990 [DIRS 109991], Tables A-1 to A-4) present data on the mean and standard deviation of the natural logarithm of the partition coefficient for individual elements for sands, loams, clays, and organic soils. This information includes the number of measurements. Sheppard and Thibault (1990 [DIRS 109991], p. 472) also cite previous work in which the partition coefficients are lognormally distributed. Finally, Sheppard and Thibault (1990 [DIRS 109991], p. 472) calculated the geometric mean and the geometric standard deviation for each element by soil texture for the mineral and organic soils.

The uncertainty analysis for this data set evaluates the tolerance interval to define an appropriate range of values. The tolerance interval is appropriate in estimating the range of variability of the underlying population (ASME PTC 19.1-1998, *Test Uncertainty, Instruments and Apparatus*

[DIRS 153195]). Standard ASME PTC 19.1-1998 ([DIRS 153195], Appendix A) provides a procedure for calculating the tolerance interval that contains a specific proportion of the population. The procedure to assess the tolerance interval for a partition coefficient at the 95 percent confidence level is:

1. $C_{T,95}$ is the factor for the tolerance interval to contain at 95 percent of the population, based on the number of samples. Obtain $C_{T,95}$ from ASME PTC 19.1-1998 ([DIRS 153195], p. 84, first column of Table A.1), which is reproduced in *Rock Mass Thermal Properties* (BSC 2001 [DIRS 155008], Attachment VIII).
2. Calculate the tolerance interval based upon the mean and standard deviation of the partition coefficient, based on the samples presented in Sheppard and Thibault (1990 [DIRS 109991], Table A-1). The confidence tolerance interval on the partition coefficient is calculated as:

$$\bar{k} \pm c_{T,95}(n) \cdot s_k$$

where \bar{k} and s_k represent the mean value and standard deviation for the natural logarithm of values for the partition coefficient of each element for sand, and n is the sample size.

3. The tolerance values can be used to construct the log-uniform distribution, or they can be compared to the lognormal distribution for the mean and standard deviation presented by Sheppard and Thibault (1990 [DIRS 109991]) for each element.

This method can be extended to calculate the tolerance interval on the basis of the combined data for sand, loam, and clay (Sheppard and Thibault 1990 [DIRS 109991], Tables A-1 to A-3). These tables present the number of samples, along with the mean and standard deviation of the natural logarithm of the partition coefficient, for measurements of sand, loam, and clay, respectively. The weighted mean value for the combined data set is given by Hahn and Shapiro (1967 [DIRS 146529], p. 38, Equation 2-31):

$$\mu_{\log} = \frac{f_s * \mu_{\log s} + f_l * \mu_{\log l} + f_c * \mu_{\log c}}{n}$$

where

- f_s = number of measurements for sand
- f_l = number of measurements for loam
- f_c = number of measurements for clay
- n = total number of measurements
- μ_{\log} = mean of the natural logarithm for the combined data set
- $\mu_{\log s}$ = mean of the natural logarithm for the sand data
- $\mu_{\log l}$ = mean of the natural logarithm for the loam data
- $\mu_{\log c}$ = mean of the natural logarithm for the clay data.

The standard deviation of the natural logarithm of the partition coefficient for the combined data is derived from the basic definition for standard deviation (Hahn and Shapiro 1967 [DIRS 146529], p. 48, Equation 2-51c):

$$s^2 = \frac{\sum_{i=1}^n (x_i - \bar{x})^2}{n-1}$$

Define a deviation value, x_D , such that the following relationship is satisfied:

$$n \cdot (x_D - \bar{x})^2 \equiv \sum_{i=1}^n (x_i - \bar{x})^2$$

The summation on the right-hand side of this equation can be replaced using the above definition of the standard deviation, s :

$$\begin{aligned} n \cdot (x_D - \bar{x})^2 &\equiv \sum_{i=1}^n (x_i - \bar{x})^2 \\ &= s^2 \cdot (n-1) \end{aligned}$$

Applying this definition to each of the samples for sand, loam, and clay and solving for the deviation values yields:

$$x_{Ds} = \sqrt{\sigma \log s^2 \cdot \frac{(fs-1)}{fs}} + \mu \log s$$

$$x_{Dl} = \sqrt{\sigma \log l^2 \cdot \frac{(fl-1)}{fl}} + \mu \log l$$

$$x_{Dc} = \sqrt{\sigma \log c^2 \cdot \frac{(fc-1)}{fc}} + \mu \log c$$

where the subscripts D_s , D_l , and D_c denote sand, loam, and clay, respectively. The standard deviation for the combined sample can then be calculated by applying the basic definition for standard deviation:

$$\sigma \log = \sqrt{\frac{(fs \cdot (x_{Ds} - \mu \log)^2 + fl \cdot (x_{Dl} - \mu \log)^2 + fc \cdot (x_{Dc} - \mu \log)^2)}{n-1}}$$

For the radionuclides listed in Table 10.3.4-1, the results of these calculations are presented in Table 10.3.4-4. The values in Table 10.3.4-4 account for small sample population effects in that the tolerance interval factor is a function of the number of measurements and the desired confidence level. The results show that:

- The tolerance intervals for the partition coefficients of americium and thorium are quite large, ranging from minimum values on the order of 10 ml/g up to maximum values on the order of 1 million ml/g.
- The tolerance intervals for the partition coefficients for iodine, neptunium, and technetium are relatively low, ranging from a minimum value on the order of 0.01 ml/g to maximum values of 6.2 ml/g for technetium, 300 ml/g for iodine, and 2,900 ml/g for neptunium.
- The tolerance interval for the partition coefficient of plutonium is intermediate between these extremes, with a range of 13 to 94,000 ml/g. The tolerance interval for the partition coefficient of uranium is also an intermediate case, with a very low minimum value (0.012 ml/g) and a maximum value of 230,000 ml/g.

Figures 10.3.4-1 through 10.3.4-7 present the results in Table 10.3.4-4 for log-uniform distributions based on the tolerance interval limits and for lognormal distributions based on the mean value and standard deviation for these data sets. The two types of distributions are essentially equivalent, considering the large variability in partition coefficients and the uncertainty in definition of the chemical environment and substrates in the waste package and invert.

The variability represented by Figures 10.3.4-1 through 10.3.4-7 and by Table 10.3.4-4 is limited to the parameter uncertainty in the selected range of literature data. This variability is a statistical measure of uncertainty, rather than an addressing of the conceptual uncertainties with the use of K_d s and a linear isotherm.

10.3.4.3.3.4 Irreversible Fractions for Desorption

Irreversible uptake can be the dominant control over contaminant transport in soils. Evidence for soil sequestering of bomb-pulse plutonium and americium and of uranium, iodine, technetium, cesium, and strontium from ore processing and reactor operations has been extensively documented in the literature (Coughtrey et al. 1983 [DIRS 132164]).

Estimates of the mean fraction of irreversible sorption for various radionuclides on soil, derived from Brady et al. (1999 [DIRS 154421], Appendix F), are presented in Table 10.3.4-5. The value of the irreversible fraction for the EBS is likely to differ from that for soils and will depend on the material that the specific radionuclide encounters, the speciation of the radionuclide, and other factors in the material and chemical environment. The important conclusion from Table 10.3.4-5 is that irreversible sorption is an important process for many radionuclides that potentially contribute to dose. A corollary to this conclusion is that the current reversible transport models are conservative if the corrosion products in the waste package and invert behave like soils in the natural environment.

10.3.4.4 Other Lines of Evidence

The EBS elements through which radionuclides can migrate are conceptually similar to a laboratory column test, where radionuclides are introduced at the top of the column and migrate downward through materials representing the waste form and invert. This similarity is relevant for many laboratory tests of radionuclide transport properties.

Advective Transport—Laboratory testing of radionuclide migration downward through a crushed tuff column was performed with several radionuclides (neptunium-237, plutonium-239, tritium, and pertechnetate) in two groundwaters with different chemical compositions (Triay et al. 1997 [DIRS 100422], Section V.A). The purpose of the tests was mainly to compare column transport characteristics with radionuclide sorption parameters from batch sorption tests. The tests, therefore, provided analogous information on advective transport modified by sorption in crushed tuff. The transport model in the invert is analogous to these laboratory tests, which demonstrate that sorption can be effective in crushed tuff.

Diffusive Transport—A different series of tests was performed to gather information on the diffusive uptake of radionuclides by intact samples of tuff (Triay et al. 1997 [DIRS 100422], Section VI). It was observed that certain radionuclides could diffuse through minute water-filled pores depending on porosity, heterogeneity of the pore structure, and sorptive retardation. The tests show that diffusion through the intact tuff is a slow process for the typical time scales of these experiments, particularly for radionuclides with strong sorption, such as the actinides. In highly unsaturated conditions, diffusive transport is very slow, again providing corroborating evidence for sorption in crushed tuff.

10.3.5 Colloidal Transport of Radionuclides

10.3.5.1 Goal of Model

The goal of this model is to quantify the impacts of uncertainties in the behavior of colloids generated from the degradation of high-level radioactive waste glass, commercial spent nuclear fuel, and DOE spent nuclear fuel, as well as colloid-facilitated transport properties of radionuclides in the engineered barrier system. It is anticipated that colloids will also be mobilized as a result of the corrosion of waste package and in-drift components, in addition to the waste forms. The abundance of colloids will depend on the extent of waste form alteration and the alteration products formed.

Colloid abundance and stability also depend on many environmental factors, including ionic strength, pH, cation concentrations, colloid content of groundwater entering the drift, presence of fulvic and humic acids, and microbe fragments. Suspended colloids may subsequently flocculate and settle by gravity, be chemically or mechanically filtered, or dissolve. If environmental factors change, colloids may be peptized; colloid-sized particles may precipitate; or other natural processes may occur. In addition, colloids may sorb readily at the interfaces between air and water in rocks and engineered barriers and, depending upon the degree of saturation of the porous medium as well as its configuration, may be retarded, even immobilized or transported. These issues are relevant to transport of radionuclides by colloids, a primary concern within the waste package, within the EBS, and in the near- and far-fields.

10.3.5.2 Identification of Unquantified Uncertainties in Total System Performance Assessment-Site Recommendation

The current TSPA-SR model for generation and transport properties of colloids resulting from waste form degradation (CRWMS M&O 2000 [DIRS 153246], Section 3.5.6 and p. 3-138 to 3-139) generally uses a bounding approach for incorporating relevant source data, and it uses conservative assumptions where the available data were thought to be limited (CRWMS M&O 2001 [DIRS 153933]; CRWMS M&O 2000 [DIRS 129280]). This approach has given rise to uncertainties, the most significant of which are summarized in Table 10.3.5-1.

10.3.5.2.1 Colloid Generation

Potential Contribution of Irreversibly Attached Radionuclides on Colloids Generated from Commercial Spent Nuclear Fuel Degradation—This is a significant uncertainty and may be addressed as results are evaluated from ongoing laboratory experiments. Irreversibly attached radionuclides, as currently used in the analysis, refers to those radionuclides that are bound within the colloid, either within the crystal structure or in a separate phase embedded in the colloid. The only existing data on irreversibly attached plutonium content from degradation of waste are for high-level radioactive waste glass (CRWMS M&O 2001 [DIRS 154071], Table 4); data from degradation of commercial spent nuclear fuel were inconclusive because few colloids could be collected for analysis (CRWMS M&O 2001 [DIRS 154071], pp. 31 to 36).

This operational definition of irreversible (see above paragraph) has been adopted for abstraction. The term is also used in the scientific literature in reference to surface complexation of a metal, including radionuclides, to strong sites, which may be irreversible under certain conditions or over certain time frames. This form of attachment may be reversed by a change in chemical conditions, such as a lowering of pH [“(acidification)”], chelation, or ion exchange. It should be emphasized that such attachment of metals and radionuclides to colloidal or fixed substrates may in fact be reversible without a change in conditions over very long times.

Quantities of Colloids Generated from Corrosion of Steel—This uncertainty is considered significant. Iron-(hydr)oxides will form from the corrosion of steel components within the repository, including the waste package and in-drift structural components. There are few data on quantities of iron-(hydr)oxide colloids that may be generated from steel corrosion under given aqueous chemical conditions. This is potentially significant because it has been determined that plutonium and americium have a strong affinity with iron-(hydr)oxide minerals, so radionuclides bound to such colloids have the potential to be transported considerable distances.

The evolution of steel degradation products is also uncertain. There is a natural tendency for progression to the higher oxides, which are more thermodynamically stable. Accordingly, ferrihydrite tends to alter to goethite, which tends to alter to hematite over time. As this happens, the degree of crystallinity increases and the size of the domains probably increase. With time, the colloids that are formed initially will tend to crystallize and agglomerate. This would have the effect of reducing the number of available colloids over time, but at the same time would provide relatively immobile substrates for sorption or other attachment of dissolved radionuclides. This uncertainty has therefore been incorporated into the colloidal transport

abstraction for the TSPA-SR sensitivity studies. Corrosion colloids are discussed further in Sections 10.3.5.3 and 10.3.4.

Potential Contribution of Colloids from U.S. Department of Energy Spent Nuclear Fuel Degradation—This uncertainty could be significant, and may be addressed as results are evaluated from ongoing laboratory experiments. Preliminary unpublished results from the experimental degradation of metallic uranium fuel indicate that the fuel degrades rapidly and produces fine particulates, including particulates of colloid size (CRWMS M&O 2001 [DIRS 153933], p. 33). The potential for colloid-facilitated migration of radionuclides derived from the degradation of metallic uranium fuel is not considered in the current colloid model.

10.3.5.2.2 Colloid Stability, Concentration, and Transport Properties

Dependence of Colloid Stability and Concentration on Temperature—This uncertainty may be significant; however, temperature effects on colloid stability, concentration, and transport properties are largely unknown. Ionic strength and pH in the waste package are calculated in the TSPA, as are colloid stability and concentration dependence on ionic strength and pH (CRWMS M&O 2001 [DIRS 153933]; CRWMS M&O 2000 [DIRS 129280]). Therefore, colloid stability and concentration response to changing chemical conditions resulting from changing temperature is incorporated into current TSPA methodology. Uncertainties would combine the uncertainties incorporated into the colloid versus. Ionic strength and pH relationships described in the waste form colloid analysis model report [DIRS 125156] and the uncertainties incorporated into the in-package calculation of ionic strength and pH. In any case, colloid stability is generally expected to decrease with increasing temperature. Actinide and metal sorption onto metal hydroxide colloids tends to increase with temperature, paralleling temperature-dependent increases in metal hydroxide anionic surface charge (Machesky 1990 [DIRS 145046]).

Smectite as a Proxy for Groundwater Colloids—This uncertainty is probably not significant, and has not been included in the TSPA-SR sensitivity studies. In the model, all groundwater colloids flowing into the in-drift materials are assumed to be smectite (CRWMS M&O 2001 [DIRS 153933], p. 56; CRWMS M&O 2000 [DIRS 129280], p. 22). However, other colloids may be present, including silica, zeolites, feldspars, and iron-(hydr)oxides. Experimental results suggest that smectite has a somewhat higher affinity for radionuclides than many of these other mineral colloids (iron-(hydr)oxides being exceptions; Lu et al. 2000 [DIRS 154422]), and therefore the assumption that all groundwater colloids are smectite may be overly conservative. Information on colloid mineralogy collected from wells in the Yucca Mountain area may provide justification to use a mixture of mineralogies, including less sorptive minerals (e.g., silica). A preliminary review of data presented in Lu et al. (2000 [DIRS 154422]) suggests that while K_d values for plutonium and americium sorption are generally higher on montmorillonite than on silica, the difference is less than one order of magnitude. Determination of the degree to which K_d values for various types of colloids differ would require a significant effort for TSPA. If the differences were not large, then incorporating additional K_d values specific to each colloid mineral type into the model would complicate the calculation without adding demonstrably to the quality of the result. Note as well that explicit consideration of degradation product colloids and the uncertainty associated with them would probably tend to outweigh any uncertainty in the groundwater colloid term.

Flow Rate Within the Waste Package—The significance of this uncertainty is probably low. The colloid model currently incorporates the assumption that colloids, incrementally “generated” at each TSPA calculation time step, leave a failed waste container and enter the drift (specifically the invert) (CRWMS M&O 2001 [DIRS 153933], pp. 20, 66, and 67). This approach is conservative, bounding, and simplifies the model. An alternative approach would be to use the calculation of flow rate within the waste package to provide a more realistic (and lower) estimate of colloid transport rate within and out of the container. The conservative, simplifying approach has been retained for the TSPA-SR sensitivity studies because the uncertainty probably is low.

Entrainment of colloidal particles within the waste package, possibly caused by flow transients, chemical gradients, or surface tension gradients, may serve to mobilize and concentrate colloids within the waste package. The potential effects of entrainment on colloid concentration have not been considered in the TSPA-SR sensitivity studies.

Colloid Sorption onto the Air-Water Interface—This uncertainty may be moderately significant. Colloids are considered to adhere strongly to the interface between air and water of thin films, bubbles, etc. (Wan and Wilson 1994 [DIRS 114430]). The analysis of this important process is site-specific (i.e., it must be tailored specifically to the system under investigation) and can be quite complex. Leaving colloid sorption onto the air-water interface out of the colloid model is likely conservative. Adhesion to a fixed interface (e.g., as part of a water film on a component in the waste package) would serve to immobilize the colloid as long as the interface remained intact. Adhesion to the surface of a freely suspended bubble, on the other hand, would enable the colloid to be transported with the bubble, although the relatively large size of the bubble may cause it to become filtered out at constrictive passageways. Colloid sorption onto the air-water interface is not considered in the current model.

Potential Effects on the Total Colloid Population of Organic Material, Including Introduced Organics and Microbes—The effects of organic materials are potentially significant and may include:

- Organic coatings on mineral colloids, which would tend to sorb radionuclides as well as destabilize the colloid suspension and cause the colloids to agglomerate (CRWMS M&O 2001 [DIRS 153933], Attachment VI, pp. VI-1 and VI-2).
- Development of colloids comprised of monocellular microbes and fragments, which could sorb and transport radionuclides or agglomerate and immobilize radionuclides (CRWMS M&O 2001 [DIRS 153933], Attachment VI, pp. VI-1 and VI-2).

Thus two competing processes, one that encourages colloid mobilization and another that encourages colloid agglomeration and flocculation, may prevail. It is uncertain which process would dominate at a particular location or point in time within the repository. Organic and particularly microbial effects are discussed at length in Section 10.3.6.

10.3.5.2.3 Radionuclide Attachment and Concentration

The model currently considers attachment of radionuclides to colloids either irreversible or reversible. As noted previously, “irreversibly attached radionuclides are those bound within the

colloid, either within the crystal structure or in a separate phase embedded in the colloid (CRWMS M&O 2001 [DIRS 153933], pp. 18, 25 to 33, 51, 52, and 59 to 62). Reversibly attached radionuclides are those attached to colloids by the sum of processes referred to as sorption. The distribution of a radionuclide between the aqueous solution and the colloid is described by its K_d .

Wide Range of Distribution Coefficients Used to Describe Sorption of Radionuclides on Colloids—This uncertainty is significant, as K_d is a sensitive parameter incorporated into several TSPA calculation sets. Results of laboratory investigations and literature review to determine or estimate K_d s for radionuclides onto relevant materials has yielded ranges of K_d s as great as six orders of magnitude (CRWMS M&O 2001 [DIRS 153933], pp. 12 to 16, 44 to 46, and Attachment XVI.1.1.2; Lu et al. 2000 [DIRS 154422]).

Better-Justified Upper-Bound Maximum Concentration of Plutonium Irreversibly Attached to Colloids—This uncertainty may or may not be significant. The dependence of irreversibly attached plutonium content from the degradation of high-level radioactive waste glass on ionic strength was derived by closely bounding a representative subset of the data produced in the glass degradation experiments at Argonne National Laboratory (CRWMS M&O 2001 [DIRS 153933], pp. 38 and 39).

Consideration of Radionuclides Other than Plutonium and Americium—This uncertainty is low to moderately significant. Abundant data exist only for plutonium from waste degradation experiments (CRWMS M&O 2001 [DIRS 154071], Table 4, p. 19). In the current waste form degradation model, americium is assumed to behave similarly to plutonium (i.e., it may be incorporated into a colloid as irreversibly attached). The quantities of both plutonium and americium irreversibly attached to colloids are determined at each time step in the TSPA-SR by the radionuclide inventory remaining at each time step (CRWMS M&O 2001 [DIRS 153933], p. 51).

In the current colloid model, plutonium and americium are treated as irreversibly attached to waste form colloids. These two radionuclides were considered potentially the most significant sparingly soluble radionuclides that could readily become irreversibly attached to colloids and subsequently be transported from the waste package. In addition to plutonium and americium, two other radionuclides, protactinium and thorium, are considered for reversible attachment to waste form colloids and subsequent transport. The fractions of release from colloids associated with other dose-important radionuclides are considered insignificant relative to their dissolved concentrations.

10.3.5.3 Quantification of Previously Unquantified Uncertainty

This section discusses alternative distributions for certain of the parameters discussed above. These parameters and the alternative distributions are summarized in Table 10.3.5-2.

Combined Groundwater and Corrosion Colloid Concentrations—Limited data exist for concentrations of iron-(hydr)oxide colloids in natural systems. At the Morro de Ferro natural analogue site (Poços de Caldas, Brazil), concentrations of iron-(hydr)oxide [$\text{Fe}(\text{OH})_3$] colloids were measured in deep groundwaters adjacent to an iron-rich rock body (CRWMS M&O 2000

[DIRS 150707], pp. 3-72 to 3-81). The measured concentration, 0.25 mg/L, is similar to concentrations of other inorganic colloids found in natural waters at other deep sites. The upper end of the range, 1.0 mg/L, imparts a fourfold conservatism relative to the concentration observed at the analogue site. The proposed distribution is triangular, with a peak at 0.25 mg/L and endpoints at 10^{-3} and 1.0 mg/L. This type of distribution was selected because the data set is small. Reasonable numbers were available for peak and extreme values, so a triangular distribution was appropriate.

Given the limited data on corrosion colloid concentrations, as well as the somewhat more abundant data on groundwater colloid concentrations, uniform distributions were chosen for uncertainty analysis for a combined population of groundwater and corrosion colloids. Suitably wide concentration ranges were evaluated for two different ranges of aqueous ionic strength. Reasonable ranges for this combined colloid population, to which radionuclides may reversibly attach, are log-uniform distributions between 10^{-6} and 10^{-1} mg/L (for ionic strength $\leq 0.05\text{M}$) and 10^{-9} and 10^{-3} mg/L (for ionic strength $> 0.05\text{M}$). Differences in affinities for aqueous metals, including radionuclides, were accommodated by assumptions regarding sorption distribution coefficient (K_d) values and distributions (see below).

Range of Plutonium Concentration Irreversibly Attached to Waste Form Colloids—Reasonable distributions for plutonium irreversibly associated with waste form colloids are log-uniform distributions between 10^{-11} and 10^{-6} mol/L (for ionic strength less than 0.05M) and 10^{-14} and 10^{-8} mol/L (for ionic strength greater than 0.05M). These distributions were selected to capture the potential uncertainty about and sensitivity to irreversible plutonium sorption in the present study in a way that tests the entire ranges of values uniformly (i.e., without weighting the values about a mean). The upper range is (approximately) centered on the bounding concentration of 8×10^{-8} mol/L defined in *Waste Form Colloid-Associated Concentrations Limits: Abstraction and Summary* (CRWMS M&O 2001 [DIRS 153933], Figures 7 and 13). The minimum value of the distribution (10^{-11}), is approximately four orders of magnitude lower than 8×10^{-8} , and the maximum value of the distribution (10^{-4}), is approximately three orders of magnitude greater. Similarly, the lower range is centered on the minimum concentration measured experimentally, 10^{-11} mol/L (CRWMS M&O 2001 [DIRS 154071], Table 4, p. 20). The minimum and maximum values of this range are then ± 3 orders of magnitude from 10^{-11} mol/L.

Sorption of Plutonium and Americium onto Colloids—A careful review of the data presented in *Waste Form Colloid-Associated Concentrations Limits: Abstraction and Summary* (CRWMS M&O (2001 [DIRS 153933], Attachment XVI) and Lu et al. (2000 [DIRS 154422]) suggests that the currently used K_d values for plutonium and americium (10^4 and 10^5 ml/g, respectively; CRWMS M&O 2001 [DIRS 153933], Table 1) are reasonable for sorption onto montmorillonite, (a proxy colloid mineral for both waste form and groundwater colloids. However, a preliminary review of the Lu et al. (2000 [DIRS 154422]) data suggests that the currently used K_d values for iron-(hydr)oxides (a proxy colloid mineral for steel corrosion colloids) may be underestimated by as much as one to two orders of magnitude. Considering the large mass of iron-(hydr)oxides that may be present in the EBS and the uncertainty in the state of degraded materials with time, it is reasonable to use the same distribution for K_d s that describe the sorption of plutonium and americium onto colloids. The alternative distribution is a lognormal distribution with a mean

value of 10^5 ml/g and a standard deviation of two orders of magnitude. Lognormal distributions are useful for distributions in which mean values have been reasonably well determined, but in this case there is considerable variability. Therefore, a large geometric standard deviation was applied (100) so that sampled values would tend to cluster about the mean, but also span a very large range of possibilities in the TSPA iterative calculations.

10.3.5.4 Other Lines of Evidence

Numerous investigations of colloid characteristics, behavior, and transport properties have been published that relate to colloid stability and transport in the environment and the ability of colloids to facilitate the transport of radionuclides and non-radioactive-metals. Common principles have been employed in the development of this model.

Colloid Stability—A colloidal dispersion must be stable for the duration of transport and must carry significant amounts of radionuclides for radionuclide-bearing colloids to affect repository performance. Transport times can range from days to years for advective transport out of a breached waste package, and up to many thousands of years for retarded transport to the accessible environment. Thus, some relatively unstable colloids generated in the waste form may persist long enough to be transported through the EBS, but not long enough to reach the accessible environment. More stable colloids, however, can remain suspended for years and travel great distances.

Colloid Analogues—There is field evidence of colloid-facilitated transport of radionuclides. Buddemeier and Hunt (1988 [DIRS 100712], p. 536) found plutonium and americium more than 30 m below a low-level waste site in unsaturated tuff after approximately 30 years of operation. In a test at the Nevada Test Site, the isotope ratio of plutonium-240 to plutonium-239 in groundwater showed that plutonium had been transported more than 1.3 km over a 30-year period, although plutonium is assumed strongly sorbed at the Nevada Test Site and assumed to be immobile (Kersting et al. 1999 [DIRS 103282]). Plutonium is often found attached to colloids in water samples from the Nevada Test Site. In the Pahute Mesa drainage, Buddemeier and Hunt (1988 [DIRS 100712], p. 537) found colloid concentrations of 0.8 mg/L to 6.9 mg/L for particles greater than 30 nm in size.

Treated liquid wastes containing traces of plutonium and americium have been released into Mortandad Canyon at Los Alamos National Laboratory (Triay et al. 1997 [DIRS 100422], Section V.D., p. 172). The shallow alluvium at that location is composed of sandy to silty clays formed from weathering of volcanic rocks. Detectable amounts of plutonium and americium have been observed in monitoring wells up to 3.4-km (2.1-miles) downgradient from the discharge point. Sorption studies predicted that movement of plutonium and americium would be restricted to a few meters. This suggests that plutonium and americium are strongly associated with colloids that can be mobile for large distances (Triay et al. 1997 [DIRS 100422], Section V.D., p. 172).

Although colloid-facilitated plutonium transport in a qualitative sense has been “observed” in the field, the phenomenon has not been studied to the extent that other contaminants have been studied. For this reason, the model relies heavily on experiments in which conditions anticipated in the repository were simulated (to the extent possible). Accordingly, one

non-radionuclide-related natural analogue, Morro de Ferro (CRWMS M&O 2000 [DIRS 150707], pp. 3-72 to 3-81), was directly used in this model, in lieu of experimental data, to estimate concentrations of iron-(hydr)oxide colloids resulting from corrosion of steel components in the EBS.

10.3.6 Microbial Sorption and Transport

10.3.6.1 Goal of Model

The goal of this model is to quantify the impact of potential microbial communities on sorption of radionuclides to microbes and the ability of microbes to be transported as colloids through the EBS. The transport of microbes through the EBS is a function of the uptake of dissolved radionuclides onto the cell walls and the subsequent mobility of microbes through the waste package and invert.

Adsorption of radionuclides to microbes occurs in one of two ways. First, radionuclides can be adsorbed when a microbe is exposed to a radionuclide-laden aqueous solution. This uptake typically occurs when a bond is formed by surface sites on the microbial wall that have a chemical affinity for the radionuclide. This mechanism is a common one because it provides a means of protection for the cells against the toxic effects of the dissolved metals. Once a metal (or radionuclide) is adsorbed or precipitated onto the cell wall, its toxicity to microbes is greatly reduced. Second, microbes will create intracellular traps and precipitate crystalline metal deposits within the cell wall. This is also done to protect the cell against toxicity.

Sorption of uranium and plutonium onto microbes has been documented (Hersman 1997 [DIRS 100763]; Suzuki and Banfield 1999 [DIRS 154445]), and an extrapolation of uranium data for thorium and plutonium has been proposed (Macaskie 1991 [DIRS 154446]). Therefore, as a minimum, these three radionuclides must be considered for accumulation in and transport on microbial cells.

Once an individual microbe has sorbed the available radionuclides within or on its cell walls, the radionuclides become subject to the transport regime imposed on the microbe by the EBS. As discussed in Section 10.1.1, water saturation and the availability of an air-water interface within an unsaturated porous media can be related to the time-dependent saturation of the invert. Liquid saturation is a key parameter for determining whether the partition between radionuclides that adsorb onto microbes is retained within the invert and radionuclides will be available for additional "colloidal" transport into the UZ via microbes.

10.3.6.2 Identification of Unquantified Uncertainties in Total System Performance Assessment-Site Recommendation

The TSPA-SR (CRWMS M&O 2000 [DIRS 153246], Section 3.6) model does not account for the potential for microbial sorption or for transport of microbes as colloids. However, the *In-Drift Microbial Communities* model (CRWMS M&O 2000 [DIRS 151561], Section 6.6.5.2) reports that there is a potential for microbial colloids and gives a bounding value for the numbers of organisms per milliliter of flux ($1.16 \times 10^{+12}$) that could leave the EBS. This is a rather large number of potential "colloids" and could become a significant source of dose at the accessible environment, especially in light of the uncertainty work that is associated with sorption in the

EBS, as discussed in Section 10.3.4. Microbial transport, when coupled with irreversible sorption onto corrosion products, could yield significant decreases in noncolloidal releases from the EBS.

10.3.6.3 Quantification of Previously Unquantified Uncertainty

10.3.6.3.1 Conceptual Model for Microbial Sorption and Transport

As *In-Drift Microbial Communities* (CRWMS M&O 2000 [DIRS 151561]) describes, several factors influence the growth and abundance of microbes. These are primarily water availability (as a function of temperature and relative humidity), nutrient, and energy availability. In all other instances, including the ranges of pH and salinity expected in the drift, there are no physical limits to microbial growth. Microbes differ from traditional colloids in that they are able to facilitate several processes that will allow them to coexist with colloidal particles. First, microbes can agglomerate irreversibly onto existing colloids; they can also adsorb colloids onto their surfaces. These processes are joined with the ability that microbes have to make changes in their immediate environment, where gradients exist in and around themselves. Thus, microbes can establish a great diversity that would otherwise not occur in such close proximity (Hersman 1997 [DIRS 100763]). Biological processes that contribute to the mobility of microbes mainly revolve around the characteristics of the cell surface. The cell surface is prone to adhere to surfaces. The size and shape of microbes influence their ability to move, as do sedimentation, motility, and chemotaxis. These issues are discussed in some detail in Mills (1997 [DIRS 100800]). Mills also points out that in unsaturated media, gas-water interfaces may be the most important factor in controlling the movement of bacteria.

The conclusions presented in *In-Drift Microbial Communities* (CRWMS M&O 2000 [DIRS 151561]) indicate that microbial communities of some size will be present in the EBS. Associated with these communities will be opportunities to sorb and transport radionuclides. This is based on the observed capabilities of microbes to sorb and transport radionuclides, as well as the size of the microbial community that could be supported within the EBS.

10.3.6.3.1.1 Radionuclide Uptake

In a detailed discussion, Suzuki and Banfield (1999 [DIRS 154445]) report mechanisms for accumulation of radionuclides on microbes. Two types of mechanisms are discussed. One is the metabolism-dependent precipitation of uranium. This mechanism depends on changes in redox states due to the metabolic processes that microbes use to grow and subdivide. It is a complex process that depends on complex geochemical models. Suzuki and Banfield (1999 [DIRS 154445], p. 402) also report that this mechanism is small compared to the metabolism-independent uptake (or adsorption) of uranium. Therefore, only the largest effect (metabolism-independent uptake) will be quantified because the completeness gained by including both mechanisms would result in only small changes to the TSPA.

Metabolism-independent uptake (or adsorption) of uranium is modeled using a data set compiled from 25 separate literature sources for microbial uranium accumulation by microorganisms (bacteria, fungi, algae, and lichens) reported in Suzuki and Banfield (1999 [DIRS 154445], Table 2). The data set was pared down to represent only the uranium uptake by 45 species of

bacteria and fungi over a range of "optimum" pH values (i.e., pH values of 1 to 7), as shown in Figure 10.3.6-1. These data can be used to represent the uptake of uranium by potential microbial communities in the repository. Because uranium has many similarities to other actinides in terms of chemical properties, it has been demonstrated that it is possible to extrapolate data for microbial uranium accumulations to other actinides (Macaskie 1991 [DIRS 154446], pp. 42 to 55). Because U^{+4} is similar to Th^{+4} and Pu^{+4} , it can be assumed that the data in Figure 10.3.6-1 can be used as a surrogate for data on the uptake of thorium and plutonium.

10.3.6.3.1.2 Transport

As discussed in Section 10.1.1, data from laboratory column tests from Jewett et al. (1999 [DIRS 154325], Table 2) and Wan et al. (1994 [DIRS 154367]) show a strong dependence of microbial transport on the level of water saturation in the porous media (Figure 10.3.6-2). The retention of microbes in the EBS can then be linked directly to saturation levels in the invert, assuming that the analogue data are sufficient for quantifying uncertainty and that the granular invert backfill is similar to a packed sand column.

The advective transport of microbes out of the EBS can be limited by the findings of Jewett et al. (1999 [DIRS 154325]) and Wan et al. (1994 [DIRS 154367]) above a liquid saturation level of 44 percent. However, below this level, no specific control can be devised. Therefore, an assumption can be made that saturations at or below 44 percent will be able to move 5 percent of the microbes (at 44 percent saturation, 95 percent of the microbes are retained). This assumption is likely to be conservative because microbial movement will be progressively more limited as saturation decreases. Other evidence that may partially support this assumption is the work reported on the Large Block Test (Chen et al. 1999 [DIRS 154447]), which shows that bacterial transport could occur during heating, where one would expect the initial saturation levels in the fractures and matrix to decrease because of the thermal movement of water. Chen et al. (1999 [DIRS 154447]) also report that some of the bacterial tracers used to conduct the transport test had migrated to the collection points. This information indicates that some level of microbial transport occurs under these conditions.

10.3.6.3.2 Representation of a Total System Performance Assessment Model for Microbial Sorption and Transport

The representation of this model in the TSPA can be accomplished in the following manner. First, a source term for microbial biomass must be generated each time step (see Section 10.3.6.3.2.1). Second, the sorption of uranium and plutonium onto that biomass must be calculated. The uptake of uranium and plutonium is discussed in Section 10.3.6.3.2.2. Finally, the fraction of microbes that will be retained in the invert versus the fraction that will be released as colloids from the EBS must be determined (see Section 10.3.6.3.2.3).

10.3.6.3.2.1 Microbial Source Term

The source term for microbes through time is abstracted from the results of the in-drift microbial communities model (CRWMS M&O 2000 [DIRS 151561]; DTN: MO0010MWDMIN38.031 [DIRS 154299]). The values used were the cumulative growth curves through time for each of

the commercial spent nuclear fuel waste package (21-PWR) modeling runs (Cases 1 to 5 and 7) and the high-level radioactive waste package modeling runs (Cases 15 to 19 and 21) that included biomass growth from waste package failure and waste form degradation. These results were plotted in SigmaPlot 4.0 and regressed using third- and fourth-order linear regression of a log/log plot to best fit the data (Figures 10.3.6-3 and 10.3.6-4). Based on the regression analysis, the following equations represent the microbial source terms for the commercial spent nuclear fuel and high-level radioactive waste glass, respectively. The cumulative microbes produced (*CMP*) is measured in units of grams (dry weight) per meter of waste package, and *T* is time in years.

$$\log CMP_{csnf} = -5.7846 + 7.5541 (\log t) - 2.0501 (\log t)^2 + 0.1891 (\log t)^3$$

$$\log CMP_{hlw} = 1.4824 + 0.4394 (\log t) + 0.4545 (\log t)^2 - 0.1887 (\log t)^3 + 0.0207 (\log t)^4$$

The predicted biomass available for radionuclide uptake in any given year, *t*, is determined by taking *CMP* calculated at time *t* and subtracting from it the value for *CMP* at time *t*-1.

10.3.6.3.2 Radionuclide Uptake

The data for uranium uptake are taken from Suzuki and Banfield (1999 [DIRS 154445], Table 2). These values, which represent uranium uptake for 45 species of bacteria and fungi, were averaged, and the results are shown in Table 10.3.6-1.

The average, or mean, value in Table 10.3.6-1 (162.88 mg U/gm) is smaller than the midpoint of the minimum and maximum values (330 mg U/gm). In this situation, a normal distribution with the mean and standard deviation given in Table 10.3.6-1 is biased away from the maximum values. The distribution of uptake for TSPA purposes should therefore be a triangular distribution with a range between 45.2 and 615 mg U/gm and a median value of 111.33 mg U/gm to capture the observed range of data and provide the median value as the most likely uptake. As discussed above, plutonium and thorium are also expected to sorb onto microbes. Since there are no specific data for uptake of these two elements, the distribution for uranium uptake will also be used for plutonium and thorium. In addition, because the abundance of these two radionuclides is smaller than that of uranium, a second modeling assumption will be that plutonium and thorium are sorbed in proportion to the ratios of their dissolved concentrations with respect to uranium prior to uptake.

10.3.6.3.2.3 Transport of Microbes in the Invert

A regression of data found in Jewett et al. (1999 [DIRS 154325], Table 2, p. 85) will govern the release of microbes from the invert when saturation levels in the invert are equal to or greater than 0.45. This regression fit, which is validated by data from Wan et al. (1994 [DIRS 154367], Figure 9), is shown in Figure 10.3.6-2. The regression equation is:

$$\text{Fraction of Microbial Mass Retained in Invert} = 1.3256 + (\text{Invert Saturation})(-0.8417)$$

This equation is valid over the range of invert saturation from 0.45 to 1.0. For matrix saturation levels below 0.45, there are no data available. However, as discussed above, a conservative assumption would be that, below a saturation of 0.45, 5 percent of the microbes are transported

as colloids for any given time step, since this is the value bounded by the data from Jewett et al. (1999 [DIRS 154325], Table 2, p. 85; see also Figure 10.3.6-1). The remaining 95 percent of the microbes would no longer be able to participate in transport. This would remove 95 percent of the uranium, plutonium, and thorium sorbed to microbes from being able to contribute to overall dose.

10.3.6.4 Other Lines of Evidence to Support Model

The information compiled by Suzuki and Banfield (1999 [DIRS 154445]) and Hersman (1997 [DIRS 100763]) indicate that there is a substantial experimental basis documenting radionuclide uptake by microbes and their subsequent movement as colloidal particles in unsaturated environments.

10.4 SUMMARY AND PARAMETERS PROVIDED TO TOTAL SYSTEM PERFORMANCE ASSESSMENT

This section defines the computational algorithms for TSPA-SR sensitivity studies related to transport through the EBS. It is structured to parallel the six subsections in Section 10.3, summarizing the conceptual and mathematical models for diffusion in the waste package, transport from the waste package to the invert, diffusion through the invert, sorption of dissolved radionuclides, colloidal transport, and microbial sorption and transport. The emphasis in this section is on definition of the algorithms for TSPA; detailed technical discussions and references can be found in the corresponding portions of Section 10.3.

10.4.1 Diffusion in the Waste Package

The general approach for the commercial SNF (21-PWR and 44-BWR) waste packages is to consider three limiting pathways for diffusion: along failed fuel rods, through porous corrosion products inside the package, and through porous corrosion products filling breaches (either stress corrosion cracks or general corrosion patches) in the outer layer of the waste package. Starting from the time when a package is first breached, the extent of degradation is determined. This parameter is the basis for estimating the amount of corrosion product present inside a package and the size of penetrations, and allows the water saturation and effective diffusion coefficient to be computed. The diffusive flux for releases along failed fuel rods and through corrosion products within the package is calculated, and the larger of these two is selected. Next, the diffusion rate through breaches in the package is computed. The smaller of the in-package diffusion rate and the breach diffusion rate is selected as the net diffusive release. This is a reasonable approach because the net diffusive release from the waste package is limited by the smaller of the in-package diffusion rate and the breach diffusion rate. In other words, these pathways are sequential, so the smallest diffusion rate will be the controlling parameter. Within the waste package, however, radionuclides will diffuse along the fastest independent pathway that is available.

Figure 10.4.1-1 is a flow chart that summarizes the computational algorithms for the in-package diffusion model. The elements in Figure 10.4.1-1 have been identified with the letters that correspond to the major steps in the computational algorithm. These elements also include the section number where the equation or parameter is discussed in Section 10.3.1. The major steps in the flow chart are:

- Figure 10.4.1-1, Item A. Determine the extent of degradation of the iron-based internal components of the waste package and the resulting surface area available for adsorption of water vapor. This is a two-step process. First, the extent of degradation is computed from the estimated lifetime of the internal components. Second, the effective surface area for adsorption is interpolated between the initial surface area and the fully degraded surface area as a function of the component lifetimes and the current simulation time.

First Step—Assume the iron-based internal components have a lifetime equal to that of the waste package inner layer, which is 50-mm thick. The cylindrical wall of each commercial SNF waste package has an inner layer made of stainless steel and an outer layer made of Alloy 22. Compute the lifetime by dividing the inner layer thickness by the corrosion rate. Assume that one-third of the iron-based internal components are carbon steel and two-thirds are stainless steel. Each type of steel corrodes at a different rate, determined by sampling its rate distribution. The lifetime of carbon steel is then given by:

$$t_{f1} = \frac{50 \text{ mm}}{r_1} = \frac{5 \times 10^4}{r_1}$$

where r_1 is the sampled value for the corrosion rate of carbon steel [$\mu\text{m}/\text{yr}$]. Similarly, the lifetime of stainless steel is given by:

$$t_{f2} = \frac{50 \text{ mm}}{r_2} = \frac{5 \times 10^4}{r_2}$$

where r_2 is the sampled value for the corrosion rate of stainless steel [$\mu\text{m}/\text{yr}$].

Second Step—One-third of the total initial surface of the internal components is assigned to carbon steel components and two-thirds are assigned to stainless steel components, similar to the assumption for the first step. The initial surface areas are then $(1/3)(1390.8 \text{ m}^2) = 463.6 \text{ m}^2$ for carbon steel and $(2/3)(1390.8 \text{ m}^2) = 927.2 \text{ m}^2$ for stainless steel, where $1,390.8 \text{ m}^2$ is the total initial surface area for all waste package internal components (see Section 10.3.1.3.3.1). Similarly, the fully degraded surface areas are $(1/3)(2.58 \times 10^8 \text{ m}^2) = 0.86 \times 10^8 \text{ m}^2$ for carbon steel and $(2/3)(2.58 \times 10^8 \text{ m}^2) = 1.72 \times 10^8 \text{ m}^2$ for stainless steel, where $2.58 \times 10^8 \text{ m}^2$ is the total degraded surface area for all waste package internal components (see Section 10.3.1.3.3.1). Then at the current simulation time, t , the surface areas of the carbon and stainless steel components are computed as a linear interpolation over the lifetimes of the iron-based components:

$$\begin{aligned}
A_1 &= 463.6 + (0.86 \times 10^8 - 463.6) \frac{t - t_0}{t_{f1}}, \quad \text{for } t_0 < t < t_0 + t_{f1} \\
&= 0.86 \times 10^8, \quad \text{for } t > t_0 + t_{f1} \\
A_2 &= 927.2 + (1.72 \times 10^8 - 927.2) \frac{t - t_0}{t_{f2}}, \quad \text{for } t_0 < t < t_0 + t_{f2} \\
&= 1.72 \times 10^8, \quad \text{for } t > t_0 + t_{f2}
\end{aligned}$$

where A_1 is the surface area of the carbon steel components, A_2 is the surface area of the stainless steel components, and t_0 is the time of first breach of the waste package. The total surface area within the waste package is then $(A_1 + A_2)$. The surface area available for adsorption of water vapor, s_{WP} , is then calculated as the product of this total surface area and the sampled waste package surface area factor, f_{WPs} , that accounts for the uncertainty in the estimates of the surface area of corrosion products.

- Figure 10.4.1-1, Item B. Using the adsorption isotherm for Fe_2O_3 and assuming that the package void volume remains constant at 4.97 m^3 (Table 10.3.1-5), compute the amount of water vapor adsorbed (number of monolayers and film thickness) and the water saturation in the package as follows:

$$\begin{aligned}
S_e &= \frac{V_w s_{WP}}{s_{N_2} V_{WP}} \\
&= \frac{s_{WP}}{V_{cp}} \frac{M_w}{\rho_w A_w N_A} \left(\frac{-1.1}{\log_{10} RH} \right)^{\frac{1}{2.45}}
\end{aligned}$$

Symbols are defined in Sections 10.3.1.3.5.1 and 10.3.1.3.2.1.

- Figure 10.4.1-1, Items C1 and C2. Compute the effective diffusion coefficient for steel corrosion product, D_s , using Archie's Law with a fixed porosity of 0.6539 and the water saturation obtained from Item B (Item C1). Calculate $D_s A_s$, where A_s (Item C2) is the total cross-sectional area of the medium, depending on which direction diffusion is taking place. The predominant direction for diffusion will be axial (toward each end of the waste package) when only stress corrosion cracks are present; A_s should then be the cross-sectional area of a waste package. Once general corrosion patches appear in the cylindrical sides of the waste package, radial diffusion to the sides of the waste package will dominate, so A_s should then be the inside surface of the Alloy 22 layer. Both of these estimates for A_s represent upper bounds. A lower bound would be the actual area of the breaches. Depending on the direction of diffusion, sample the diffusion path length, Δx_s , uniformly from 2 cm (Alloy 22 thickness) to 4.775 m (inside length of a 21-PWR waste package) if only stress corrosion cracks are present; otherwise, sample Δx_s uniformly from 2 cm to 0.712 m (half the inside diameter of a 21-PWR waste package) when patches are present (Item C2).

- Figure 10.4.1-1, Items D1 and D2. With minimal degradation (i.e., spaces between rods are mostly free of corrosion products), diffusion occurs along failed fuel rods. Use the adsorption isotherm for ZrO_2 to obtain the thickness of the adsorbed water film on the surface of fuel rods. Compute the cross-sectional area, A_f , for diffusion along rods (see Section 10.3.1.3.5.1); multiply by number of failed rods, N_{ffr} ; then multiply this product by D_{wl} , the diffusion coefficient of radionuclides in water (using the same values used to calculate radionuclide transport in the invert) to determine $D_{wl} A_f N_{ffr}$. Sample the diffusion path length, Δx_f , uniformly from 2 cm (Alloy 22 thickness) to 4.775 m (inside length of a 21-PWR).
- Figure 10.4.1-1, Items E1, E2, and E3. Calculate the diffusion rates, $q_s = D_s A_s \Delta C / \Delta x_s$ and $q_f = D_{wl} A_f N_{ffr} \Delta C / \Delta x_f$, for diffusion in-package through porous corrosion products and for diffusion along failed fuel rods, respectively (Items E1 and E2). The concentration of radionuclides inside the package is at the solubility limit (or the concentration provided by a source term model), and the concentration outside the package can either be conservatively assumed as zero or can be the concentration in the invert, if it is available. Use the larger of the two as the in-package diffusion rate through the waste package interior (Item E3):

$$q_{ip} = \max(q_s, q_f)$$

- Figure 10.4.1-1, Item F. Obtain the total area, A_b , of all breaches in the waste package outer barrier by summing the areas of all stress corrosion cracks and general corrosion patches. Assume all penetrations are filled with corrosion products with a porosity of 40 percent. Assume corrosion products are Fe_2O_3 , and calculate the water saturation at the given RH using:

$$S_{e.cp} = 1.19419 \times 10^{-2} (-\ln RH)^{-1/2.45}$$

Use Archie's Law to get the effective diffusion coefficient for diffusion through penetrations (Equation 10-9 in Section 10.3.1.3.5.3 where the exponents on porosity and saturation are those obtained by Conca and Wright [1992 [DIRS 100436]], as discussed in Section 10.3.1.3.5.1):

$$D_s = \phi_{cp}^{1.849} S_{e.cp}^{1.8492} D_{wl}$$

Multiply the effective diffusion coefficient by the total area of all patches to evaluate the $D_{s.cp} A_b$ term in the diffusion rate expression. Sample the path length, Δx_b , uniformly from 2 cm (Alloy 22 thickness) to 7 cm (total thickness of inner and outer walls of waste package). Calculate the diffusion rate through breaches:

$$q_{cp} = D_{s.cp} A_b \Delta C / \Delta x_{cp}$$

- Figure 10.4.1-1, Item G. Compare the diffusion rates for in-package diffusion and diffusion through breaches, and select the smaller as the rate of diffusion out of the waste package:

$$q = \min(q_{ip}, q_b)$$

The only sampled parameters that are not already used in another model are the diffusion path length (Δx), the corrosion rate of steel components (r_1 and r_2), and the surface area factor for the waste package (f_{WPS}). The sampled parameters for the model are summarized in Table 10.3.1-12.

10.4.2 Transport from the Waste Package to the Invert

The baseline model for transport between the waste package and the invert will be used until additional information is available on thin film flow and until TSPA-SR sensitivity results are analyzed to determine the impacts from the other models introduced in this section. A detailed advective-diffusive transport model between the waste package and the invert may be implemented when (1) three-dimensional predictions of relative humidity and waste package temperature are available to the required level of detail, (2) the effects of surface roughness and heterogeneity for the repository system can be quantified, and (3) the maximum value of relative humidity that will prevent advective transport within the repository system can be determined.

10.4.3 Diffusion Through the Invert

The abstraction for the diffusion coefficient in the invert is as follows:

- The self-diffusivity of water is a bounding value for the free water diffusivity of all radionuclides at 25°C. The value for the self-diffusivity of water, D_0 , is 2.299×10^{-5} cm²/s. This approach is conservative by a factor of between 1 and 3.8, as explained in Section 10.3.3.3.2. This approach is unchanged from the TSPA-SR (CRWMS M&O 2000 [DIRS 153246]).
- The free water diffusion coefficient is corrected for the porosity and (liquid) saturation of the invert as a porous medium. The diffusivity, D , is calculated as:

$$D = D_0 \phi^{1.849} s^{1.849} 10^{ND(a=0, \sigma=0.223)}$$

where

D_0 is the free water diffusion coefficient

ϕ is the porosity

s is the (liquid) saturation.

ND represents a normal distribution with a mean (a) of 0 and a standard deviation (σ) of 0.223. Note that the exponent of the porosity has changed from the TSPA-SR (CRWMS M&O 2000 [DIRS 153246]). See Section 10.3.3.3.1 for additional details.

- The temperature correction for the diffusion coefficient is unchanged from the TSPA-SR (CRWMS M&O 2000 [DIRS 153246]).
- Detailed calculations with NUFT demonstrate that the use of a volume-averaged saturation for the invert is an appropriate abstraction. No changes are required from the TSPA-SR with regard to liquid saturation in the invert.

10.4.4 Sorption of Dissolved Radionuclides

Two approaches have been used to estimate ranges of partition coefficients in the EBS. The first approach uses median values and ranges for partition coefficients (K_{ds}) for americium, iodine, neptunium, plutonium, technetium, thorium, and uranium on typical soils and corrosion products, or under oxidizing conditions from a variety of sources. The results of this approach are summarized in Table 10.3.4-1 and described in more detail in Section 10.3.4.3.3.2.

An alternate approach to estimating the appropriate ranges of values for partition coefficients is based on the concept of tolerance interval. Tolerance intervals provide a statistical estimate of parameter ranges at a given confidence level from a small data set. In other words, the tolerance interval provides an estimate of the uncertainty inherent in a finite set of data, but it does not represent the conceptual uncertainties associated with linear isotherms and K_{ds} . The resulting tolerance intervals for a 95 percent confidence level for partition coefficients on sand, loam, and clay are presented in Table 10.3.4-4 and discussed in more detail in Section 10.3.4.3.3.3.

The final recommendations for partition coefficients and distribution type are presented in Table 10.4.4-1. At the low end, each range is based on the minimum value from the tolerance interval because it provides a 95 percent level of confidence. At the high end, each range is based on the maximum value for the corrosion products because the tolerance interval often has values that appear unusually high. All distributions are log uniform because K_d data is often observed to be logarithmically distributed, because a log distribution maintains uniformity of sampling in each decade, and because little is known about the distribution of K_d values throughout a given range.

Finally, the mass of iron-based corrosion products in the waste package is presented in Table 10.3.4-3. The mass of iron-based corrosion products in the invert is 1,004 kg/m of Fe_2O_3 in both the lithophysal and nonlithophysal areas of the repository.

10.4.5 Colloidal Transport of Radionuclides

The baseline model for colloidal transport of radionuclides will be used until additional information is available on colloidal concentrations and transport properties in the EBS and until the results from TSPA-SR sensitivity results are analyzed to determine the impacts on performance from the other models introduced in this section.

Combined Groundwater and Corrosion Colloid Concentrations—Reasonable ranges for this combined colloid population, to which radionuclides may reversibly attach, are log uniform distributions between 10^{-6} and 10^{-1} mg/L (for ionic strength less than or equal to 0.05) and 10^{-9} and 10^{-3} mg/L for (ionic strength greater than 0.05). Differences in affinities for aqueous metals,

including radionuclides, were accommodated by assumptions regarding sorption distribution coefficient (K_d) values and distributions.

Range of Plutonium Concentration Irreversibly Attached to Waste Form Colloids—Reasonable distributions for plutonium irreversibly associated with waste form colloids are log uniform distributions between 10^{-11} and 10^{-6} mg/L for ionic strength less than or equal to 0.05 and between 10^{-14} and 10^{-8} mg/L for ionic strength greater than 0.05.

Sorption of Plutonium and Americium onto Colloids—It is reasonable to use the same distribution for K_{ds} that describe the sorption of plutonium and americium onto colloids. The recommended distribution for this study is a lognormal distribution with a mean value of 10^5 mg/L and a standard deviation of two orders of magnitude.

10.4.6 Microbial Sorption and Transport

Microbial sorption and transport is not represented in the TSPA-SR model. This baseline (i.e., no microbial sorption and transport of radionuclides) will be used until additional information is available on microbial abundance and transport properties in the EBS and until the results from TSPA-SR sensitivity results are analyzed to determine the impacts on performance from the other models introduced in this section.

Source Term—The following equations represent the microbial source terms for commercial SNF and high-level radioactive waste glass, respectively. The cumulative microbes produced (CMP) are:

$$\text{Log } CMP_{csnf} = -5.7846 + 7.5541 (\log t) - 2.0501 (\log t)^2 + 0.1891 (\log t)^3$$

$$\log CMP_{hlw} = 1.4824 + 0.4394 (\log t) + 0.4545 (\log t)^2 - 0.1887 (\log t)^3 + 0.0207 (\log t)^4$$

where CMP is in units of grams (dry weight) per meter of waste package and t is time in years (see Section 10.3.6.3.2.1). The predicted biomass available for radionuclide uptake in any given year, t , is determined by taking CMP calculated at time t and subtracting from it the value for CMP at time $t - 1$.

Radionuclide Uptake—The uptake of uranium for TSPA sensitivity studies (McNeish 2001 [DIRS 155023]) will be a triangular distribution ranging between 45.2 and 615 mg uranium/gm and with a median value of 111.33 mg uranium/gm (Section 10.3.6.3.2.2). Plutonium and thorium are also expected to sorb onto microbes. Because there are no specific data for uptake of these two elements, the sampled value from the distribution for uranium uptake will be scaled down for the relative abundances of plutonium and thorium. That is, it will be assumed that plutonium and thorium sorb onto microbes in proportion to the ratios of their dissolved concentrations with respect to uranium prior to uptake.

Transport of Microbes in the Invert—For invert saturation levels equal to or greater than 0.45, the fraction of microbial mass retained in the invert will be represented through a regression fit to experimental data:

$$\text{Fraction of Microbial Mass Retained in Invert} = 1.3256 + (\text{Invert Saturation})(-0.8417)$$

No data are available for matrix saturation levels below 0.45. However, a conservative assumption will be to transport 5 percent of the microbes as colloids for any given time step because this is the value bounded by the experimental data (Section 10.3.6.3.2.3).

Table 10.3.1-1. Comparison of the Adsorption of Water on Various Metals

Element	RH for Monolayer Coverage (%)			H ₂ O Adsorbed at 80% RH and 25°C in N ₂ /H ₂ O (g/cm ²)
	25°C	45°C	90°C	
Gold	10	25	24	4.6×10 ⁻⁷
Copper	10	10	40	3.1×10 ⁻⁷
Nickel	35	20	20 ^a	6.2066×10 ⁻⁸
Iron	40	23	16 ^a	2.48×10 ⁻⁷

Source: Lee 1994 [DIRS 154380], Chapter 5.

NOTE: ^aThe values for nickel and iron at 90°C were measured at 85°C.

Table 10.3.1-2. Least Squares Analysis of Adsorption of Water on ZrO₂

RH	Adsorption ZrO ₂ (mg/g)	No. of Monolayers (θ _a)	Y = -ln(-ln(RH))	X = ln(θ _a)	Prediction of Y	Predicted RH
0.010	5.54	1.354	-1.527	0.303	-1.343	0.02
0.050	6.92	1.691	-1.097	0.525	-0.935	0.08
0.100	7.76	1.896	-0.834	0.640	-0.725	0.13
0.150	8.53	2.085	-0.640	0.735	-0.552	0.18
0.200	9.12	2.229	-0.476	0.801	-0.429	0.22
0.300	10.40	2.542	-0.186	0.933	-0.189	0.30
0.400	11.52	2.815	0.087	1.035	-0.002	0.37
0.500	12.80	3.128	0.367	1.140	0.191	0.44
0.600	14.56	3.558	0.672	1.269	0.427	0.52
0.658	16.00	3.910	0.871	1.364	0.600	0.58
0.700	17.81	4.352	1.031	1.471	0.797	0.64
0.784	24.00	5.865	1.413	1.769	1.343	0.77
0.840	32.00	7.820	1.747	2.057	1.870	0.86
0.880	40.00	9.775	2.057	2.280	2.279	0.90
0.917	48.00	11.730	2.446	2.462	2.613	0.93
0.947	56.00	13.685	2.910	2.616	2.895	0.95

Source: Holmes et al. 1974 [DIRS 154379], p. 367.

Table 10.3.1-3. Specific Surface Area of Oxide Samples Reported in Literature

Material	Specific Surface Area (m ² /g)	Reference
α-Fe ₂ O ₃	9.10	Jurinak 1964 [DIRS 154381], p. 480
α-Fe ₂ O ₃	10	McCafferty and Zettlemoyer 1970 [DIRS 154382], p. 453
"Iron oxide"	13.3 – 14.3	Gregg and Sing 1982 [DIRS 153010], Table 3.17
ZrO ₂	14.5	Holmes et al. 1974 [DIRS 154379], p. 368 (avg. of range listed)

Table 10.3.1-4. Characteristics of a 21-PWR Waste Package

Component	Dimensions	Qty. in WP	Total Surface Area (m ²)	Mass (kg)	Density (kg/m ³)
Fuel Rods ^e	0.94996 cm OD; 384.96 cm length; 0.11488698 m ² /rod	5544	636.933	–	–
Basket A-Sideguide	10 mm thickness	32	22.013 ^a	27	7850 ^b
Basket B-Sideguide	10 mm thickness	16	14.675 ^a	36	7850 ^b
Basket A-Stiffener	10 mm thickness	64	1.174 ^a	0.72	7850 ^b
Basket B-Stiffener	10 mm thickness	32	1.223 ^a	1.5	7850 ^b
Basket C-Stiffener	10 mm thickness	32	1.875 ^a	2.3	7850 ^b
Basket Corner Guide	10 mm thickness	16	17.121 ^a	42	7850 ^b
Basket A-Plate	7 mm thickness	8	25.037 ^a	85	7760 ^c
Basket B-Plate	7 mm thickness	8	25.037 ^a	85	7760 ^c
Basket C-Plate	7 mm thickness	16	25.920 ^a	44	7760 ^c
Basket D-Plate	5 mm thickness	8	24.889 ^a	21	2700 ^d
Basket E-Plate	5 mm thickness	8	24.889 ^a	21	2700 ^d
Basket Tube ^f	4.575 m length; 22.64 cm width; 5 mm thickness	21	177.854	–	7850 ^b
Inner Shell	1.424 m ID; 4.775 m length	1	21.362	–	–
Inner Lid	1.430 m diameter	2	3.212	–	–
Total	–	–	1023.214	–	–

NOTES: ^a Surface Area = $2mN/(\rho\Delta x)$; m = mass (kg); N = quantity; ρ = density (kg/m³); Δx = thickness (m); "2" accounts for 2 sides of a plate; edges ignored; WP = waste package.

^b CRWMS M&O (1999 [DIRS 102933], p.10; Material: SA-516 K02700).

^c CRWMS M&O (1999 [DIRS 102933], p.39; Material: Neutronit A 978).

^d CRWMS M&O (1999 [DIRS 102933], p.56; Material: A96061).

^e CRWMS M&O (1998 [DIRS 100733], Attachment I, Table 1); 264 rods/assembly.

^f Square cross section; width listed is inside dimension; ends ignored.

Basket dimensions, quantities, mass, and material from CRWMS M&O 2000 [DIRS 144128], Attachment I, Sketch SK-0175.

W1717WL chosen as average assembly.

Table 10.3.1-5. Porosity Calculation for a 21-PWR Waste Package
(Density, Mass, and Sources Listed in Table 10.3.1-4)

Component	Mass each (kg)	Quantity in WP	Total Volume (m ³)
Fuel Rods	(272.845 cm ³ /rod)	5544	1.5127
Basket A-Sideguide	27	32	0.1101
Basket B-Sideguide	36	16	0.0734
Basket A-Stiffener	0.72	64	0.0060
Basket B-Stiffener	1.5	32	0.0061
Basket C-Stiffener	2.3	32	0.0094
Basket Corner Guide	42	16	0.0856
Basket A-Plate	85	8	0.0876
Basket B-Plate	85	8	0.0876
Basket C-Plate	44	16	0.0907
Basket D-Plate	21	8	0.0622
Basket E-Plate	21	8	0.0622
Basket Tube	164	21	0.4387
Total Solids Volume	-	-	2.6323
Inner WP Volume	1.424 m ID; 4.775 m length	1	7.6047
Total Void Volume	-	-	4.9724

NOTE: WP = waste package.

Table 10.3.1-6. Masses and Materials for the Three Types of Waste Packages That Will Comprise the Bulk of Waste in the Repository

Material	21-PWR Mass (kg)	44-BWR Mass (kg)	5-DHLW Mass (kg)
Alloy C-22	6663	6812	8260
Stainless Steel Type 316NG	11249	11531	11296
A 516 carbon steel	5723.68	7245	3805
Neutronit A 978	2064	2152	-
Stainless Steel Type 304L	-	-	2500
Aluminum 6061	336	336	-
Commercial SNF ^a	172.6	182.1	-
Zircaloy	2244 ^b	2063 ^c	-
DOE High-Level Waste Glass	-	-	8410 ^d

Source: CRWMS M&O 2000 [DIRS 151561], Tables III-1 to III-4.

NOTES: ^a Includes only the mass of elements C, N, P, S, Mn, and Fe; does *not* include masses of U, UO₂ or Zr (CRWMS M&O 1998 [DIRS 100737], pp. I-2 and III-2).

^b Based on 5544 fuel rods; 0.94996 cm (0.374 in.) outer diameter; 0.05715 cm (0.0225 in.) cladding thickness; 384.9624 cm (151.560 in.) length (DOE 1992 [DIRS 102588], p. 2A-30). Includes only the cladding. Density of Zircaloy 4 = 6560 kg/m³ (CRWMS M&O 1999 [DIRS 102933], p. 44). The calculation is as follows:

$$\begin{aligned}
 m &= \pi \left\{ D_o^2 - (D_o - 2t_{clad})^2 \right\} L \rho N / 4 \\
 &= \left(\frac{\pi}{4} \right) \left\{ (0.94996 \text{ cm})^2 - [(0.94996 \text{ cm}) - 2(0.05715 \text{ cm})]^2 \right\} \\
 &\quad (3849624 \text{ cm/rod}) (6560 \text{ kg/m}^3) (5544 \text{ rods}) (10^{-6} \text{ m}^3/\text{cm}^3) \\
 &= (61.70828 \text{ cm}^3 / \text{rod}) (5544 \text{ rods/WP}) (6560 \text{ kg/m}^3) (10^{-6} \text{ m}^3/\text{cm}^3) \\
 &= (0.3421107 \text{ m}^3 / \text{WP}) (6560 \text{ kg/m}^3) \\
 &= 2244.25 \text{ kg/WP}
 \end{aligned}$$

^c GE BWR/4-6 8x8 Assembly (DOE 1992 [DIRS 102588], p. 2A-20); 63 fuel rods/assembly; 2772 rods total; 1.25222 cm (0.493 in.) outer diameter; 365.76 cm (144 in.) length; 0.08636 cm (0.034 in.) cladding thickness; Zircaloy 2 density: 6550 kg/m³ (CRWMS M&O 1999 [DIRS 102933], p. 41). The calculation is as follows:

$$\begin{aligned}
 m &= \left(\frac{\pi}{4} \right) \left\{ (1.25222 \text{ cm})^2 - [(1.25222 \text{ cm}) - 2(0.08636 \text{ cm})]^2 \right\} \\
 &\quad (365.76 \text{ cm}) (6550 \text{ kg/m}^3) (2772 \text{ rods/WP}) \\
 &= (0.31491492 \text{ m}^3 / \text{WP}) (6550 \text{ kg/m}^3) \\
 &= 2062.7 \text{ kg/WP}
 \end{aligned}$$

^d CRWMS M&O 2000 [DIRS 151561], p. IV-4.

Table 10.3.1-7. Elemental Composition of Each Waste Package Material

	316NG Stainless Steel		A516 Steel		Neutronit A978		Aluminum 6061		Commercial SNF		Total
	Wt %	mol	Wt %	Mol	Wt %	mol	Wt %	mol	Wt %	mol	mol
Fe	61.8	124481	97.9	100336	66.7	24651	0.7	42	95.7	2958	252468
Mo	3.0	3518	0.0	0	0.0	0	0.0	0	0.0	0	3518
Cr	18.0	38942	0.0	0	18.5	7344	0.4	26	0.0	0	46311
Ni	14.0	26824	0.0	0	13.0	4570	0.0	0	0.0	0	31407
Al	0.0	0	0.0	0	0.0	0	96.0	11955	0.0	0	11955
Other	3.2	6446	2.1	2153	1.8	665	2.9	174	4.3	133	9571
Total	100.0	200211	100.0	102489	100.0	37230	100.0	12197	100.0	3091	355218

Source: CRWMS M&O 2000 [DIRS 151561], pp. III-4 to III-6, IV-3.

NOTE: Treat "other" as iron.

Table 10.3.1-8. Surface Area Available for Adsorption of Water Inside a 21-PWR Waste Package

Condition	Surface Area (m ²)	Comments
Initial emplacement	1023.2	Surfaces of intact fuel rods, basket components
Initial emplacement	1390.8	Includes area of SNF in 2.2 failed rods per assembly
Initial emplacement	48220.8	Includes area of SNF in all 5,544 fuel rods, but excludes surface area of fuel rod cladding
Fully degraded steel	2.58×10 ⁸	Stainless steel inner liner and all basket components converted to moles of iron that is fully oxidized to Fe ₂ O ₃

NOTE: Information based on calculations presented in Section 10.3.1.3.3.1.

Table 10.3.1-9. Effective Water Saturation in Waste Package Resulting from Adsorption of Water Vapor

WP Surface Area (m ²)	RH = 80%	RH = 90%	RH = 95%	RH = 99%
1023.2	1.584×10 ⁻⁷	2.152×10 ⁻⁷	2.887×10 ⁻⁷	5.615×10 ⁻⁷
1390.8	2.153×10 ⁻⁷	2.925×10 ⁻⁷	3.924×10 ⁻⁷	7.633×10 ⁻⁷
48220.8	7.466×10 ⁻⁶	1.014×10 ⁻⁵	1.361×10 ⁻⁵	2.646×10 ⁻⁵
2.58×10 ⁸	3.995×10 ⁻²	5.426×10 ⁻²	7.280×10 ⁻²	1.416×10 ⁻¹

NOTE: WP = waste package. Information based on Equation 10-5 and surface areas presented in Table 10.3.1-8.

Table 10.3.1-10. Values of Diffusion Coefficient Normalized to the Diffusion Coefficient in Water for Various Waste Package Surface Areas and Relative Humidities

Relative Humidity	D_s / D_{wl}			
	$S_{WP} = 1023.2 \text{ m}^2$	$S_{WP} = 1390.8 \text{ m}^2$	$S_{WP} = 48220.8 \text{ m}^2$	$S_{WP} = 2.58 \times 10^8 \text{ m}^2$
0.1	2.15×10^{-15}	3.97×10^{-15}	4.77×10^{-12}	1.37×10^{-04}
0.2	2.88×10^{-15}	5.32×10^{-15}	6.40×10^{-12}	1.83×10^{-04}
0.3	3.65×10^{-15}	6.74×10^{-15}	8.11×10^{-12}	2.32×10^{-04}
0.4	4.56×10^{-15}	8.43×10^{-15}	1.01×10^{-11}	2.90×10^{-04}
0.5	5.73×10^{-15}	1.06×10^{-14}	1.27×10^{-11}	3.64×10^{-04}
0.6	7.35×10^{-15}	1.36×10^{-14}	1.63×10^{-11}	4.67×10^{-04}
0.7	9.85×10^{-15}	1.82×10^{-14}	2.19×10^{-11}	6.26×10^{-04}
0.8	1.45×10^{-14}	2.67×10^{-14}	3.21×10^{-11}	9.19×10^{-04}
0.9	2.67×10^{-14}	4.93×10^{-14}	5.92×10^{-11}	1.70×10^{-03}
0.95	4.80×10^{-14}	8.86×10^{-14}	1.07×10^{-10}	3.05×10^{-03}
0.99	1.82×10^{-13}	3.35×10^{-13}	4.03×10^{-10}	1.15×10^{-02}

Table 10.3.1-11. Summary of Cross-Sectional Areas for Diffusion for Various Configurations at a Relative Humidity of 95 Percent

Component/ Configuration	Diffusive Path	Path Length (m)	Cross-Sect. Area (mm ²)	Diffusion Coefficient ^a (m ² /s)	$\frac{D_s A}{\Delta x}$ (m ³ /s)
Single fuel rod	Axially along fuel rod, 1/2 WP length	2.388	4.22×10^6	2.299×10^{-9}	4.06×10^{-21}
46.2 fuel rods/WP	Axially along fuel rod, 1/2 WP length	2.388	1.09	2.299×10^{-9}	1.05×10^{-15}
Initial WP surface consolidated	Axially through full length of WP	4.775	0.297	2.299×10^{-9}	1.43×10^{-16}
Initial WP surface consolidated; 46.2 failed fuel rods	Axially through full length of WP	4.775	0.405	2.299×10^{-9}	1.95×10^{-16}
Initial WP surface consolidated; no cladding	Axially through full length of WP	4.775	14.0	2.299×10^{-9}	6.74×10^{-15}
Initial WP surface as porous medium	Axially through 1/2 length of WP	2.388	1.593×10^6 ^c	2.04×10^{-22} ^d	1.36×10^{-22}
SCCs (filled with porous corrosion products)	Axially through SCCs in lids	0.135 ^b	102.	1.126×10^{-12}	8.50×10^{-16}
Fully degraded WP surface consolidated	Axially through 1/2 length of WP	2.388	7.5×10^4	2.299×10^{-9}	7.22×10^{-11}

Table 10.3.1-11. Summary of Cross-Sectional Areas for Diffusion for Various Configurations at a Relative Humidity of 95 Percent (Continued)

Component/ Configuration	Diffusive Path	Path Length (m)	Cross-Sect. Area (mm ²)	Diffusion Coefficient ^a (m ² /s)	$\frac{D_s A}{\Delta x}$ (m ³ /s)
Fully degraded WP; porous medium	Axially through ½ length of WP	2.388	1.593×10 ^{6c}	1.80×10 ⁻¹²	1.20×10 ⁻¹²
Corrosion patch (1)	Radially outward through patch in Alloy 22	0.02	2.346×10 ⁴	1.126×10 ⁻¹²	1.32×10 ⁻¹²
Corrosion patch (10)	Radially outward through patches in Alloy 22 layer	0.02	2.346×10 ⁵	1.126×10 ⁻¹²	1.32×10 ⁻¹¹
DHLW surface consolidated	Axially through ½ length of WP	2.388	0.932 ^e	2.299×10 ⁻⁹	8.96×10 ⁻¹⁶

NOTES: ^a Self-diffusion coefficient of water is used except for porous media in waste packages and in corrosion patches, which use effective diffusion coefficients.

^b For 21-PWR; thickness of inner lid and closure lid plus the air gap between lids (CRWMS M&O 2000 [DIRS 153940], p. 65).

^c WP cross section; inner diameter = 1.424 m (see Table 10.3.1-4).

^d $D_s / D_{wl} = 8.86 \times 10^{-14}$ (for initial surface area = 1,390.8 m²/waste package, as in Table 10.3.1-10).

^e From adsorption isotherm (Equation 10-1), 15.73 monolayers adsorbed at a relative humidity of 0.95. Thickness of each monolayer of water is 2.83×10^{-10} m from Equation 10-3. From CRWMS M&O (2001 [DIRS 153846], p. 45, Table 6), the mean surface area of each of 5 glass logs in a DHLW package is 100 m², or 500 m²/waste package. Then area = (15.73 monolayers) (2.83×10^{-10} m/monolayer) (500 m²/package)/(2.388 m) = 9.32×10^{-7} m².

WP = waste package.

Table 10.3.1-12. Parameters to be Sampled for In-Package Diffusion Model

Parameter		Range	Distribution	Comments
Path length (m)	1	0.02 – 4.775	Uniform	Applicable range depends on controlling diffusion pathway: 1. In-package along fuel rods 2. In-package axially through porous corrosion products (only breaches are stress corrosion cracks) 3. In-package radially through porous corrosion products (general corrosion patches present) 4. Through breaches.
	2	0.02 – 4.775	Uniform	
	3	0.02 – 0.712	Uniform	
	4	0.02 – 0.07	Uniform	
Steel corrosion rate ($\mu\text{m}/\text{yr}$)	1	23.5 – 95.34	Normal; median = 59.42	First range and distribution applies to 1/3 of total mass of steel; second applies to 2/3 of total mass, in approx. proportion to mass of mild steel and stainless steel in waste package (see Table 10.3.1-7). Ranges and median values from CRWMS M&O 2001 [DIRS 153846], Tables 26 & 29
	2	0.0879 – 45.5	Log uniform	
Waste package surface area factor, f_{WPs}		0.01 to 100	Log triangular; most likely value = 1.0	Multiplies surface computed from extent of degradation

Table 10.3.4-1. Summary of Partition Coefficient Ranges on Corrosion Products, Sand, and Loam

Element	Substrate or Conditions	Median or Best Estimate (ml/g)	Range (ml/g)	Source/Comments
Americium	Sand	1,900	8.2 to 300,000	Sheppard and Thibault 1990 [DIRS 109991], Table 3
	Loam	9,600	400 to 48,309	
	Iron (hydr)oxides	10,000	1,000 to 20,000	EPRI 2000 [DIRS 154149], Table 6-9
	Oxidizing ^a	5,000	85 to 40,000	Onishi et al. 1981 [DIRS 154420], Table 8.96
	Iron oxide	–	1,000 to 5,000	CRWMS M&O 2001 [DIRS 154024], Table 2a
Iodine	Sand	1	0.04 to 81	Sheppard and Thibault 1990 [DIRS 109991], Table 3
	Loam	5	0.1 to 43	
	Iron (hydr)oxides	0	0 to 1	EPRI 2000 [DIRS 154149], Table 6-9. Maximum value based on IO_3^- on magnetite and goethite.
	Oxidizing ^a	10	0 to 75	Onishi et al. 1981 [DIRS 154420], Table 8.96
	Copper oxide and copper sulfide	–	58 to 1,375	Balsley et al. 1998 [DIRS 154439], Table 1, p. 135

Table 10.3.4-1. Summary of Partition Coefficient Ranges on Corrosion Products, Sand, and Loam
(Continued)

Element	Substrate or Conditions	Median or Best Estimate (ml/g)	Range (ml/g)	Source/Comments
Neptunium	Sand	5	0.5 to 390	Sheppard and Thibault 1990 [DIRS 109991], Table 3
	Loam	25	1.3 to 79	
	Iron (hydr)oxides	1	0.1 to 1,000	EPRI 2000 [DIRS 154149], Table 6-9. Values reduced by about 2 orders of magnitude because uranium species will dominate sorption sites
	Oxidizing ^a	10	0.2 to 127	Onishi et al. 1981 [DIRS 154420], Table 8.96
	Iron oxide	–	500 to 1,000	CRWMS M&O 2001 [DIRS 154024], Table 2a
Plutonium	Sand	550	27 to 36,000	Sheppard and Thibault 1990 [DIRS 109991], Table 3
	Loam	1,200	100 to 5,933	
	Iron (hydr)oxides	10,000	1,000 to 20,000	EPRI 2000 [DIRS 154149], Table 6-9
	Oxidizing ^a	50,000	100 to 100,000	Onishi et al. 1981 [DIRS 154420], Table 8.96
	Iron oxide	–	1,000 to 5,000	CRWMS M&O 2001 [DIRS 154024], Table 2a
Technetium	Sand	0.1	0.01 to 16	Sheppard and Thibault 1990 [DIRS 109991], Table 3
	Loam	0.1	0.01 to 0.4	
	Iron (hydr)oxides	0	0 to 1,000	EPRI 2000 [DIRS 154149], Table 6-9. Maximum value assumes reduction of technetium on iron oxide surface
	Oxidizing*	5	0 to 100	Onishi et al. 1981 [DIRS 154420], Table 8.96
	Copper oxide and copper sulfide	–	31 to 67	Balsley et al. 1998 [DIRS 154439], Table 2, p. 139
	Sediment	4.3 (Oxic) 13.7 (Anoxic)	Not provided	Bird and Schwartz 1997 [DIRS 154488]. Sediment-water ratio is 1 percent; sand-water and clayey silt/sand-water ratios are 10 percent
	Sand	0.2 (Oxic) (Anoxic)		
Clayey silt and sand	(Oxic) 0.5 (Anoxic)			
Thorium	Sand	3,200	207 to 150,000	Sheppard and Thibault 1990 [DIRS 109991], Table 3
	Loam	3,300	No Data	
	Iron (hydr)oxides	10,000	1,000 to 20,000	EPRI 2000 [DIRS 154149], Table 6-9
	Oxidizing ^a	10,000	10 ³ to 10 ⁶	Onishi et al. 1981 [DIRS 154420], Table 8.96
	Iron oxide	–	1,000 to 5,000	CRWMS M&O 2001 [DIRS 154024], Table 2a
Uranium	Sand	35	0.03 to 2,200	Sheppard and Thibault 1990 [DIRS 109991], Table 3
	Loam	15	0.2 to 4,500	

Table 10.3.4-1. Summary of Partition Coefficient Ranges on Corrosion Products, Sand, and Loam (Continued)

Element	Substrate or Conditions	Median or Best Estimate (ml/g)	Range (ml/g)	Source/Comments
Uranium (continued)	Iron (hydr)oxides	1,000	50 to 10,000	EPRI 2000 [DIRS 154149], Table 6-9
	Oxidizing ^a	50	16 to 1000	Onishi et al. 1981 [DIRS 154420], Table 8.96
	Iron oxide	-	100 to 1000	CRWMS M&O 2001 [DIRS 154024], Table 2a

NOTE: ^aData encompass values in fresh water and seawater, with an emphasis on oxidizing conditions. Values shown are the minimums of the fresh or seawater cases for these elements.

Table 10.3.4-2. Expected Material Lifetimes of Invert, Pallet, and Waste Package Components in the Drift

Component	Material	Thickness (mm)	Lifetime ^a (yrs)	Source for Components, Materials, and Thickness
Invert and Pallet Components				
Transverse support beam	Mild carbon steel	14.61	246	BSC 2001 [DIRS 154441], Table 1 for the W 12 x 53 beam and Section 5.1.10
Gantry rail	Mild carbon steel	31.75	534	BSC 2001 [DIRS 154441], Table 1 for the crane rail and Section 5.1.5
Waste Package Components				
WP inner barrier	316NG stainless steel	50	25000	CRWMS M&O 2000 [DIRS 151561], Table 24
Basket guide	A 516 carbon steel	10	168	CRWMS M&O 2000 [DIRS 151561], Table 24
Basket plate	Neutronit A 978	7	175	CRWMS M&O 2000 [DIRS 151561], Table 24

NOTE: ^aLifetime is calculated as thickness divided by median corrosion rate. The median corrosion rates are 0.05942 mm/yr for mild carbon steel, 0.002 mm/yr for Stainless Steel Type 316L, and 0.04 mm/yr for borated stainless steel similar to Neutronit A 978 (CRWMS M&O 2000 [DIRS 151561], Tables 29, 26, and 30, respectively). Lifetimes for components fabricated from Alloy 22 or titanium are not shown because they are longer than for steel components and because iron-(hydr)oxides are the main sorbers of interest. WP = waste package.

Table 10.3.4-3. Calculated Mass of Sorbing Material in the Waste Package

Waste Package Type	Mass of Iron (kg/WP)	Mass of Fe ₂ O ₃ (kg/WP)
21-PWR	13,932	19,904
44-BWR	15,655	22,364
5-DHLW	12,333	17,619
Naval SNF	10,758	15,369

Source: Schreiner 2001 [DIRS 155038], Item 3.

NOTE: WP = waste package; SNF = spent nuclear fuel.

Table 10.3.4-4. Summary of Tolerance Interval Calculations for Sand, Loam, and Clay Data Sets

Element	Number of Data Points	ln(Mean)	ln(SD)	Mean K_d (ml/g)	K_d Range (ml/g)	Tolerance Interval Factor	Tolerance Interval (ml/gm)
Americium	60	2.2	2.21	4400	82 to 400,000	2.33	25 to 770,000
Iodine	63	0.86	2.1	2.4	0.04 to 81	2.37	0.02 to 300
Neptunium	31	2.2	1.7	10.8	0.4 to 575	2.54	0.039 to 2,900
Plutonium	78	1.9	1.7	1100	24 to 190,000	2.28	13 to 94,000
Technetium	33	1.5	1.8	0.16	0.01 to 16	2.51	0.004 to 6.2
Thorium	16	2.2	2.1	3600	24 to 160,000	2.91	6.8 to 1,900,000
Uranium	39	3.4	3.2	53	0.03 to 390,000	2.45	0.012 to 230,000

Source: Schreiner 2001 [DIRS 155038], Items 1, 5, 6, 8, 9, 10, and 11.

Table 10.3.4-5. Fraction of Contaminant Metal Irreversibly Sorbed

Element	Fraction Irreversibly Sorbed
Americium	0.6
Iodine	0.9
Plutonium	0.99
Technetium	0.1
Thorium	0.99
Uranium	0.1

Source: Brady et al. 1999 [DIRS 154421], Table 3.4.

Table 10.3.5-1. Summary of Uncertainties Considered for Engineered Barrier System Colloids

Uncertainty	Estimated Significance	Considered in TSPA-SR ^a
Potential contribution of irreversibly attached radionuclides on colloids generated from commercial spent fuel	High	No
Quantities of colloids generated from corrosion of steel	High	Yes
Potential contribution of colloids from degradation of metallic fuel	Potentially high	No
Colloid stability and concentration dependence on temperature	Unknown	No
Suitability of smectite as proxy for all groundwater colloids	Low	Yes
Flow rate within the waste package	Low	No
Colloid sorption onto the air-water interface	Potentially moderate	No
Potential effects on the total colloid population of organic material, including introduced organics and microbes	Potentially high	Partially
Wide range of distribution coefficients (K_d s) used to describe sorption of radionuclides on colloids	High	Yes
Better-justified upper-bound maximum concentration of plutonium irreversibly attached to colloids	Unknown	Yes
Consideration of radionuclides other than plutonium and americium	Low to moderate	No

NOTE: ^a CRWMS M&O 2000 [DIRS 153246], Section 3.5.6.

Table 10.3.5-2. Summary of Recommended Parameter Changes for Total System Performance Assessment

Parameter	TSPA-SR ^a Parameter Values			New Recommendations for TSPA		
	Value	Range	Distribution	Value	Range	Distribution
Combined corrosion and groundwater colloids	Determined by function	Corrosion: 10 ⁻³ mg/L to 1 mg/L Groundwater: 3 x 10 ⁻⁶ to 3 x 10 ⁻² mg/L	–	Sampled	3 x 10 ⁻⁶ to 10 ⁻¹ mg/L for I ≤ 0.05M; 10 ⁻⁹ to 10 ⁻³ mg/L for I > 0.05M	Log uniform
Range of irreversibly attached plutonium concentration on waste form colloids	Determined by function	8 x 10 ⁻⁸ mol/L to 1 x 10 ⁻¹¹ mol/L	–	Sampled	10 ⁻¹¹ to 10 ⁻⁶ mol/L for I ≤ 0.05M; 10 ⁻¹⁴ to 10 ⁻⁸ mol/L for I > 0.05M	Log uniform
K _d s of plutonium and americium on colloids	Pu: 10 ⁴ ml/g Am: 10 ⁵ ml/g	–	Log-normal σ = 10	Sampled with geometric mean values of 10 ⁵ ml/g for Pu and Am	–	Log-normal with geometric standard deviation σ = 100

NOTE: ^a CRWMS M&O 2000 [DIRS 153246], Section 3.5.6. I = ionic strength.

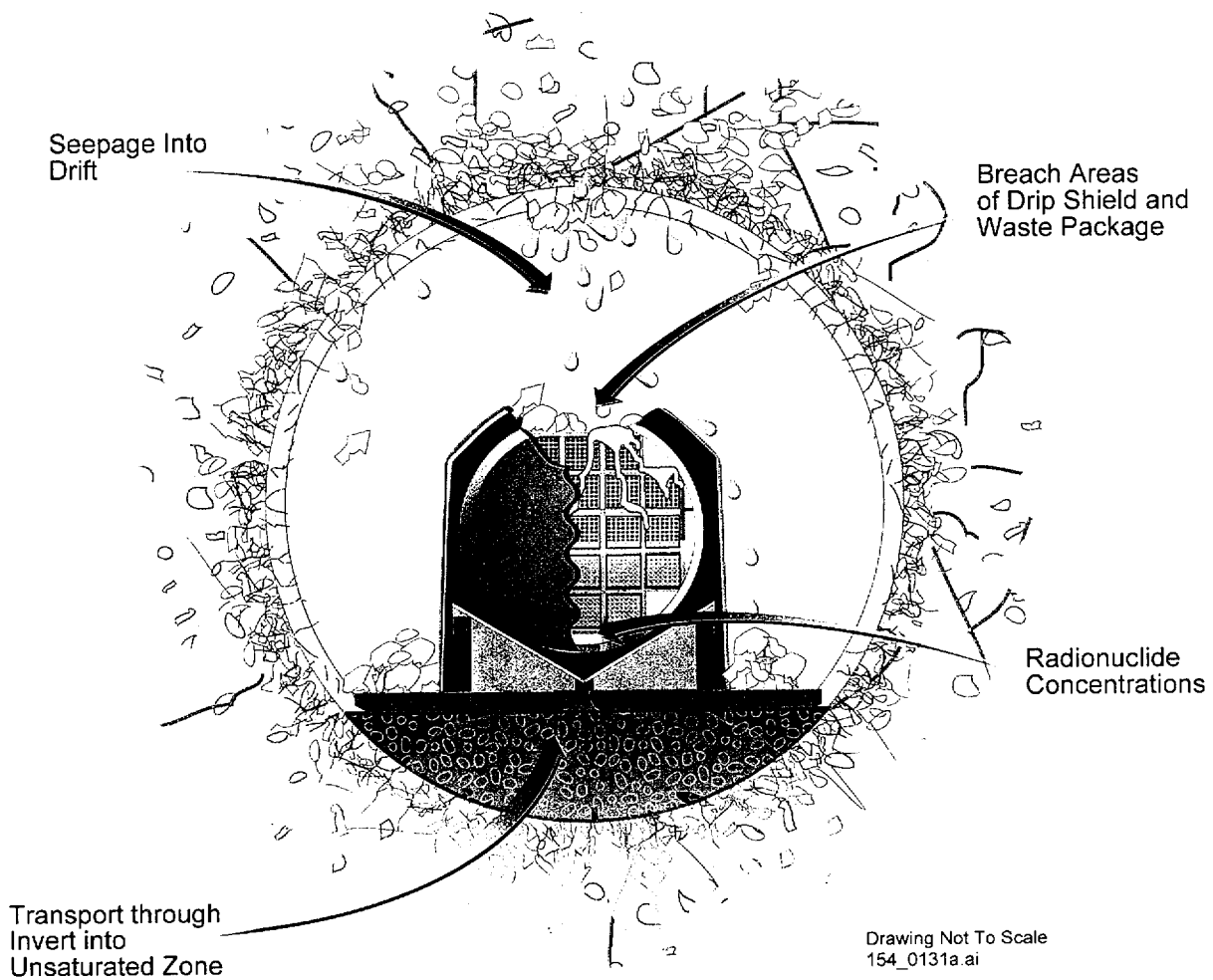
Table 10.3.6-1. Distribution of Uranium Uptake for Microbial Transport

Statistical Parameter	mg Uranium/gm Dry Cell Weight
Average (mean)	162.88
Median	111.33
Standard deviation	133.05
Minimum value	45.2
Maximum value	615

Source: Jolley 2001 [DIRS 154823].

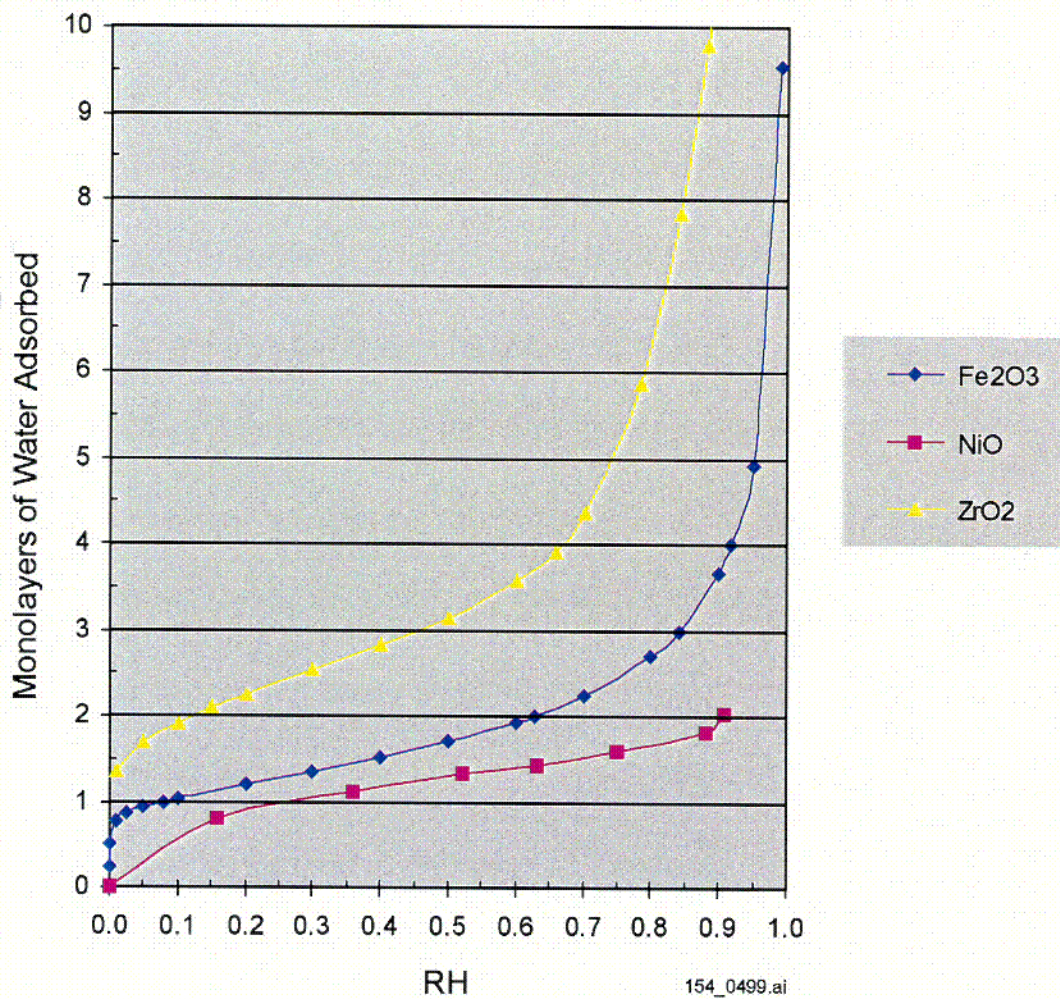
Table 10.4.4-1. Recommended Ranges and Distribution Type for the Partition Coefficients (K_ds) of Dissolved Radionuclides

Element	K _d Range for Corrosion Products (ml/g)	K _d Range from Tolerance Interval (ml/g)	Recommended K _d Range (ml/g)	Recommended Distribution Type
Americium	85 to 5,000	25 to 770,000	25 to 5,000	Log uniform
Iodine	0 to 10	0.02 to 300	0.02 to 10	Log uniform
Neptunium	0.1 to 79	0.039 to 2,900	0.039 to 79	Log uniform
Plutonium	100 to 5,000	13 to 94,000	13 to 5,000	Log uniform
Technetium	0 to 5	0.004 to 6.2	0.004 to 5	Log uniform
Thorium	1,000 to 5,000	6.8 to 1,900,000	6.8 to 5,000	Log uniform
Uranium	0.2 to 1,000	0.012 to 230,000	0.012 to 1,000	Log uniform



154_0131a.ai

Figure 10.2-1. Conceptualization of an Emplacement Drift after the Drip Shield and Waste Package are Breached and Radionuclides can Transport through the Engineered Barrier System

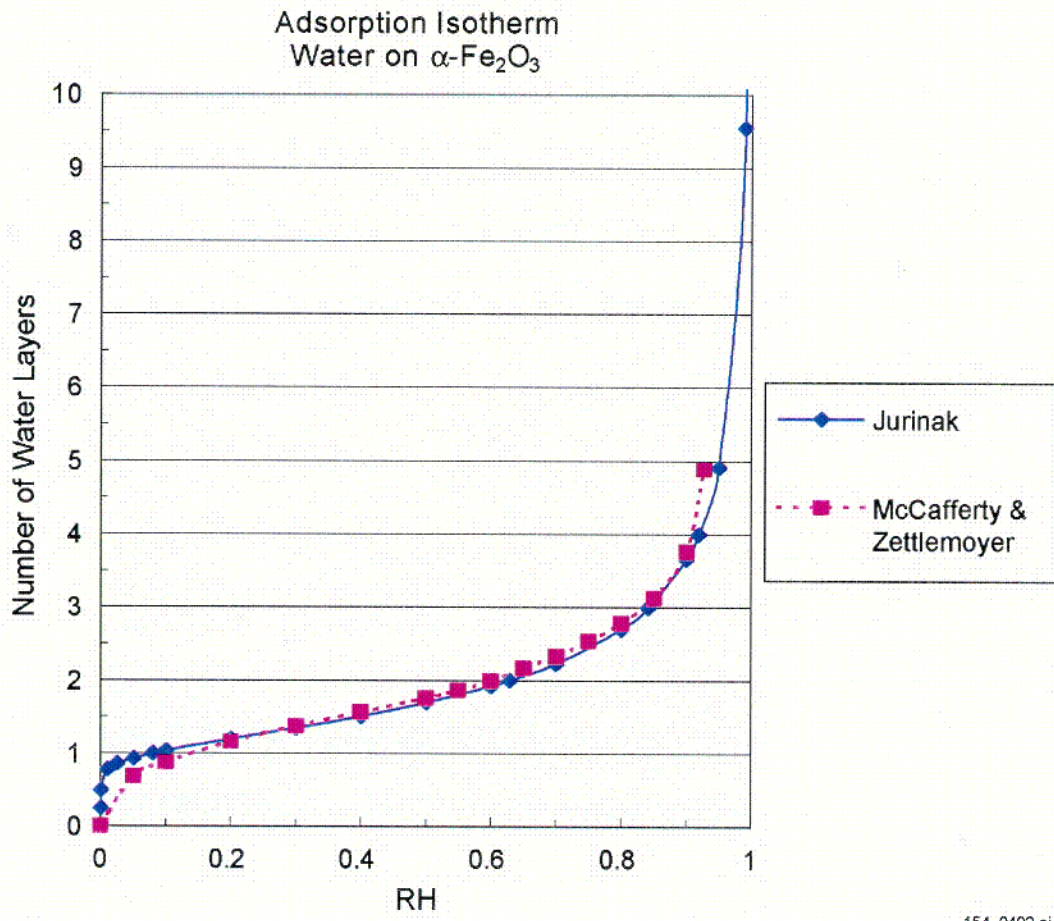


154_0499.ai

Source: Jurinak 1964 [DIRS 154381]; Lee 1994 [DIRS 154380]; Holmes et al. 1974 [DIRS 154379].

Figure 10.3.1-1. Comparison of Adsorption Isotherms for Water Vapor on Fe₂O₃, NiO, and ZrO₂

COI



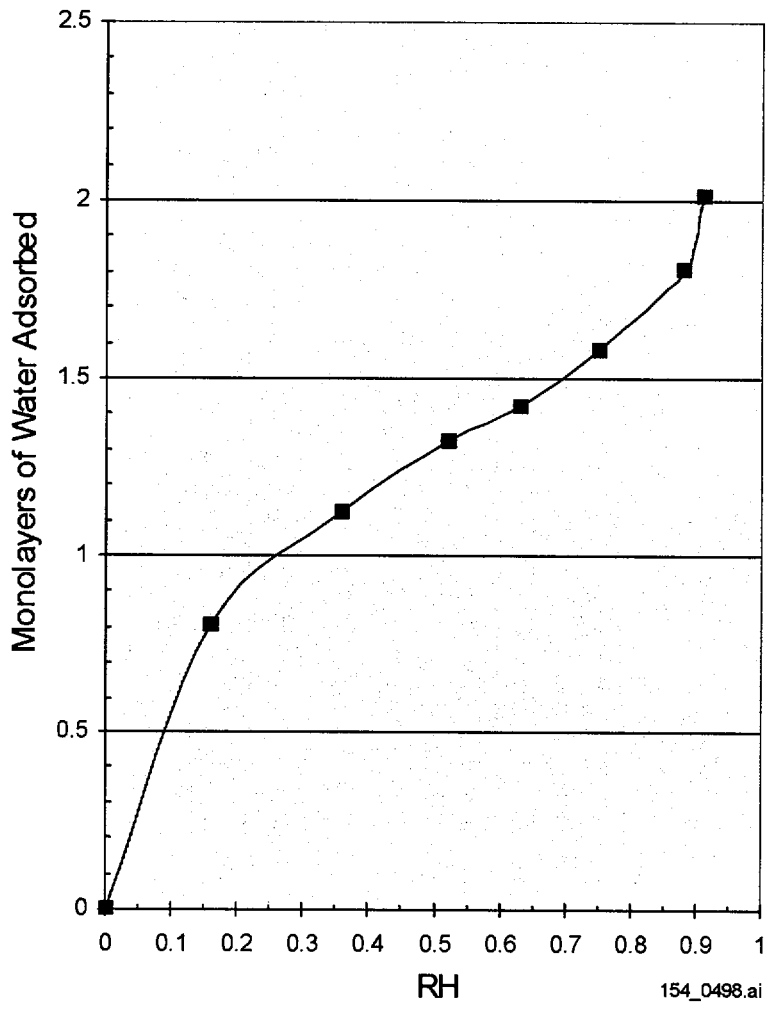
154_0402.ai

154_0402.ai

Source: Jurinak curve: Jurinak 1964 [DIRS 154381]; McCafferty and Zettlemoyer curve: McCafferty and Zettlemoyer 1970 [DIRS 154378].

Figure 10.3.1-2. Adsorption Isotherm for Water Vapor on $\alpha\text{-Fe}_2\text{O}_3$

CO2



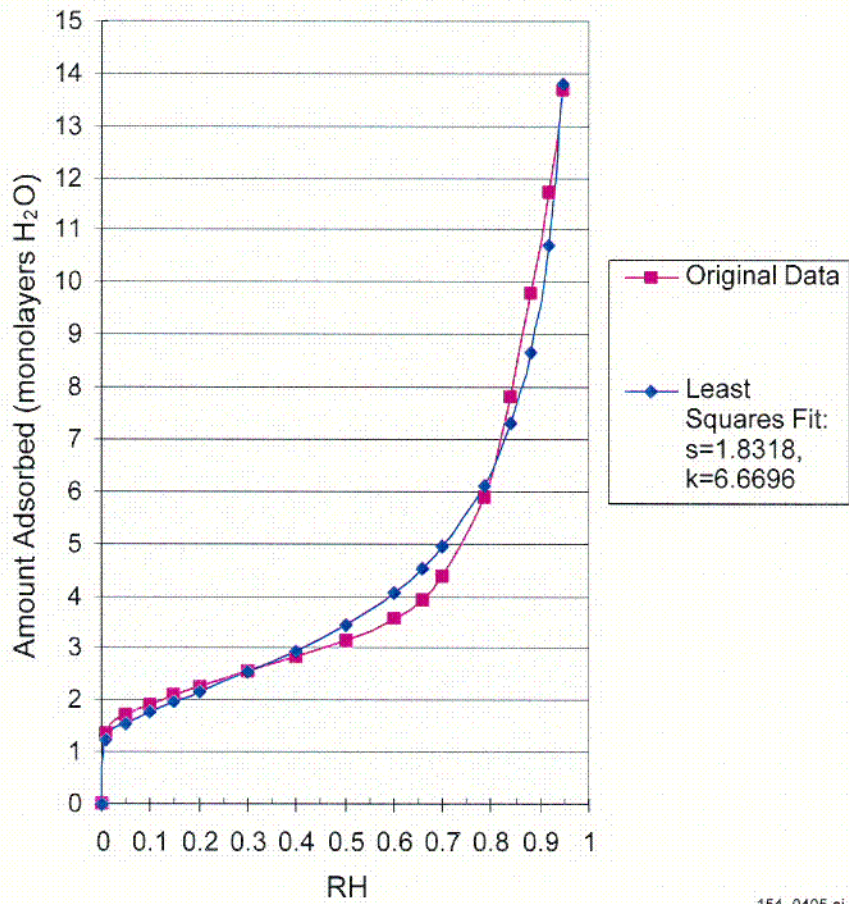
154_0498.ai

Source: Lee 1994 [DIRS 154380].

NOTE: RH = relative humidity.

Figure 10.3.1-3. Adsorption Isotherm for Water on Nickel

Adsorption of Water on ZrO_2 at 25°C
 Least Squares Fit to: $\theta_a = [-k/\ln RH]^{1/s}$



154_0405.ai

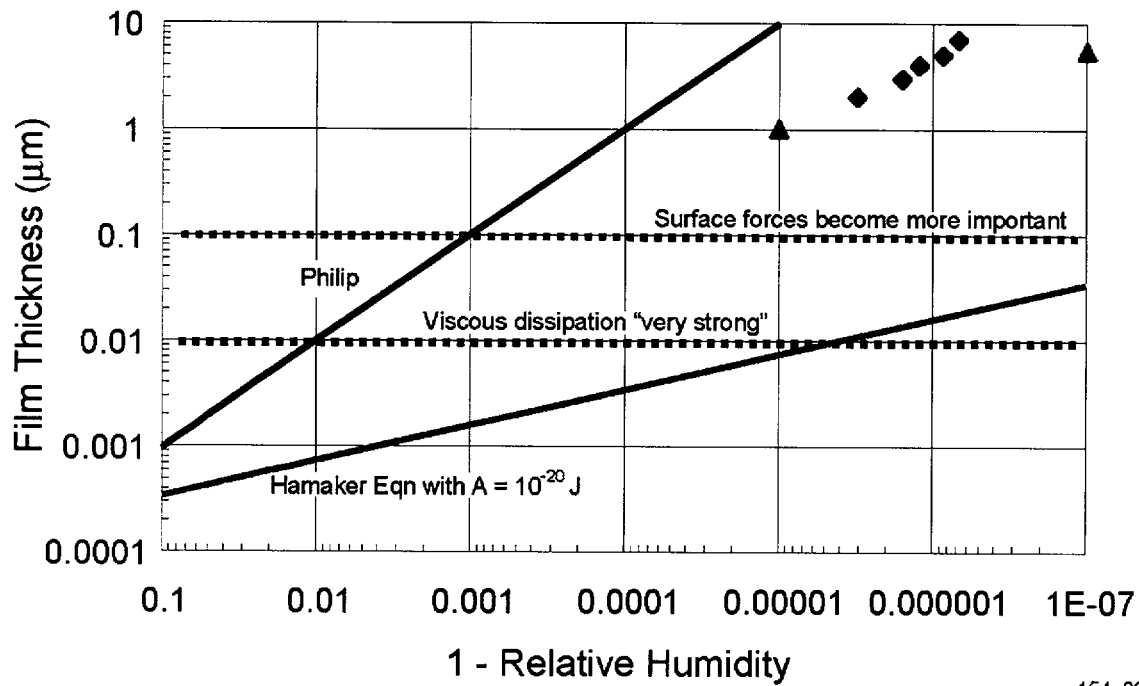
154_0405.ai

Source: Holmes et al. 1974 [DIRS 154379].

NOTE: $R^2 = 0.98$.

Figure 10.3.1-4. Regression Fit to Adsorption Isotherm Data for Water Vapor on ZrO_2

CO3A



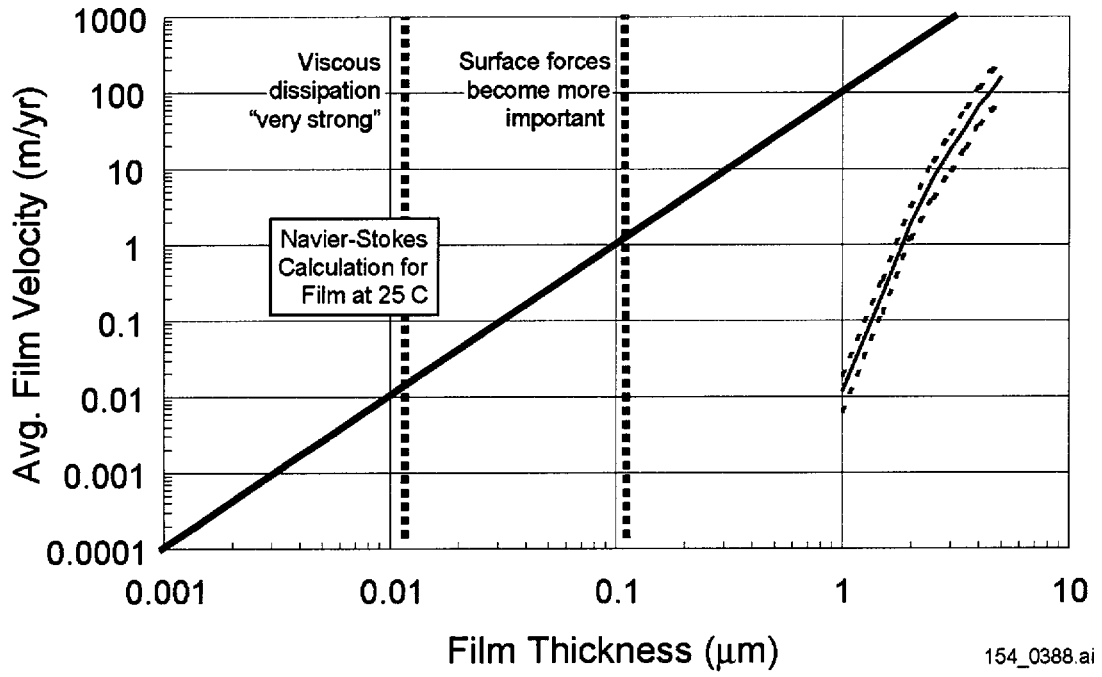
154_0387.ai

154_0387.ai

Source: Tokunaga and Wan 1997 [DIRS 139195]; Tokunaga et al. 2000 [DIRS 152914]; Philip 1977 [DIRS 152255].

NOTE: Literature data from Tokunaga and Wan (1997 [DIRS 139195]) for Bishop Tuff representing the range from Tokunaga et al. (2000 [DIRS 152914]) for rough glass.

Figure 10.3.2-1. Film Thickness Data and Predictive Relationships from the Literature

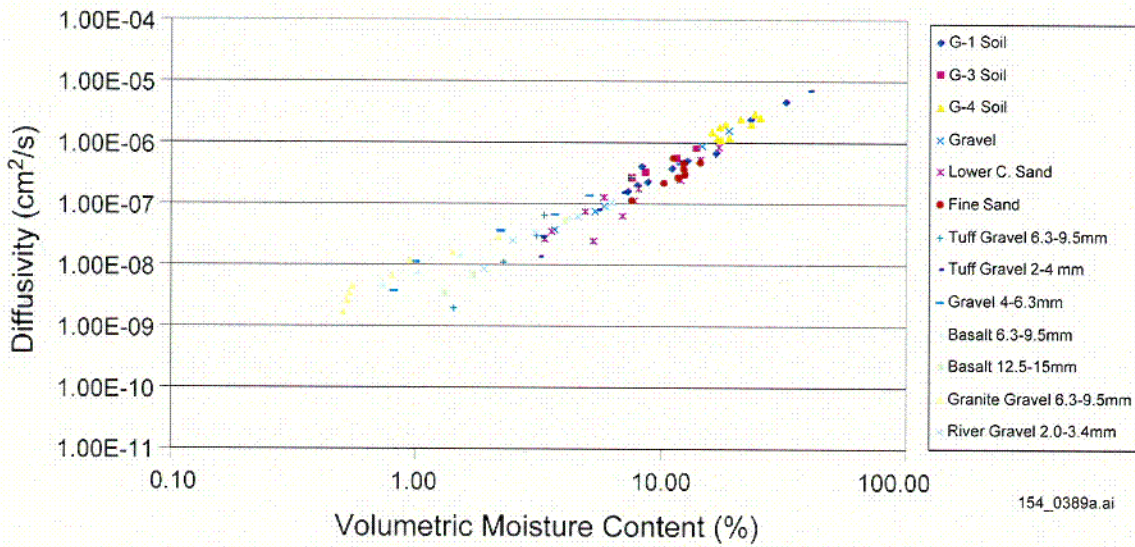


154_0388.ai

Source: Fluid velocity and uncertainty from Tokunaga et al. (2000 [DIRS 152914], Figure 10).

NOTE: Comparison of fluid velocity and uncertainty results with the one-dimensional Navier-Stokes calculation for a Newtonian fluid.

Figure 10.3.2-2. Average Film Flow Velocity versus Film Thickness



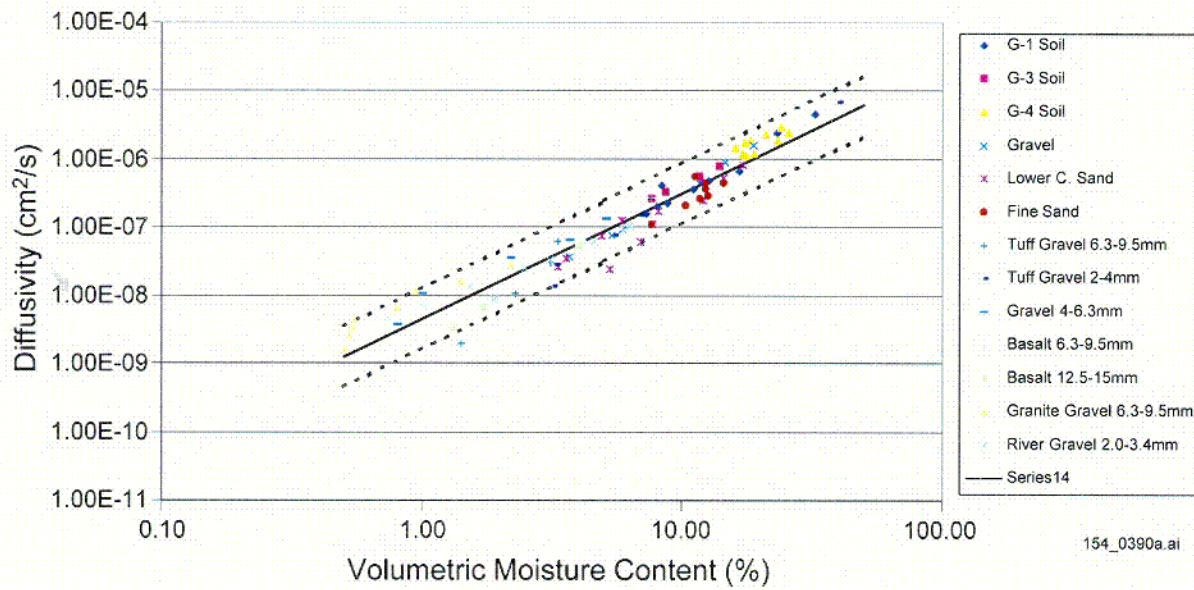
154_0389a.ai

Source: Conca and Wright 1992 [DIRS 100436]; DTN: MO9810SPA00026.000 [DIRS 137076].

NOTE: Moisture content in the range of 0.5 percent to 40 percent.

Figure 10.3.3-1. Measured Diffusivity for Various Granular Media as a Function of Volumetric Moisture Content

CO3B



154_0390a.ai

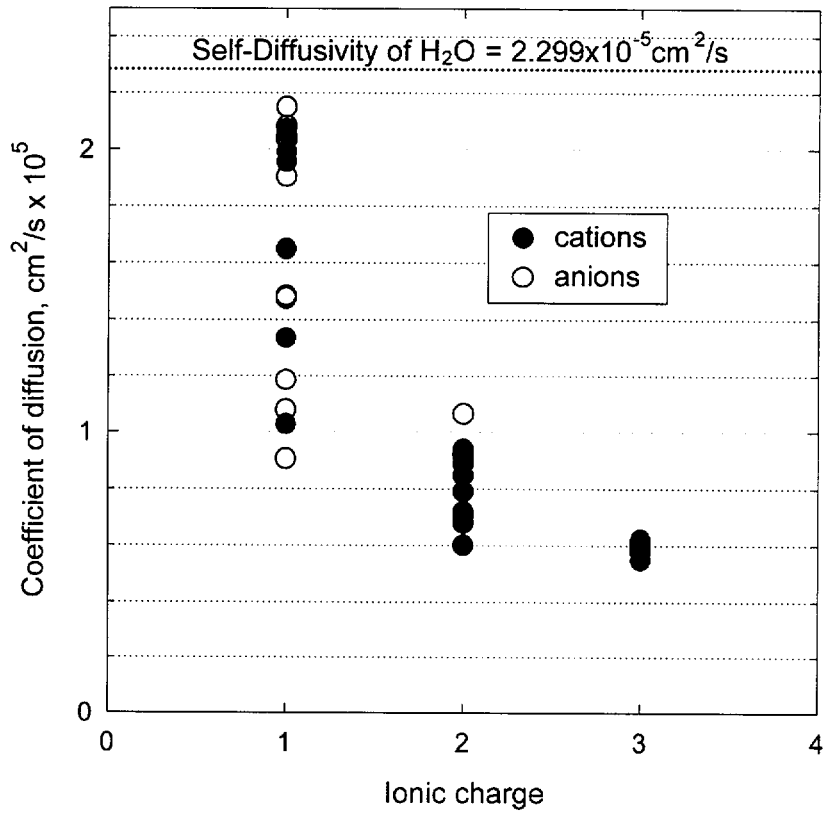
Source: Schreiner 2001 [DIRS 155038], Item 2.

NOTE: The dashed lines correspond to two standard deviations above and below the statistical fit to the data. This uncertainty was included in the TSPA-SR (CRWMS M&O 2000 [DIRS 153246]).

Figure 10.3.3-2. Uncertainty in the Statistical Fit for the Diffusion Coefficient

C04

Limiting diffusion coefficients for anions and simple (non-complexed) cations

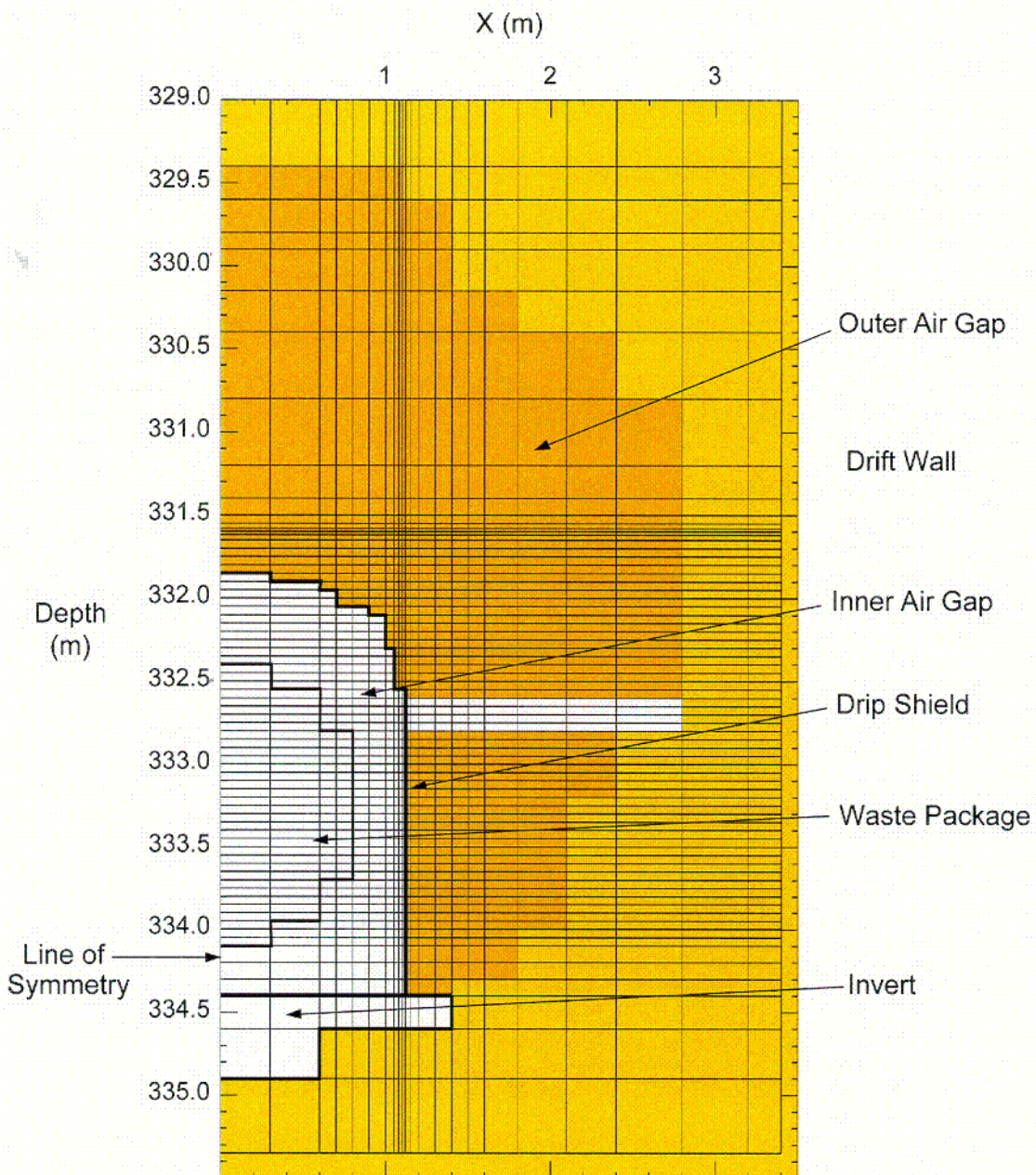


154_0391.ai

154_0391.ai

Source: CRWMS M&O 2000 [DIRS 153940], Section 6.4.1.1.

Figure 10.3.3-3. Limiting Diffusion Coefficients for Anions and Simple (Non-Complexed) Cations



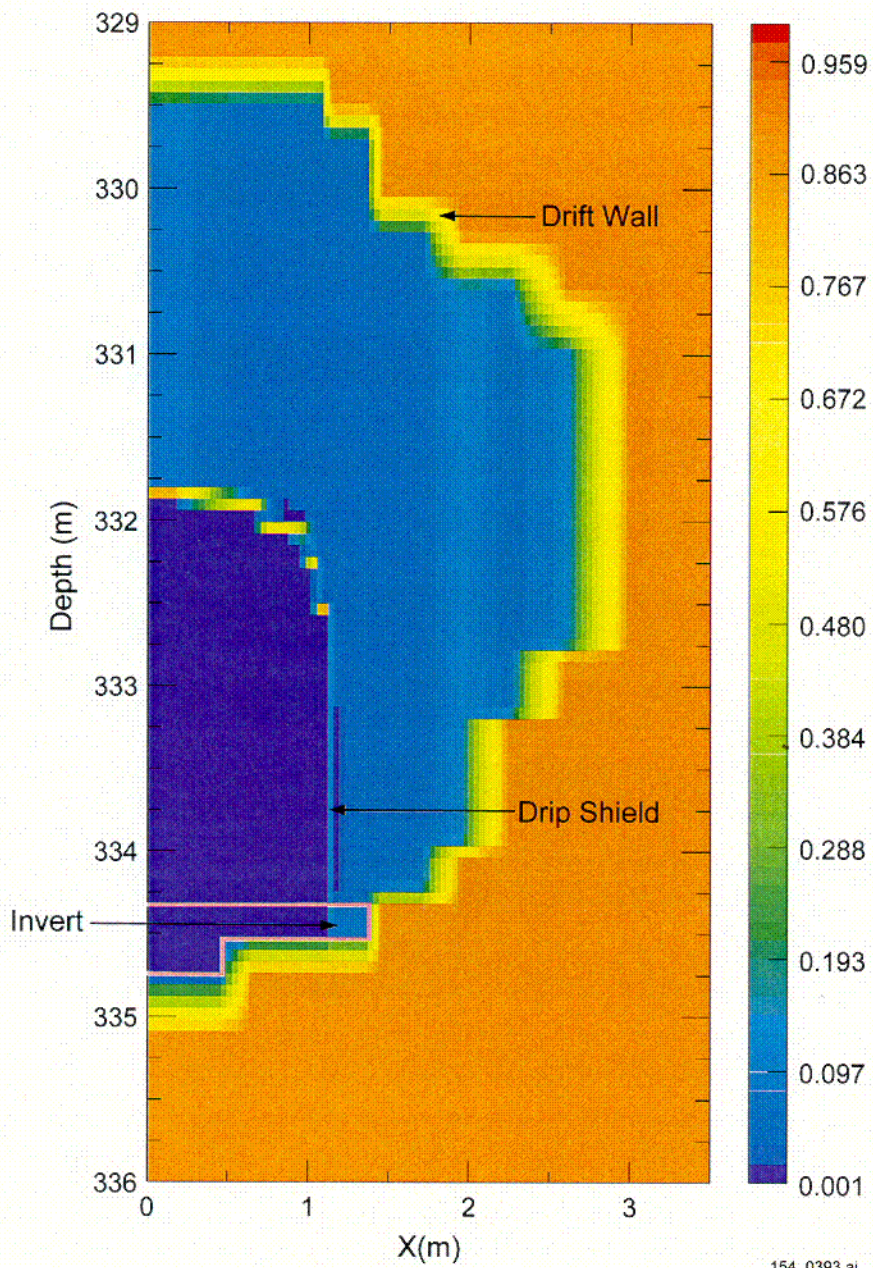
154_0392.ai

154_0392.ai

Source: Schreiner 2001 [DIRS 155038], Item 7.

Figure 10.3.3-4. Grid for NUFT Calculation of Invert Saturation

C05



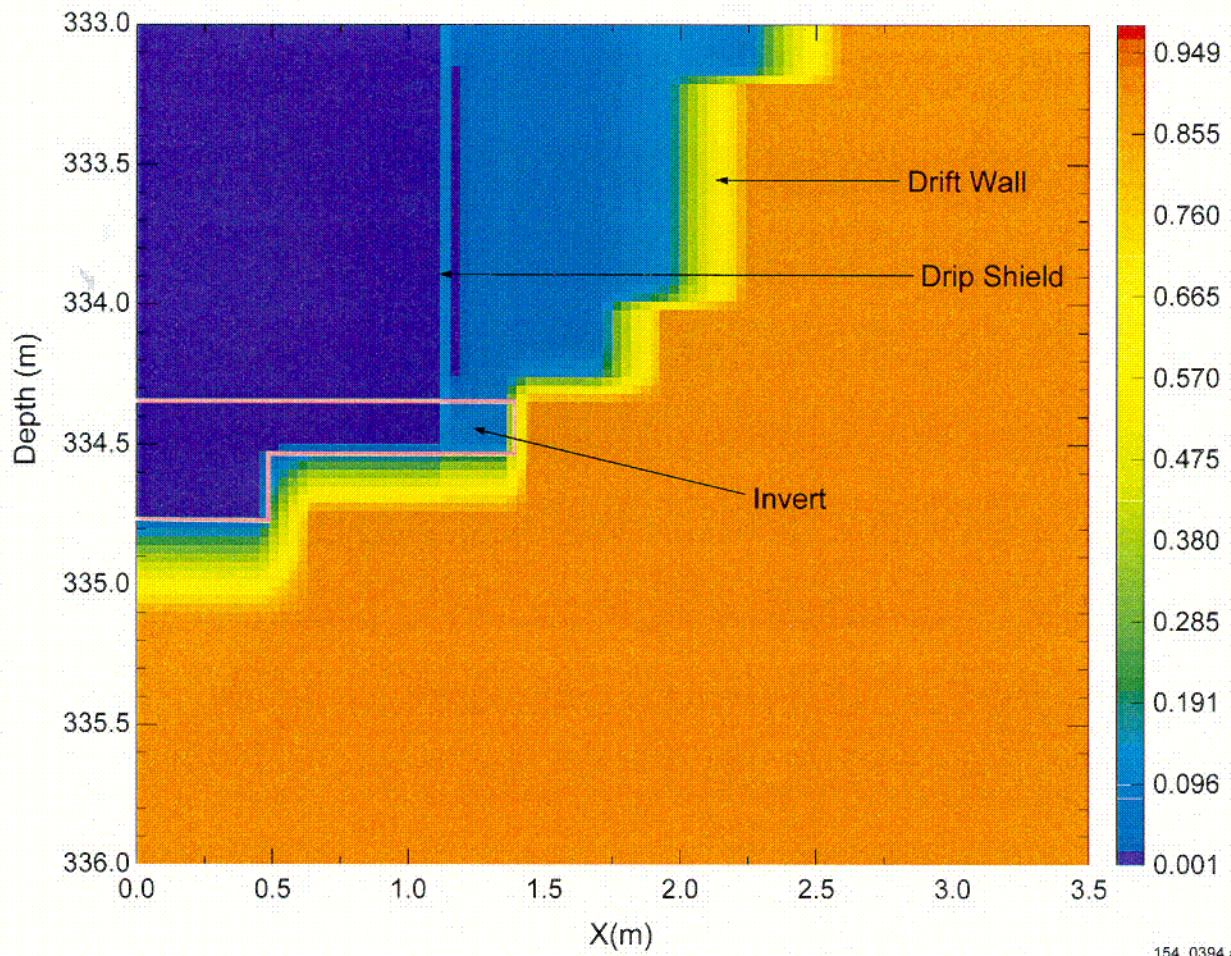
154_0393.ai

Source: Schreiner 2001 [DIRS 155038], Item 7.

NOTE: Infiltration rate of 35 mm/yr.

Figure 10.3.3-5. Liquid Saturation in the Engineered Barrier System at 10,000 Years

CO6



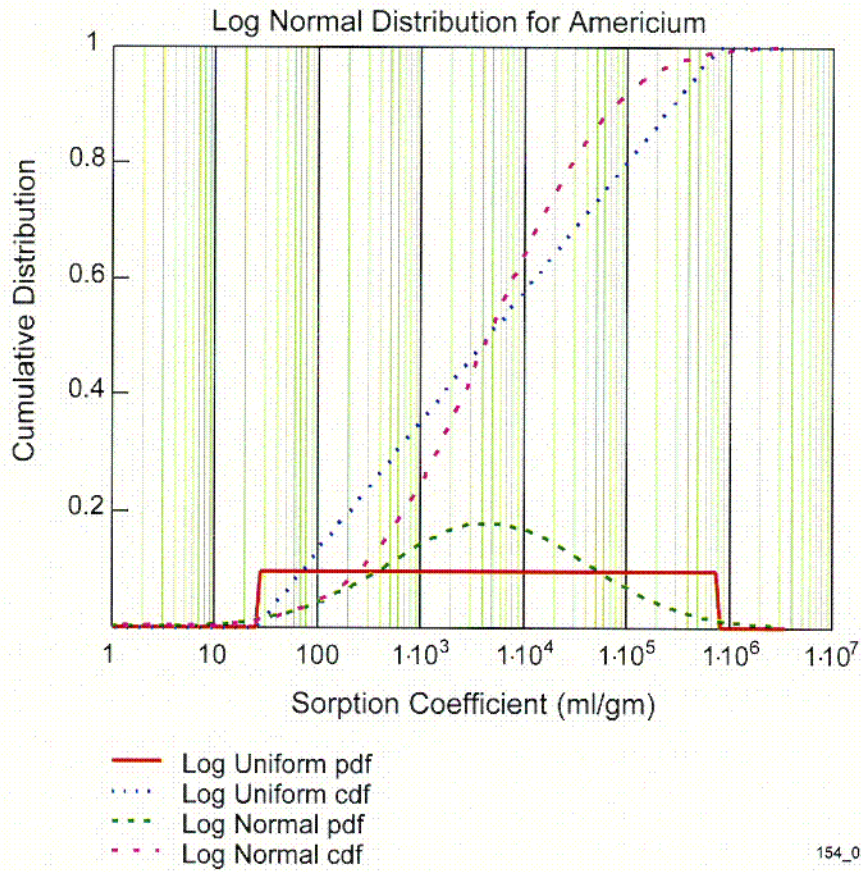
154_0394.ai

Source: Schreiner 2001 [DIRS 155038], Item 7.

NOTE: Infiltration rate of 35 mm/yr.

Figure 10.3.3-6. Liquid Saturation in the Invert at 10,000 Years

C07



154_0395.ai

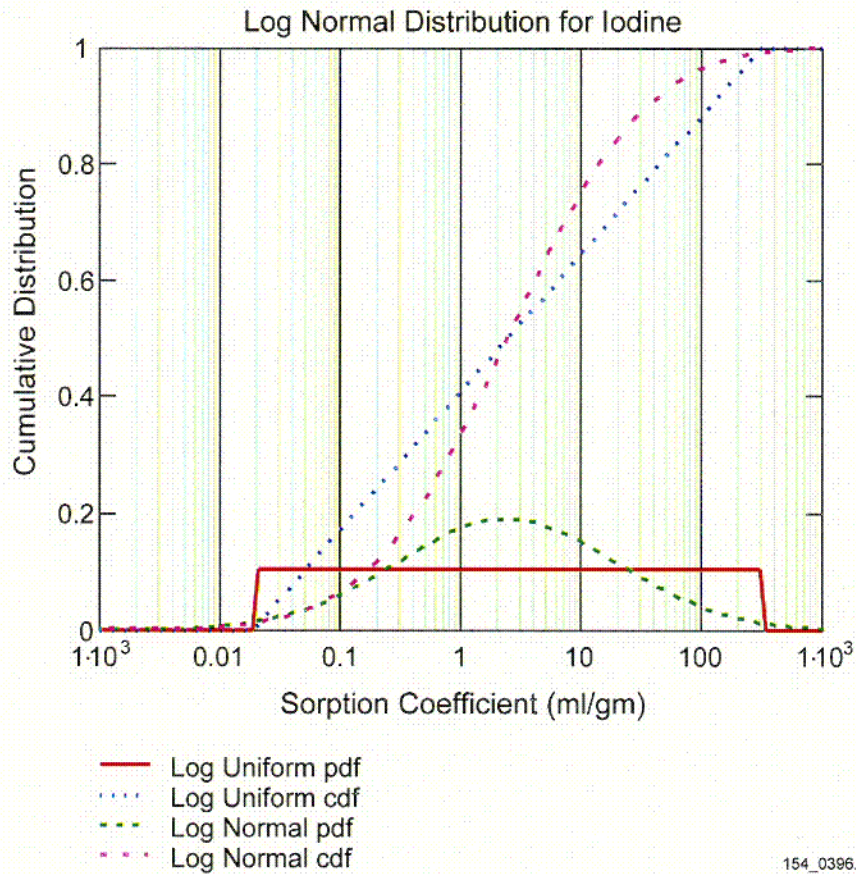
154_0395.ai

Source: Sheppard and Thibault 1990 [DIRS 109991].

NOTE: Comparison based on the tolerance interval for the 95 percent confidence level with the combined sand, loam, and clay data sets.

Figure 10.3.4-1. Comparison of Log-Normal and Log-Uniform Distributions for the Partition Coefficient of Americium

C08



154_0396.ai

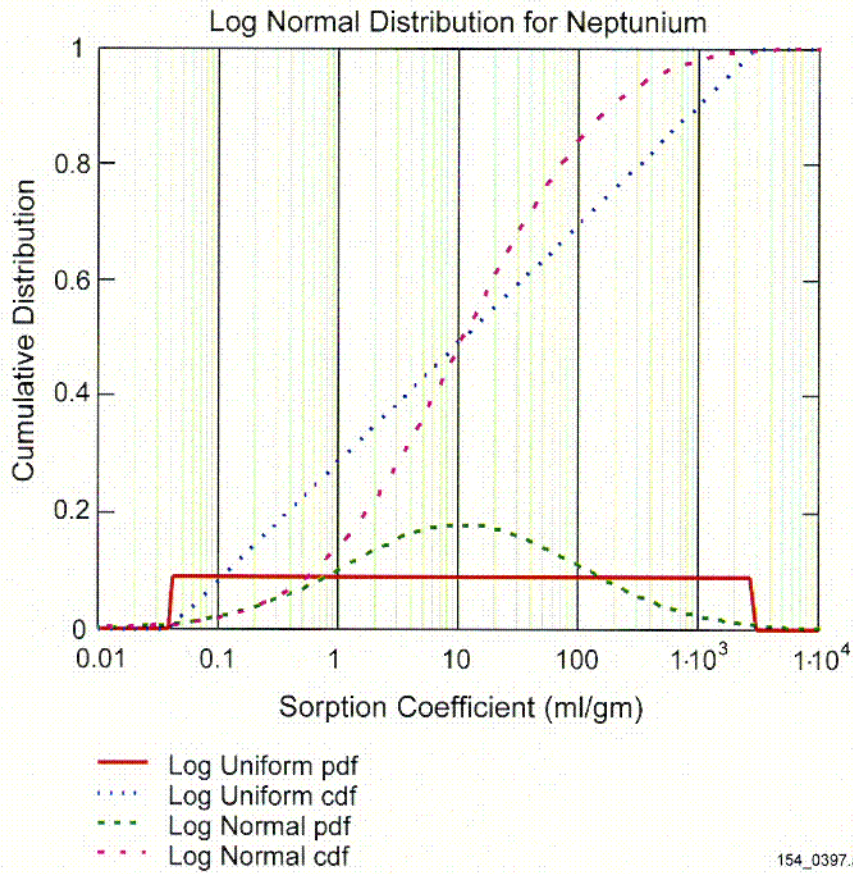
154_0396.ai

Source: Sheppard and Thibault 1990 [DIRS 109991].

NOTE: Comparison based on the tolerance interval for the 95 percent confidence level with the combined sand, loam, and clay data sets.

Figure 10.3.4-2. Comparison of Lognormal and Log Uniform Distributions for the Partition Coefficient of Iodine

CO9



154_0397.ai

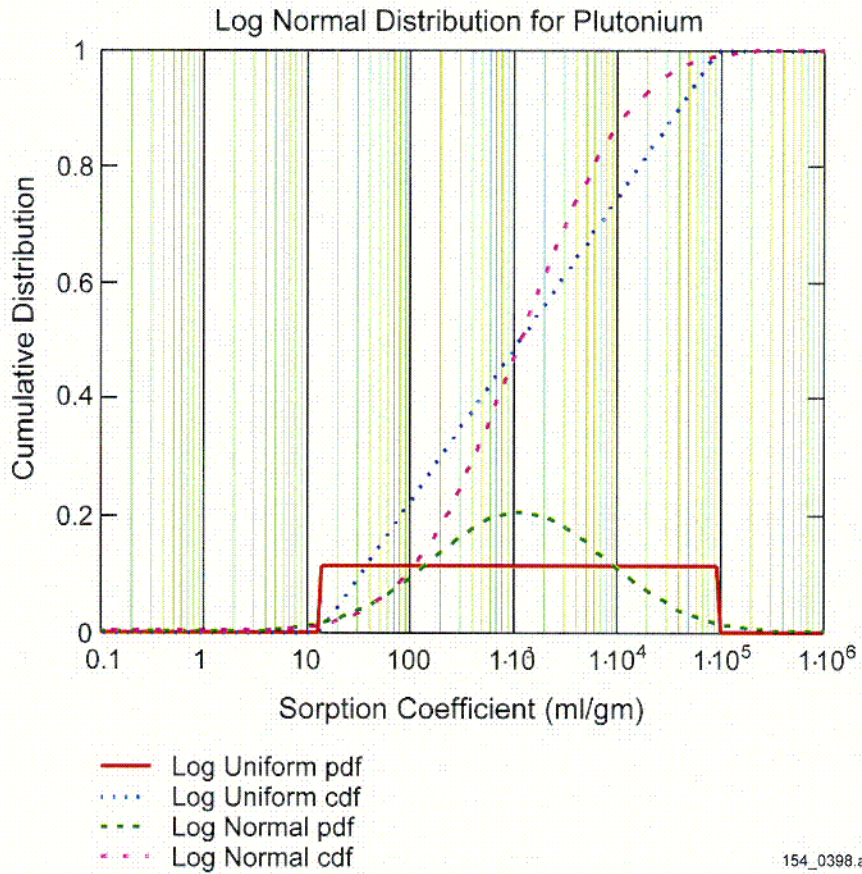
154_0397.ai

Source: Sheppard and Thibault 1990 [DIRS 109991].

NOTE: Comparison based on the tolerance interval for the 95 percent confidence level with the combined sand, loam, and clay data sets.

Figure 10.3.4-3. Comparison of Lognormal and Log Uniform Distributions for the Partition Coefficient of Neptunium

C10



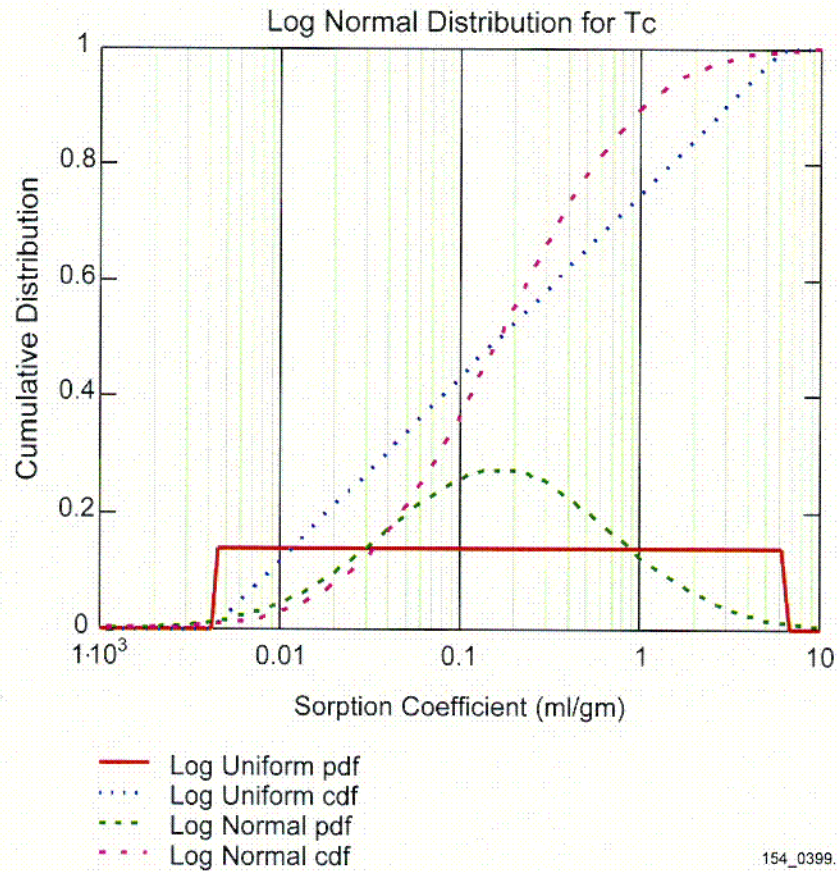
154_0398.ai

Source: Sheppard and Thibault 1990 [DIRS 109991].

NOTE: Comparison based on the tolerance interval for the 95 percent confidence level with the combined sand, loam, and clay data sets.

Figure 10.3.4-4. Comparison of Lognormal and Log Uniform Distributions for the Partition Coefficient of Plutonium

C11



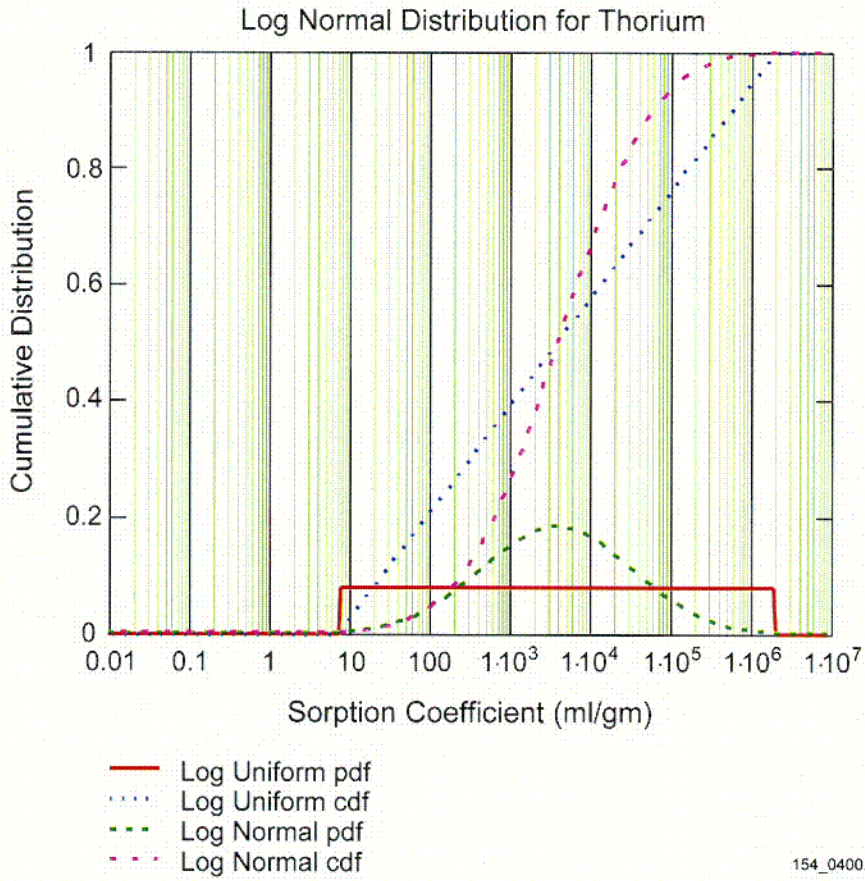
154_0399.ai

154_0399.ai

Source: Sheppard and Thibault 1990 [DIRS 109991].

NOTE: Comparison based on the tolerance interval for the 95 percent confidence level with the combined sand, loam, and clay data sets.

Figure 10.3.4-5. Comparison of Lognormal and Log Uniform Distributions for the Partition Coefficient of Technetium



154_0400.ai

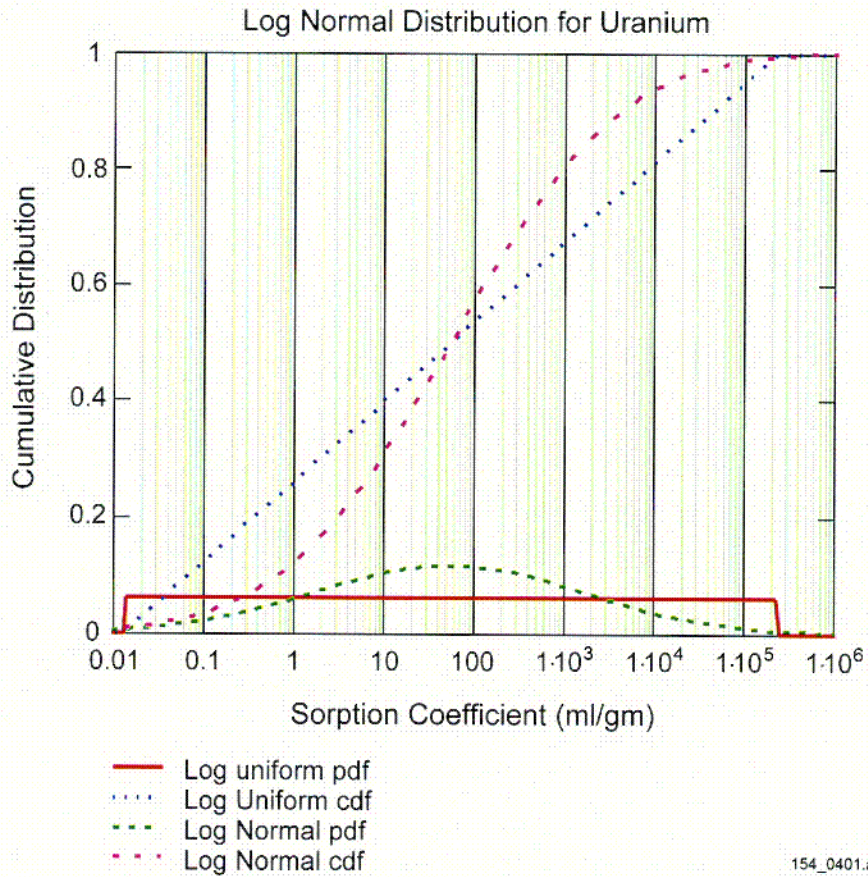
154_0400.ai

Source: Sheppard and Thibault 1990 [DIRS 109991].

NOTE: Comparison based on the tolerance interval for the 95 percent confidence level with the combined sand, loam, and clay data sets.

Figure 10.3.4-6. Comparison of Lognormal and Log Uniform Distributions for the Partition Coefficient of Thorium

C13



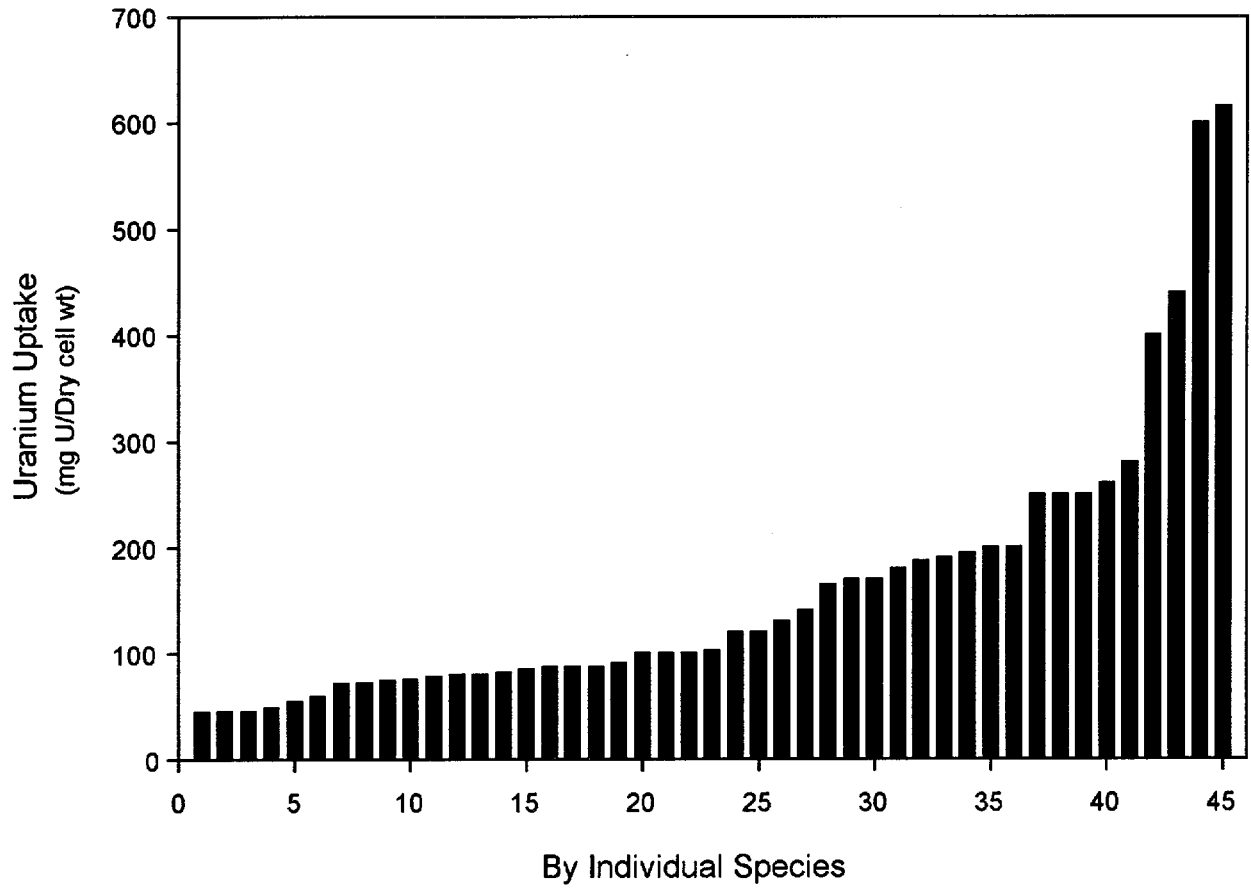
154_0401.ai

Source: Sheppard and Thibault 1990 [DIRS 109991].

NOTE: Comparison based on the tolerance interval for the 95 percent confidence level with the combined sand, loam, and clay data sets.

Figure 10.3.4-7. Comparison of Lognormal and Log Uniform Distributions for the Partition Coefficient of Uranium

C14

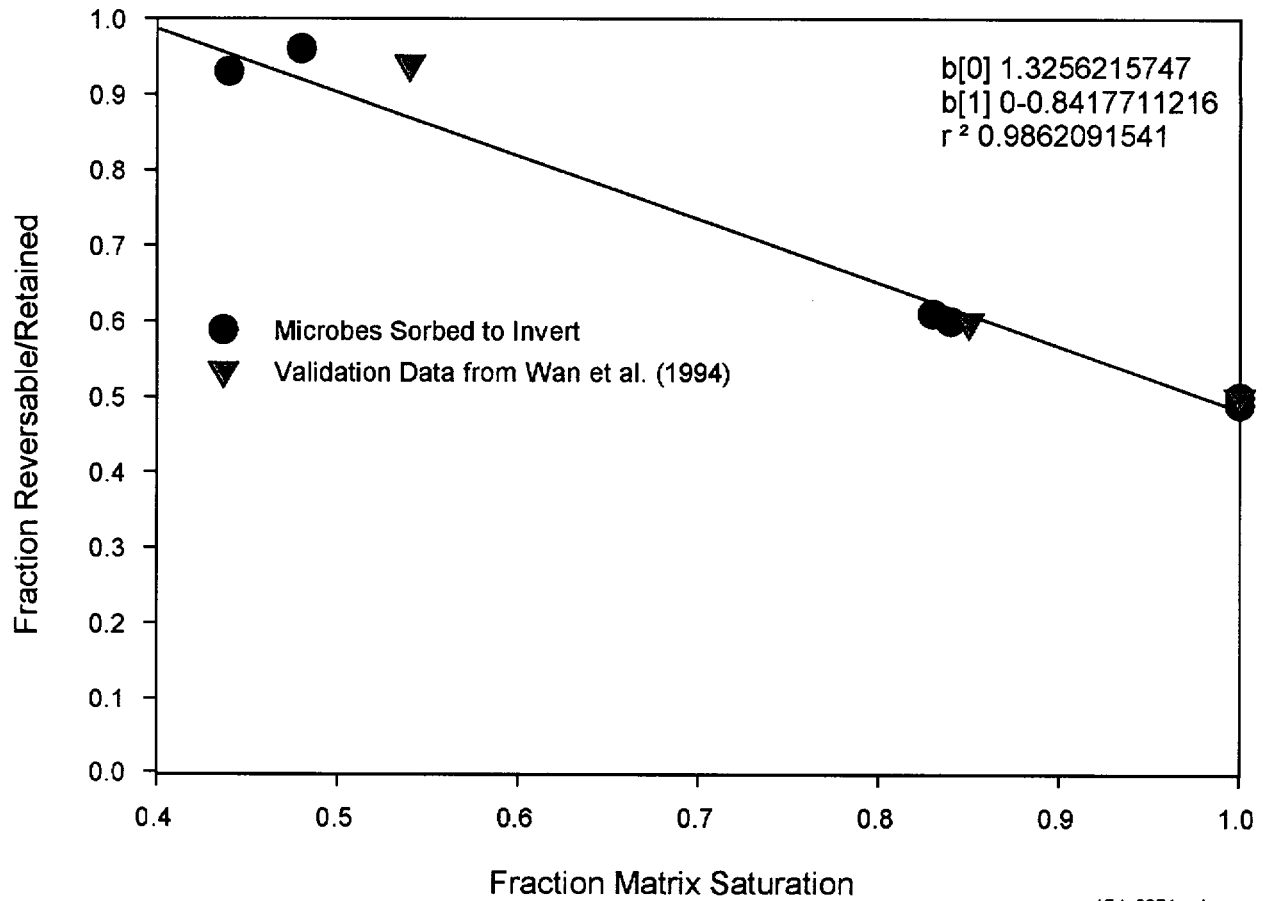


154_0350a.ai

154_0350a.ai

Source: Suzuki and Banfield 1999 [DIRS 154445].

Figure 10.3.6-1. Uranium Uptake for 45 Species of Bacteria and Fungus

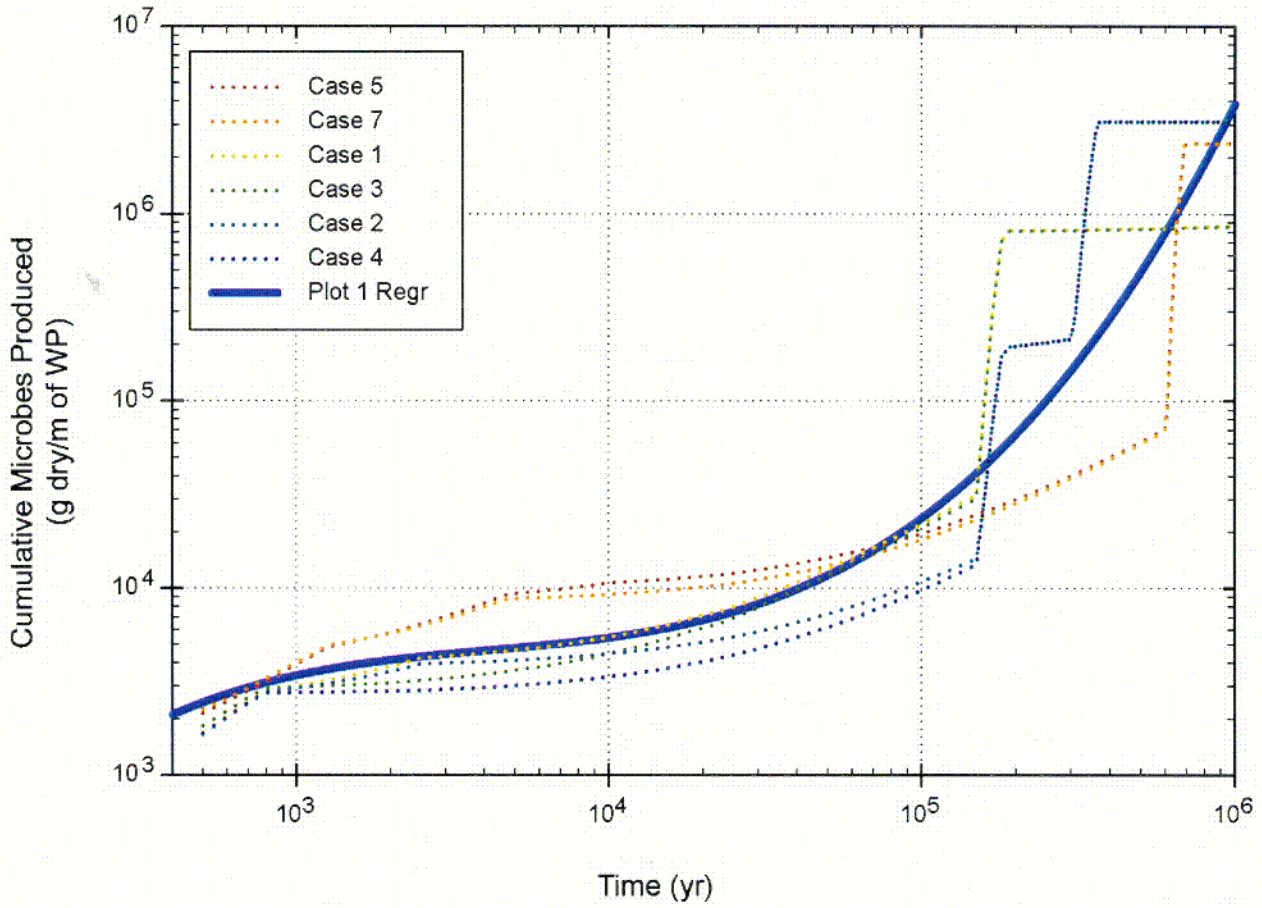


154_0351a.ai

154_0351a.ai

Source: Regression data from Jewett et al. 1999 [DIRS 154325]; validation data from Wan et al. 1994 [DIRS 154367].

Figure 10.3.6-2. Retention of Microbes on Air-Water Interfaces in Unsaturated Sand Column Experiments



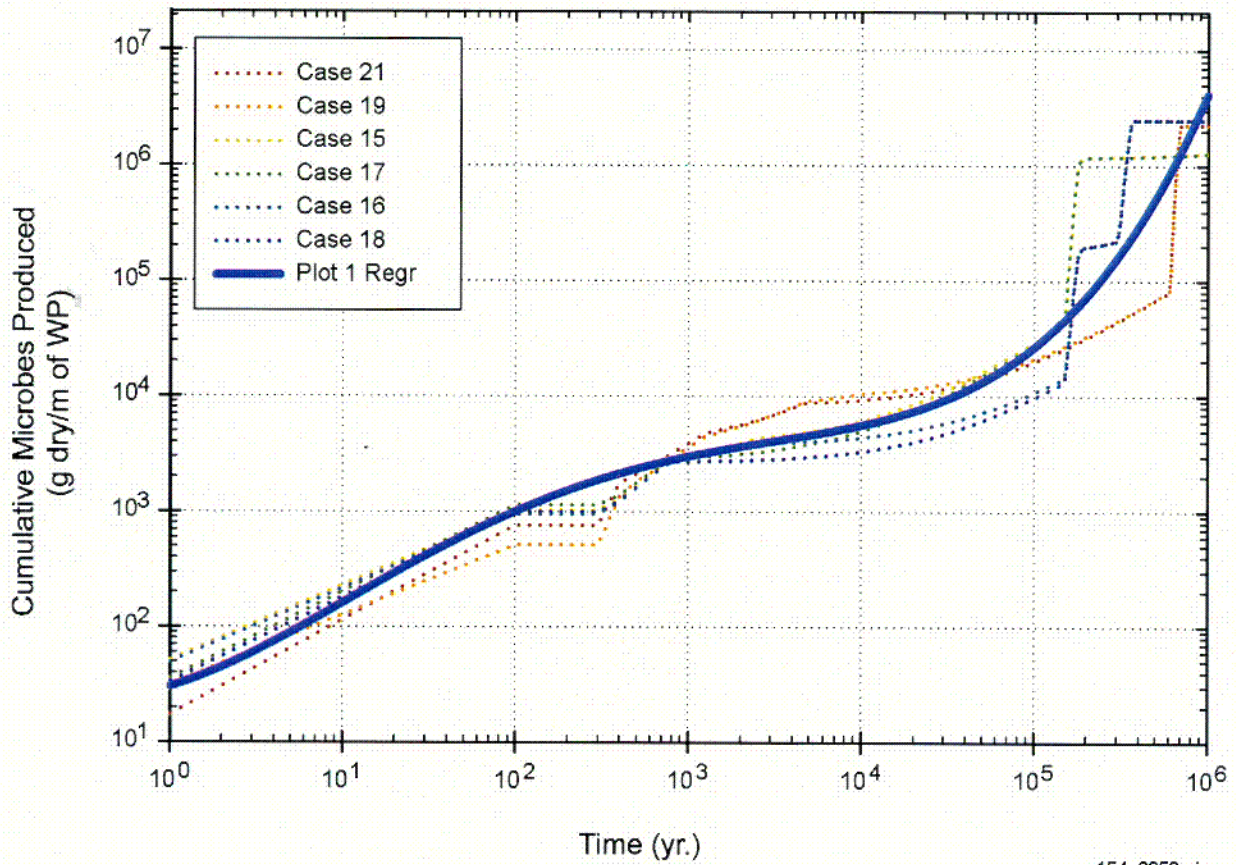
154_0352.ai

154_0352.ai

Source: Microbial growth data from CRWMS M&O 2000 [DIRS 151561]; microbial growth data documented in DTN: MO0010MWDMIN38.031 [DIRS 154299].

Figure 10.3.6-3. Third-Order Linear Regression Fit of Cumulative Microbial Growth Data for Modeling Runs Containing Commercial Spent Nuclear Fuel Waste Packages

C15



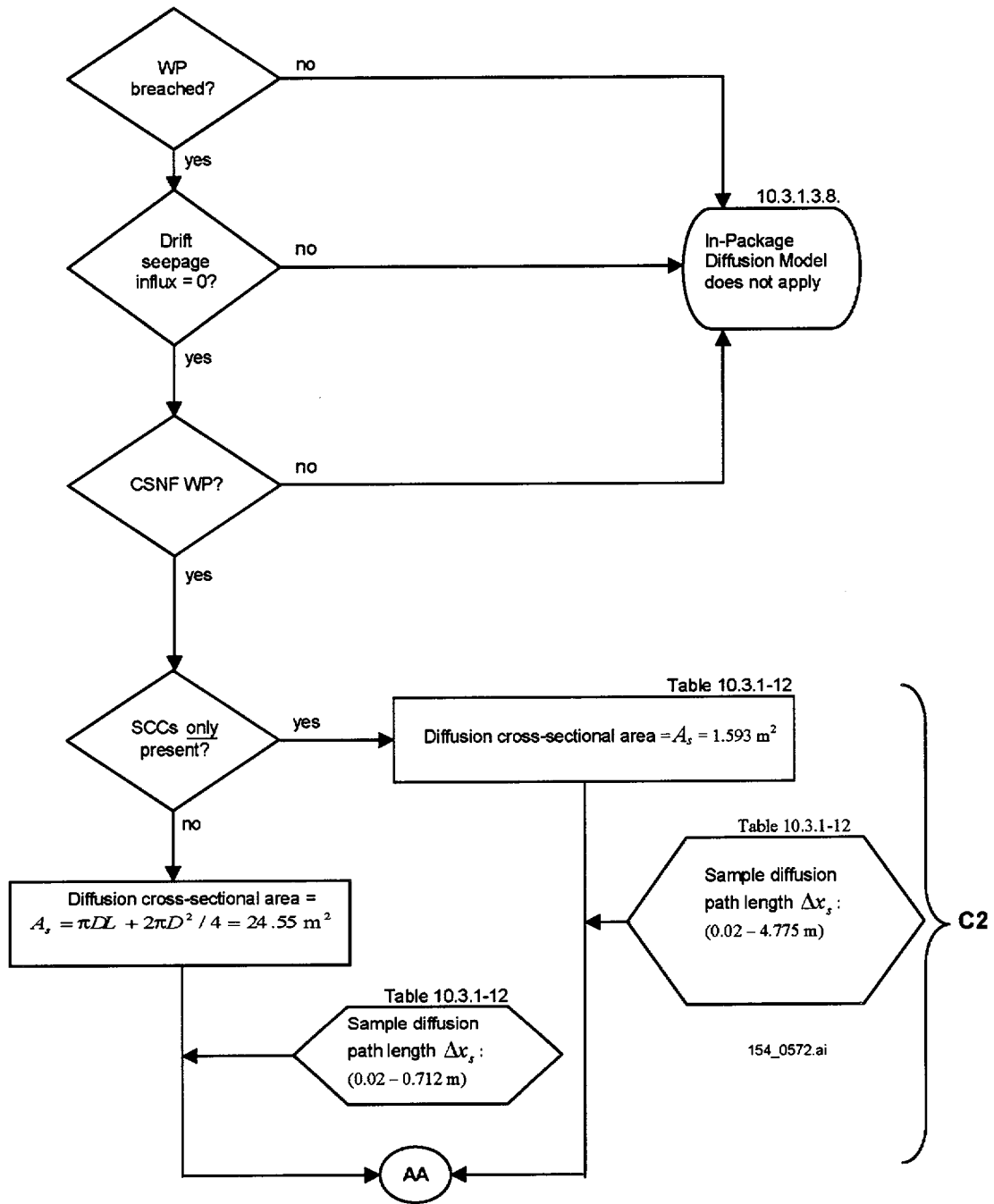
154_0353.ai

154_0353.ai

Source: Microbial growth data from CRWMS M&O 2000 [DIRS 151561]; microbial growth data documented in DTN: MO0010MWDMIN38.031 [DIRS 154299].

Figure 10.3.6-4. Fourth-Order Linear Regression Fit of Cumulative Microbial Growth Data for Modeling Runs Containing High-Level Waste Packages

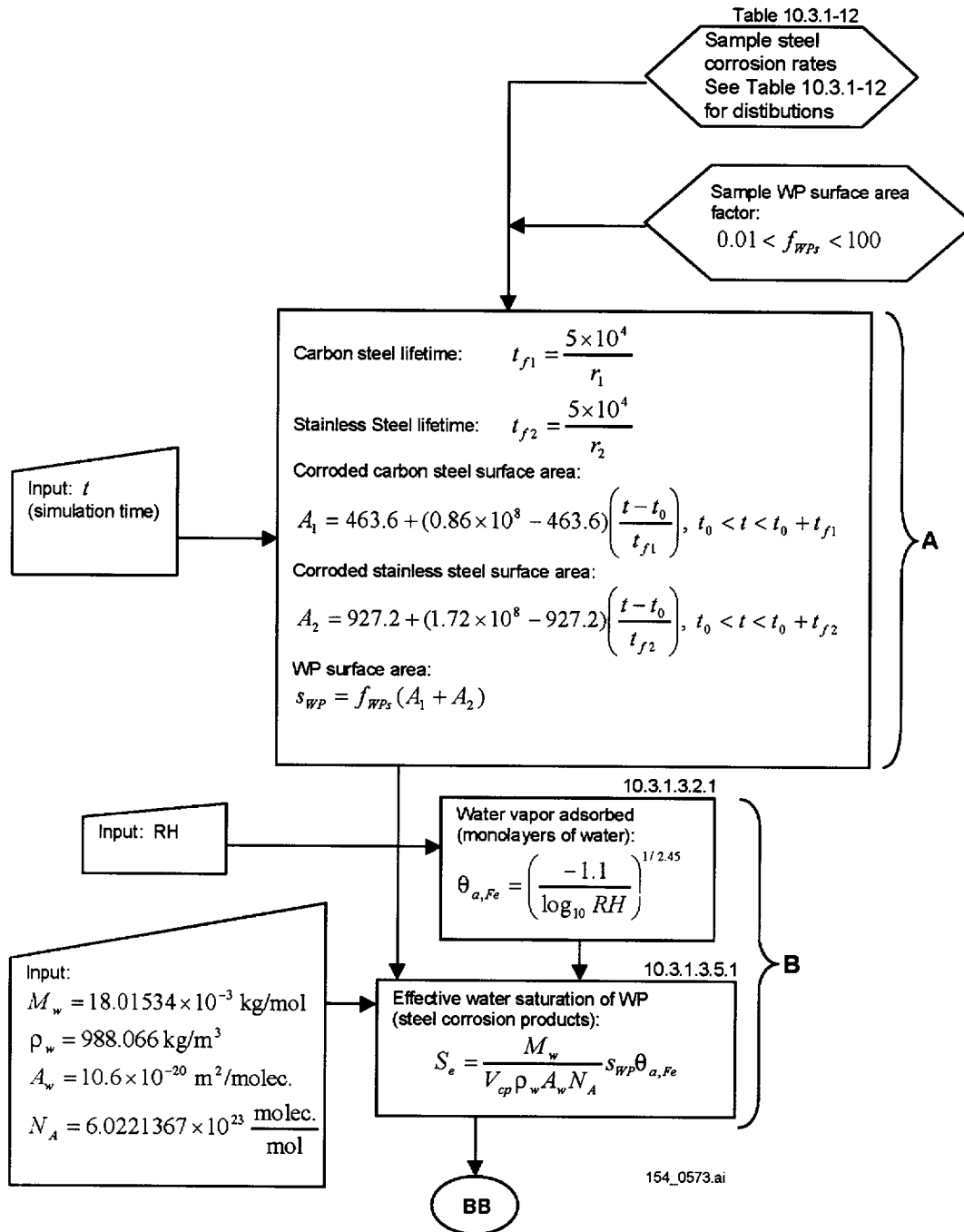
C16



154_0572.ai

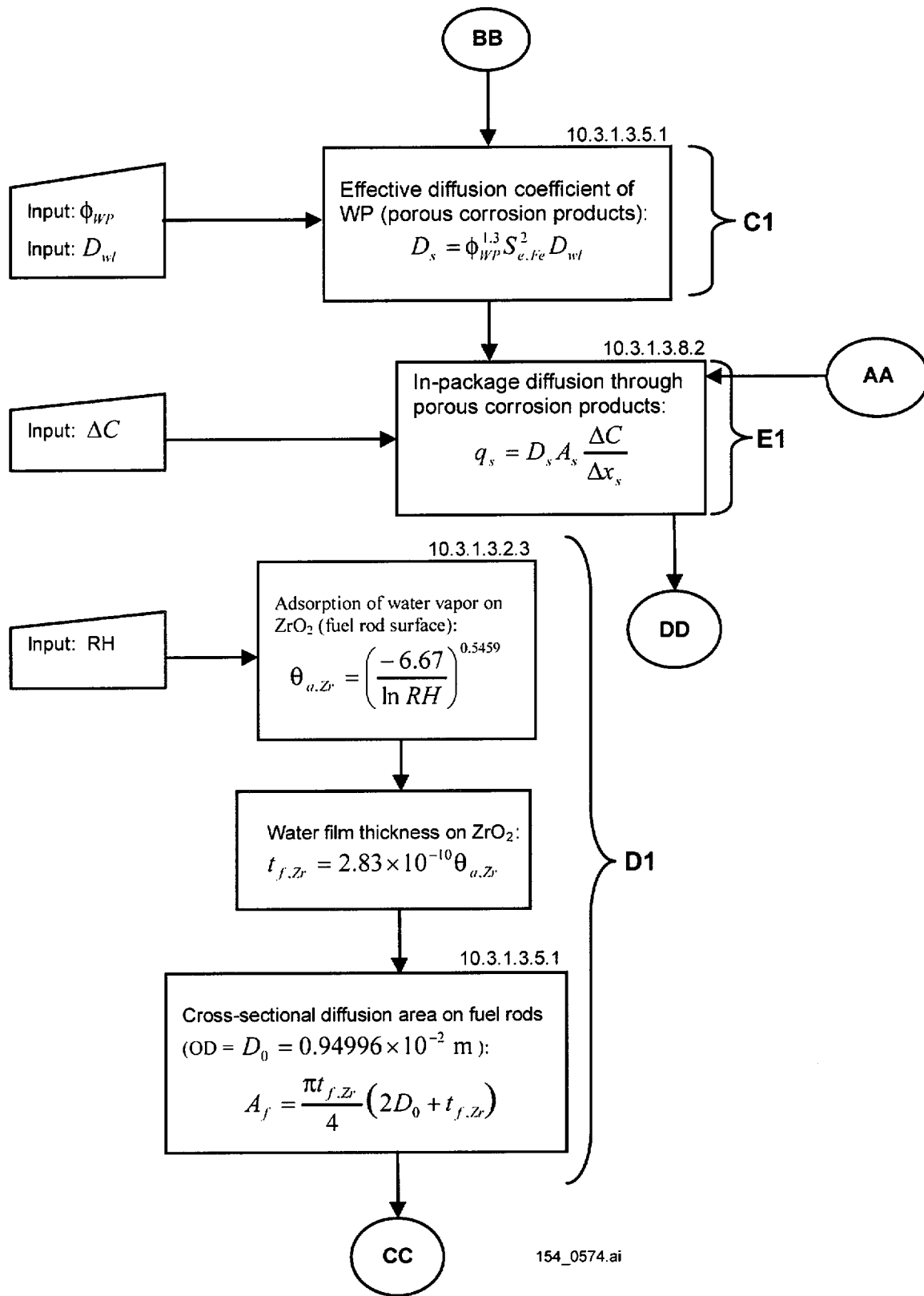
NOTE: WP = waste package; SCC = stress corrosion cracks; CSNF = commercial spent nuclear fuel; OD = outer diameter; RH = relative humidity.

Figure 10.4.1-1. Flowchart for In-Package Diffusion Model



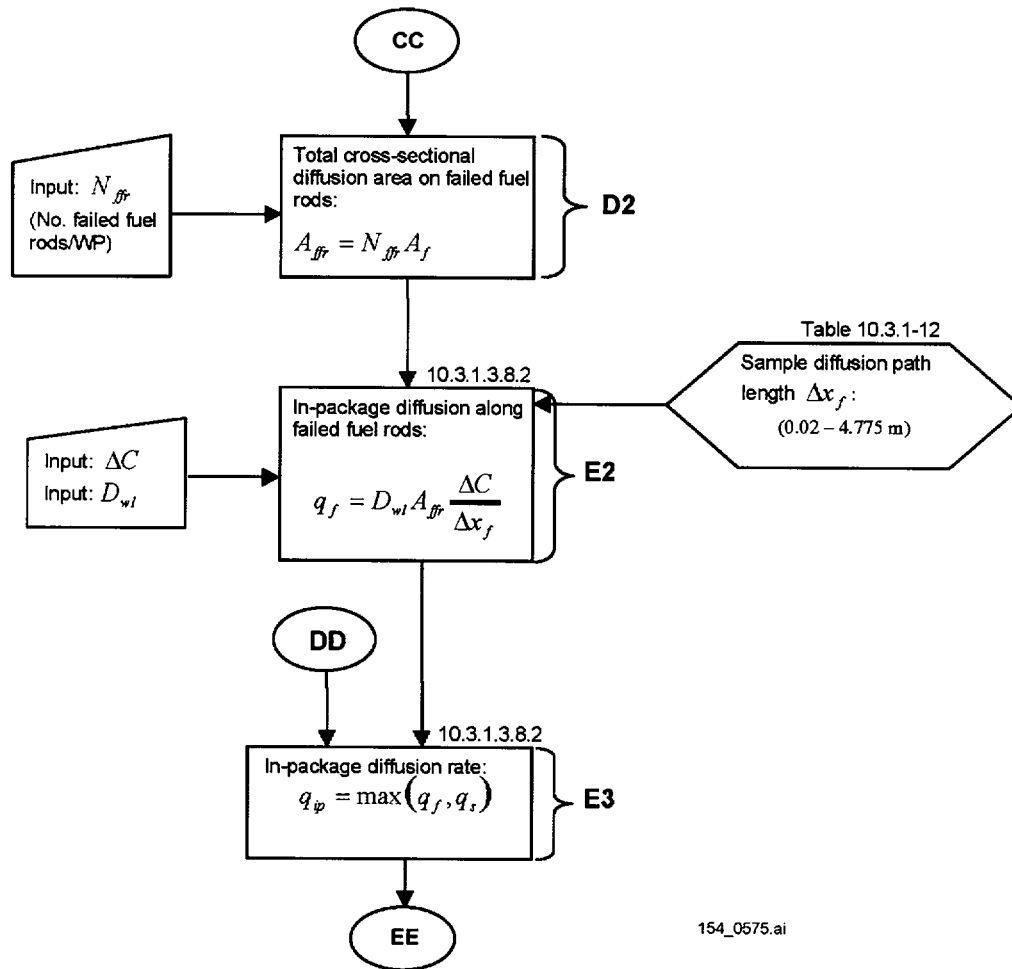
154_0573.ai

Figure 10.4.1-1. Flowchart for In-Package Diffusion Model (Continued)



154_0574.ai

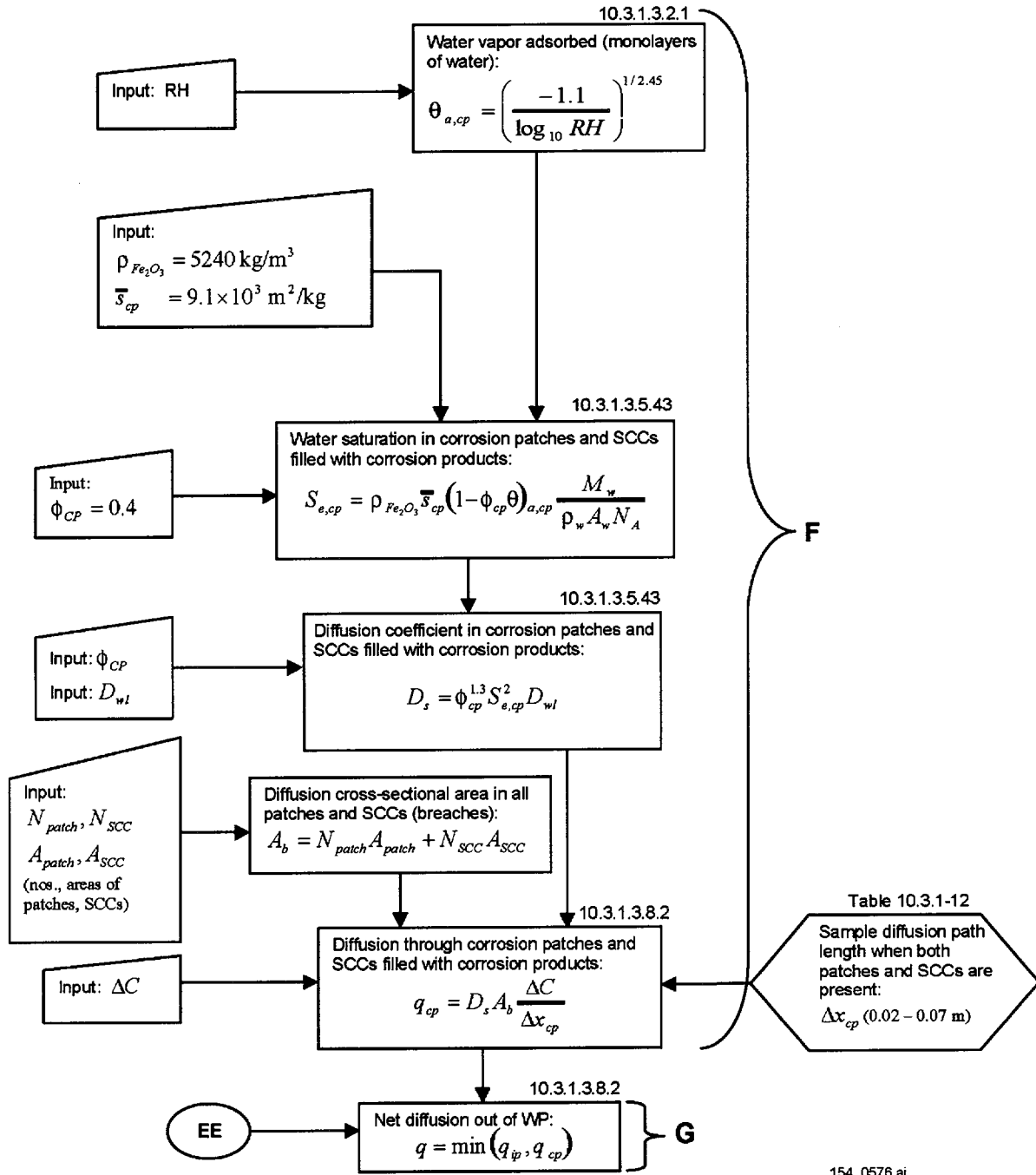
Figure 10.4.1-1. Flowchart for In-Package Diffusion Model (Continued)



154_0575.ai

154_0575.ai

Figure 10.4.1-1. Flowchart for In-Package Diffusion Model (Continued)



154_0576.ai

154_0576.ai

Figure 10.4.1-1. Flowchart for In-Package Diffusion Model (Continued)

INTENTIONALLY LEFT BLANK